Safety in Mines Research Advisory Committee

Final Report

Determine the effect of repeated dynamic loading on the performance of tunnel support systems

Authors: Güler, G., Kuijpers, J.S., Wojno, L., Milev, A., and Haile, A.

Research Agency: Mining Technology, a Division of CSIR

Project No.: GAP 616

Date : March 2001

Executive Summary

Seismicity causes the most severe loading conditions for tunnel support systems in deep-level South African gold mines. The design of such support systems should therefore incorporate the potential effect of seismicity on support requirements.

Unfortunately, this is presently not possible, as such effects have not yet been adequately quantified. Within the current project, an attempt has been made to address this shortcoming.

The findings of rock burst investigations were used to identify support failure mechanisms in tunnels after large seismic events. These findings allowed for a qualitative evaluation of support requirements and support influence and were used as a basis for the actual testing programme.

The main objective of this project was to determine the support capacity of various support systems and components under dynamic loading conditions. Deficiencies in the performance of fabric support were highlighted in these and other investigations. The lack of adequate criteria or methods for the design of fabric support is therefore a shortcoming, which needs to be overcome in order to obtain improved fabric support.

A special testing rig was redesigned in such a way that a tunnel support system could be incorporated in a realistic rock mass environment. The effects of repeated impact loading could be evaluated by monitoring displacements and velocities in response to each impact. This evaluation showed the effects of lacing, shotcrete and Evermine on the energy absorption capacity, deformations and local instabilities. Tendons, supporting the specimens, were excessively excited by the impact loads imposed on these specimens, and did not yield. All the other support components were however prone to failure, after sufficient deformation was imposed upon them. In this respect, it should be emphasized that the differential behaviour between tendons and typical fabric support correctly reflects the mechanisms involved in a deep-level mine tunnel in fractured rock. In sufficiently fragmented rock, the loading demand on tendons would be limited to the (lower) capacity of the fabric support. In such cases, the capacity of the entire support system would thus also be limited to the capacity of the fabric support. It is this capacity which was evaluated in these impact tests.

In addition, individual support components such as tendons, mesh and lacing were evaluated separately in different laboratory tests. One of the more revealing findings from these tests was the fact that the capacity of lacing can be significantly reduced by the clamping device used. This was also observed in the impact tests and may represent a realistic limitation on actual

support performance. Nevertheless, the presence of lacing always contributed strongly to the performance of a support system.

A model for impact testing is also presented here. With this model, various influencing parameters can be quantified and the monitored impact tests can be analysed in more detail. One of the most important parameters in this model is the resisting force, which is made up of an internal rock mass resistance and a support resistance. The relationship between induced displacements and impact energy is also represented by this model. This relationship is typically non-linear, a phenomenon which was also observed in the impact tests. The results from the impact tests can be interpreted with confidence using this model, as the influence of various parameters can be assessed directly.

Underground monitoring at a site on Tau Tona, to determine the effects of seismic events on support systems, has been completed. The effects of the seismic events, to which this site was subjected during the monitoring period, were relatively small, compared to the impact testing results as maximum velocities of 67 mm/s were measured at this site. Typical laboratory testing velocities from even the smaller impacts were an order of magnitude larger. Nevertheless, it was possible to establish a relationship between induced velocities and tendon support loading from the underground monitoring data. This relationship should be extremely useful for the design of these tendons in relation to seismic activity.

The importance of correct design of fabric support has been highlighted in this project and a conceptual design methodology has been formulated. It is considered important that further testing of fabric type support elements should be carried out, while the design methodology should be developed and evaluated in more detail as well.

Acknowledgements

The work presented here results from funding provided by SIMRAC. The co-operation, support and constructive criticism of the members of SIMRAC were appreciated and are acknowledged.

The authors would also like to thank the Tau Tona Shaft Management Team for their support and co-operation.

The following material suppliers are also gratefully acknowledged: Kloof Gold Mine, Haggie Rand Limited, Meshrite (PTY) Ltd and Freyssinet S.A. (PTY) Ltd.

Table of Contents

Executive Summary ..... **ii**

Acknowledgements ..... **iv**

Table of Contents ..... **v**

List of Figures ..... **vii**

List of Tables ..... **xii**

1 Introduction **1**
1.1 Aims and objectives 1
1.2 Research methodology 3

2 Literature survey **3**
2.1 Design methodologies 3
2.1.1 Design based on rock mass retention/ containment 6
2.1.2 Summary 9
2.2 Design considerations 9
2.2.1 Repeated dynamic demand on the support system 10
2.2.2 Capacity of the support systems 10

3 Physical evaluation **12**
3.1 Drop test rig 12
3.1.1 Introduction 12
3.1.2 Description of changes 12
3.1.3 Tests performed 15
3.1.4 Results 17
3.1.5 Discussion of the results and Conclusions 18
3.2 Laboratory evaluations 23
3.2.1 Introduction / Methodology 23
3.2.2 Tests performed 24
3.2.2.1 Tendons 24
3.2.2.2 Mesh 33
3.2.2.3 Lacing 35

4 Preliminary design recommendations **38**

5 Detailed underground evaluation **40**
5.1 Site selection / history 40
5.2 Evaluation of support system performance 42
5.2.1 General 42
5.2.2 Observations and monitoring 44
5.2.3 Support used in the monitored area of the 100-3c-x/c south 49
5.3 Underground monitoring results 52
5.3.1. Quasi-static and dynamic monitoring 52

6 Impact test model **58**
6.1 Parameter study on support requirements for impact loading 58
6.2 Discussion and Conclusions 65

7 Formulation of design criteria..... 71

8 Recommendations for future work..... 75

References..... 77

Appendix A..... 79

List of Figures

Figure 2.1. Definition of principle methodologies of excavation stabilization (Gürtunca and Haile, 1999).....4

Figure 2.2. Generalized deformation characteristics for principal support methodologies under high loading conditions (Gürtunca and Haile, 1999).....4

Figure 2.3. Rock mass unravelling between rock bolts (background) and rock bolt failure (foreground) (Gürtunca and Haile, 1999).....7

Figure 2.4. Relationship between accumulated impact kinetic energy and deformation for contained simulated rock mass system (Stacey and Ortlepp, 1997).....11

Figures 3.1 a and b. General views of the main test rig.....13

Figure 3.2. Sketch of the test frame with artificial rock mass and support system. 14

Figure 3.3. Plan view illustrating the position of various geophones at the bottom of an assembly supported with Evermine and lacing. 17

Figure 3.4. Peak particle velocities measured on the surface of the sample with Evermine and lacing.....18

Figure 3.5. In situ relationship between PPVs and distance from a rock bolt reinforcement unit (Haile and Le Bron, 2001).....19

Figure 3.6. Results for 10 cm drops for various fabric supports (1 kJ per drop)...20

Figure 3.7. Results for 50 cm drops for various fabric supports (5 kJ per drop)...20

Figure 3.8. Servo controller with 2000 kN capacity.....25

Figure 3.9. Various types of elements to be tested and mechanism of locking jaw. 25

Figure 3.10. An example of re-bar testing results 26

Figure 3.11. Deformation curve of the smooth bar. 27

Figure 3.12. Failure mechanisms of smooth and re-bars.....27

Figure 3.13. Deformation curve of the wire cable.....28

Figure 3.14. Failure mechanisms of wire cable.....28

Figure 3.15. Energy absorption capabilities of re-bar under different types of loadings. 29

Figure 3.16. Energy absorption capabilities of smooth bar under different types of loadings.....30

Figure 3.17. Deformation curves for all re-bars tested.....31

Figure 3.18. Deformation curves for all smooth bars tested.....31

Figure 3.19. Cumulative energy absorbed (kJ) by all re-bars tested.....32

Figure 3.20. Cumulative energy absorbed (kJ) by all smooth bars tested.....32

Figure 3.21. Deformation curves for all diamond meshes tested.....33

Figure 3.22. Cumulative energy absorbed in all diamond meshes tested.....34

Figure 3.23. Deformation curves for all welded meshes tested.....34

Figure 3.24. Cumulative energy absorbed in all welded meshes tested.....35

Figure 3.25. Lacing tested with clamping jaws.....36

Figure 3.26. Lacing tested with a single friction clamping device.....36

Figure 3.27. Lacing tested with three friction clamping devices.....37

Figure 5.1. Mine layout, geological structures and seismicity around the site. Data from the Rock Mechanics Department, Tau Tona Gold Mine.....40

Figure 5.2. A plan view of the monitoring site and de-stressing slot.....41

Figure 5.3. Instrumented rock tendons.....42

Figure 5.4. Layout of excavations and position of de-stressing slot.....43

Figure 5.5. Overall tunnel condition around monitoring position 1. (October 2000).....45

Figure 5.6. Overall tunnel condition around the monitoring position 2.....46

Figure 5.7. Measuring hangingwall – footwall closure at monitoring position 2...46

Figure 5.8. Section of monitored excavation in proximity of position 3.....47

Figure 5.9. Close-up of the hangingwall condition adjacent to position 3.....48

Figure 5.10. Overall stability of hangingwall in the vicinity of position 3.....48

Figure 5.11. Wire mesh, rope lacing and shotcrete integrated support.....49

Figure 5.12. Pre-tensioned and post-grouted cable anchor.....50

Figure 5.13. General condition of the hangingwall in the 100-3c cross-cut south. 50

Figure 5.14. A close-up of the hangingwall condition.....51

Figure 5.15. Rehabilitated area, exposing a brow. 51

Figure 5.16. A cross-sectional view of the tunnel and the position of the monitoring instrumentation; G_{SW} and G_{HW} are geophones, S_1 to S_6 are strain gauges and T_1 and T_2 are tendons. 52

Figure 5.17. PPVs recorded on the hangingwall and the sidewall of the tunnel....53

Figure 5.18. The strain at site T_1 as the face of the de-stressing slot progressed towards the instrumentation.....53

Figure 5.19. The strain at site T_2 as the face of the de-stressing slot progressed towards the instrumentation.....54

Figure 5.20. The dynamic strain measured in site T_1 as function of the PPVs measured on the hangingwall.....55

Figure 5.21. The dynamic strain measured in site T_2 as function of the PPVs. 55

Figure 5.22 Relationship between velocities and non recoverable strain 57

Figure 6.1. Relationship between the impact force, resisting force, and time.....59

Figure 6.2. Relationship between impulse velocity and time for given parameters. 62

Figure 6.3. Relationship between impulse displacement and time for given parameters.....65

Figure 6.4. Model of impact testing. 66

Figure 6.5. Displacement magnification factors for different ratios between impact force and resisting force with increasing drop heights. 68

Figure 7.1. Relationship between distance from the seismic source and the induced stresses in solid rock and induced forces (volume of 1 cubic metre) for various magnitudes.....73

Figure 7.2. Theoretical relationship between strength and span for varying thicknesses of uniformly loaded WMRSC, based on a single calibration test. 74

Figure 7.3. Cost analysis graph for cone bolts and WMRSC. 74

Figure A.1. Preparation of bricks assembly.....80

Figure A.2. Preparation of brick assembly. 80

Figure A.3. Brick assembly completed.....80

Figure A.4. Ready for testing.....80

Figure A.5. Ready for testing.....81

Figure A.6. Evermine and lacing 50 cm. drops.....81

Figure A.7. Evermine and lacing 50 cm. drops.....81

Figure A.8. Evermine and lacing 50 cm drops.....81

Figure A.9. Evermine and lacing 50 cm. drops.....82

Figure A.10. Evermine and lacing 50 cm. drops. 82

Figure A.11. Evermine and lacing 50 cm. drops. 82

Figure A.12. Evermine and lacing 50 cm. drops. 82

Figure A.13. Evermine and lacing 50 cm. drops. 83

Figure A.14. Evermine and lacing 50 cm. drops. 83

Figure A.15. Evermine and lacing 10 cm. drops. 83

Figure A.16. Evermine and lacing 10 cm. drops. 83

Figure A.17. Evermine and lacing 10 cm. drops. 84

Figure A.18. Evermine and lacing 10 cm. drops. 84

Figure A.19. Evermine and lacing 10 cm. drops. 84

Figure A.20. Evermine and lacing 10 cm. drops. 84

Figure A.21. Evermine 10 cm. drops. 85

Figure A.22. Evermine 10 cm. drops. 85

Figure A.23. Evermine 10 cm. drops. 85

Figure A.24. Evermine 10 cm. drops. 85

Figure A.25. Evermine 10 cm. drops. 86

Figure A.26. Evermine 10 cm. drops. 86

Figure A.27. Evermine 10 cm. drops. 86

Figure A.28. Evermine 10 cm. drops. 86

Figure A.29. Evermine 10 cm. drops. 87

Figure A.30. Evermine 10 cm. drops. 87

Figure A.31. Evermine 10 cm. drops. 87

Figure A.32. No fabric support 10 cm. drops.....87

Figure A.33. No fabric support 10 cm. drops.....88

Figure A.34. No fabric support 10 cm. drops.....88

Figure A.35. No fabric support 10 cm. drops.....88

Figure A.36. No fabric support 10 cm. drops.....88

Figure A.37. Lacing 10 cm. drops. 89

Figure A.38. Lacing 10 cm. drops. 89

Figure A.39. Lacing 10 cm. drops. 89

Figure A.40. Lacing 10 cm. drops. 89

Figure A.41. Detail of lacing.....90

Figure A.42. Shotcrete 50 cm. drops.....90

Figure A.43. Shotcrete 50 cm. drops.....90

Figure A.44. Shotcrete 50 cm. drops.....90

Figure A.45. Final failure of shotcreted assembly.....91

Figure A.46. Final failure of shotcreted assembly.....91

Figure A.47. Final failure of shotcreted assembly.....91

Figure A.48. Shotcrete and lacing 50 cm. drops.....91

Figure A.49. Shotcrete and lacing 50 cm. drops.....92

Figure A.50. Shotcrete and lacing 50 cm. drops.....92

Figure A.51. Shotcrete and lacing 50 cm. drops.....92

Figure A.52. Pull test diamond mesh (A). 92

Figure A.53. Pull test diamond mesh (A). 93

Figure A.54. Pull test diamond mesh (B). 93

Figure A.55. Pull test diamond mesh (B). 93

Figure A.56. Pull test diamond mesh (B). 93

Figure A.57. Pull test diamond mesh (B). 94

List of Tables

Table 4.1. Support recommendations. *39*

Table 5.1. Stress history for monitoring positions along 100-3c cross-cut south. *44*

1 Introduction

In deep-level mining environments, tunnel support systems may be subjected to quasi-static and dynamic loading. In this project, the effects of repeated dynamic loading conditions were specifically addressed. Both *in situ* and experimental data were used to investigate the influence of tunnel support systems on the stability of the supported rock mass structure under such loading conditions.

While most data was obtained from laboratory tests and physical model evaluations, additional monitoring data from an underground site was also included. Owing to the nature of the problem addressed here, seismic excitation was required to render the underground data relevant. A site, with a history of substantial seismic activity, was therefore selected in anticipation of a continuation of this historical trend.

In order to analyse the interaction between support components and the rock mass under repeated dynamic loading conditions, a realistic, physical model was developed. This model was based on a drop test rig and a simulated rock mass. Repeated dynamic loading was induced by multiple impacts of constant magnitudes. Both the energy absorption capacity of a particular fabric and the accumulation of deformations, caused by repeated impacts, could thus be quantified. It is especially the cumulative nature of these impacts, which determines the effect of dynamic loading; both the number and the magnitude of impacts are of relevance in this respect.

Support components were also assessed individually in separate laboratory tests. A variety of tendons were subjected to dynamic and repeated axial stretching in a special loading device (Terra-Tek). The same device was also used to test different types of mesh and lacing, which were supported in a separate frame. While these tests are useful for the determination of the capacity of support components, they do not enable an immediate assessment of a support system. The interaction of the various support components with the rock mass structure will, to a large extent, determine the effect of the total system.

1.1 Aims and objectives

The main aim of the project was to gain an understanding of the effect of repeated loading on typical tunnel support systems and to present recommendations on the life of tunnel support systems under such conditions. In addition, improved practical design considerations were investigated.

A literature survey into current tunnel support design considerations provided a basis for this work. The focus of the literature study was on dynamic loading, both its quantification and its possible effects on support systems. Loading history is considered to be of major importance and was therefore also investigated.

Most of the literature used for this project comprised case studies of rockbursts. It is believed that these studies provide a unique opportunity to assess "worst case" conditions on which any realistic design should be based. Failure of support systems under rockburst conditions needs to be understood in order to allow any formulation of a design methodology. As these case studies only allow for a post mortem analysis, some relevant information such as loading history, time effects, etc. may be lacking. However, the mechanisms of support failure may be clearly identified from these case studies.

Typical support components such as rock bolts and cables, various meshes and lacings were evaluated under multiple impact loading conditions in suitable laboratory tests. The purpose of these tests was to establish the behaviour of these support components under such dynamic loading conditions. In addition, the analysis of a model of realistic rock mass – support systems under controlled laboratory conditions was also included. This should allow the quantification of the interaction between support system and rock mass.

In situ monitoring of support behaviour by installation of suitable instrumentation was the third and final component of data collection. An underground site at Tau Tona Mine, 100 level was selected for this purpose.

Based on the data from the case studies, the laboratory tests and the instrumented haulage, a conceptual model of support behaviour under dynamic loading conditions was formulated. This model can be implemented in numerical tools so that comparative studies can be done. A methodology for the design of rockburst resistant tunnel support systems was formulated. This methodology allows for the cost effective design of a system consisting of tendons and fabric support. In addition, practical guidelines for the selection of support systems for different rock mass and loading conditions were developed (Table 4.1).

1.2 Research methodology

The project was divided into two phases:

Phase 1

- survey of current practices and knowledge (literature survey and evaluation of current design processes),
- physical evaluation (laboratory testing of support components, i.e. rock bolts, meshes, lacings and membrane support components and laboratory testing of simulated tunnel support – rock mass system), and

Phase 2

- underground evaluation (site selection and *in situ* evaluation of support system performance),
- numerical modelling, and
- design recommendations.

2 Literature survey

2.1 Design methodologies

The principal design methods for support systems are based on either containment or the creation of a reinforced rock mass shell. Containment of the rock mass is achieved by ensuring anchorage beyond the limit of rock mass instability in stable rock, with sufficient capacity within the support system to accommodate the full rock mass loading and deformation. Alternatively the support system may act to reinforce the skin of the unstable rock mass and thus create a reinforced rock mass structure, again capable of withstanding the envisaged loading conditions. Within most support systems some combination of both these support mechanisms can be expected to act upon the rock mass. The principal design considerations as discussed above are shown in Figure 2.1.

Of importance is the ability to estimate the depth of rock mass instability around the excavation, to enable the determination of a suitable anchor length. This may be based on historical data of anticipated depths of instability, empirical relationships, or numerical modelling analysis.

The influence of the mechanism of the support system interaction with the rock mass, on the deformation characteristics of the excavation, is illustrated in Figure 2.2.

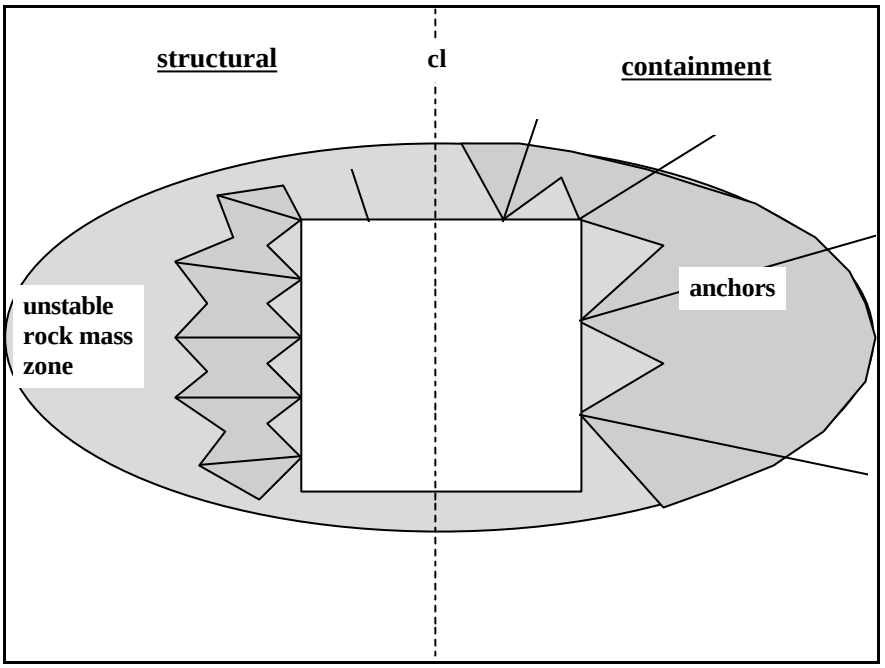

Figure 2.1. Definition of principle methodologies of excavation stabilization (Gürtunca and Haile, 1999).

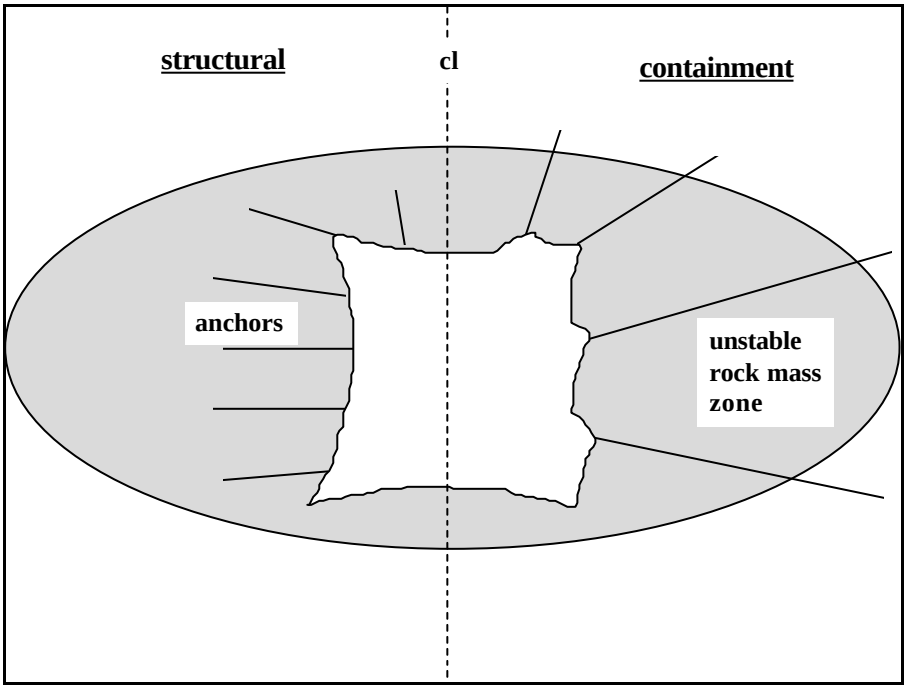

Figure 2.2. Generalized deformation characteristics for principal support methodologies under high loading conditions (Gürtunca and Haile, 1999).

These deformation mechanisms are clearly illustrated by the rockburst case studies, where deformations often occurred to the extent that failure of components of the support system resulted. Analysis of the case studies indicated the characteristic deformation mechanisms and also revealed the shortcomings of the current support systems. The main findings from these case studies are as follows:

- Bulking of the rock mass between tendons was observed at all rockburst sites. At 70 per cent of the sites this bulking resulted in failure of the fabric support. Unravelling of the fragmented rock mass around the tunnel could subsequently be observed.

- At only 30 per cent of the sites no failure of the fabric support was observed. In these cases the fabric support was capable of retaining the unstable rock between the rock bolts.

- In all rockburst sites investigated the majority of tendons had not failed in either tension or shear. In the majority of cases the rock mass had unravelled around the tendons, either due to fabric support failure, or due to the absence of fabric support. In these cases the tendons would not have been subjected to the loads associated with the tributary area theory.

- Tensile failure of some of the rock bolts was observed at 60 per cent of the rockburst sites in both sidewalls and hangingwalls. In most cases this could be associated with large block sizes and a relatively unfractured rock mass. Failure in tension was often observed on corroded tendons. In such cases, discontinuities, which would expose these tendons to a corrosive medium, were typically present. Even the interface between shotcrete and the wall rock was observed to create such a corrosive environment.

- Instability of tunnel hangingwalls was often associated with shear failure of rock bolts. Consideration of the shear capacity of tendons is not catered for in conventional support design, but examples of this type of failure were observed in 70 per cent of the rockburst case studies. Slip along bedding planes is assumed to induce this type of failure.

- Large, uniform sidewall deformations were observed in the Klerksdorp region. This type of failure was associated with a lack of retention due to insufficient tendon length in relation to the depth of instability and the inability to create a structural shell of sufficient strength for these particular geotechnical conditions.

- Shotctrete was observed to have a significant effect on the stability of a fragmented rock mass around a tunnel. Even a relatively thin layer of shotcrete could stabilize fragmented rock, where the absence of such a fabric was associated with damage and failure.

2.1.1 Design based on rock mass retention/ containment

The methodology of excavation stabilization based on retention /containment is considered to be a robust support design methodology, but it is critical that anchorage of the system within stable ground be achieved. The design mechanism often used in deep-level gold mines is the retention of a rock mass based on the tributary area loading of the rock bolts, and the depth of instability. The depth of instability is typically derived from historical data such as rock fall statistics. The required demand from fabric support is not considered.

Although the engineer should strive to design the support system in order to maximize the inherent strength of the rock mass structure, and thus minimize the support requirements, the support design should allow for the loss of rock mass strength around the excavation. The design methodology must therefore carefully consider the interaction of the individual components of the support system with the rock mass, and the anticipated demand on these units. To maximize the inherent rock mass strength, for optimum design considerations, the yield capacity of the anchors should be compatible with the envisaged rock mass deformation characteristics. That is, yield of the anchors must be compatible with the dilation of the rock mass between anchor points in order to minimize differential deformations. Incompatibility will result in loosening within the rock mass structure, particularly between the tendons, with resultant loss of rock mass strength. The incorporation of high quality, relatively stiff fabric support systems would result in a more even load distribution between the rock mass directly confined by the rock bolts and the potentially unstable rock mass between the rock bolt reinforcement. However, if the inherent strength of the rock mass is lost owing to the degree of rock mass discontinuity, or deformation, then increased demand on the fabric component of the support system must be considered.

The current design recommendations for tunnels in deep-level mining (DME, 1996) indicate the necessity for yielding tendons, particularly under dynamic loading conditions associated with major seismic events, to ensure sufficient energy absorption capacity. However, throughout numerous case studies, it was observed that relatively stiff re-bar rock bolts, with very limited yield capability and thus energy absorption, would survive the major dynamic deformations and damage (see Fig. 2.3).

This is due to the poor interaction between the rock bolts and the rock mass in these environments. This causes the direct loading of the rock bolts at levels far lower than anticipated by the design process. Under these conditions dynamic energy associated with the unstable rock mass is dissipated through the deformation of the rock mass contained by the relatively soft mesh and lace fabric support systems, resulting in the often observed bulking

profile of the tunnel. This bulking process between the rock bolt reinforcement, and the associated differential deformations will result in a further reduction of the rock bolt interaction with the rock mass. Thus, this mechanism, although not catered for in the design process, reduces the supporting capacity of the tunnel support system to that of its weakest component, namely the fabric. The survival of non-yielding rock bolts under dynamic loading conditions can readily be explained by this mechanism as well.

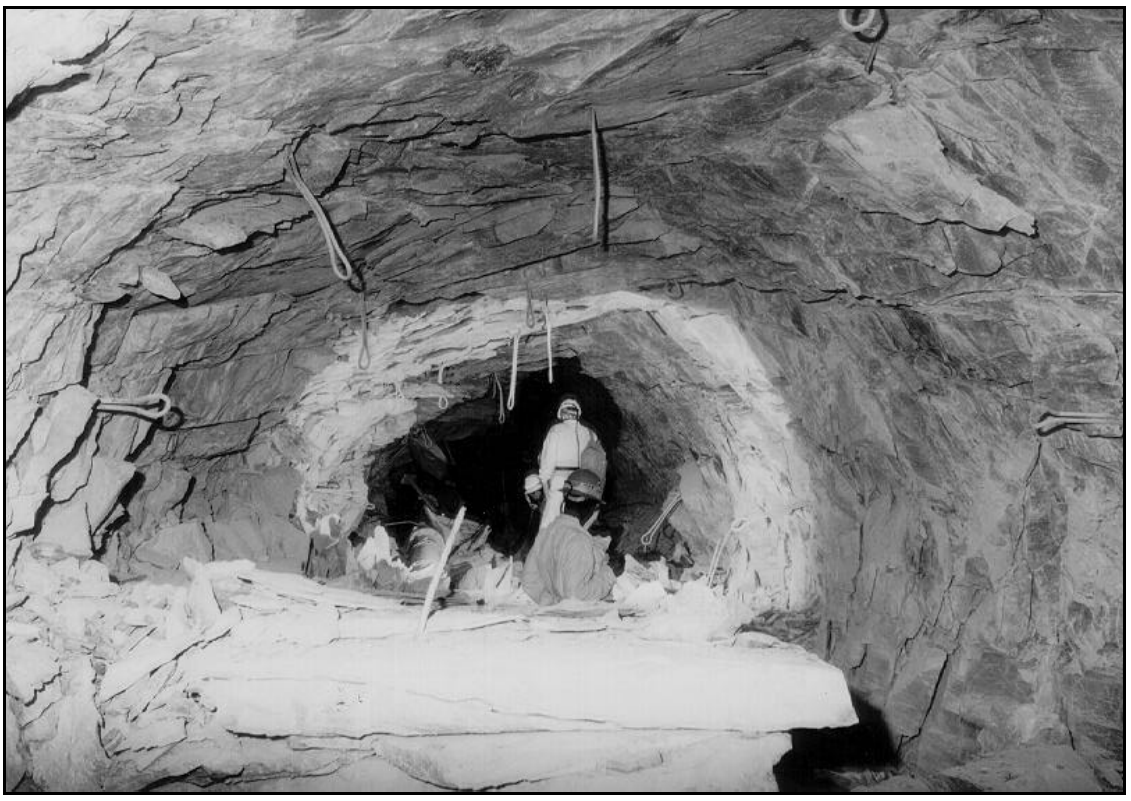

Figure 2.3. Rock mass unravelling between rock bolts (background) and rock bolt failure (foreground) (Gürtunca and Haile, 1999).

If stiffness and strength of the fabric support were increased in order to limit the deformations of the rock mass, then the distribution of loading between the fabric and the rock bolts would change. This would result in increased direct loading of the rock bolt reinforcement, which in turn might lead to failure of the rock bolt and subsequent unravelling of the support system unless yielding tendons with sufficient energy absorption capacity were used.

Of major relevance to these considerations is the nature of the fragmentation of the supported rock mass. Massive blocks can be pinned by rock tendons only and may not require additional fabric. On the other hand, rock tendons may be totally inefficient in highly fragmented rock, as

the support capacity would be limited by the capacity of the fabric in that case. At present, there is a large discrepancy between the support capacity of a typical tendon (around 100 kN) and that of a typical mesh for instance. It is evident therefore that a dominating parameter, namely fragmentation of fractured/failed rock, is not taken into account in current design considerations. Although it is inherently assumed that the rock mass is capable of distributing the tendon forces according to tributary area theory, this assumption is generally invalid. The effect of the associated forces on the potential for disintegration of the rock mass itself is not considered at all. As can be observed from most of the case studies, rock mass disintegration and unravelling is a very real and serious problem, which renders current design methodologies quite unrealistic.

The most recent tunnel support design system, developed in projects GAP 335 and GAP 035, recommends the following main considerations with regard to the design of tunnel support systems in deep-level mining environments:

- The extent of natural rock mass instability, under conditions of quasi-static and dynamic stress fracturing, can be estimated in the proposed design analysis.

- The dilation rates for the reinforced and un-reinforced rock mass can be estimated, as a function of the anticipated stress change over the life of the excavation. Analysis of the deformation mechanisms has indicated the importance of the consideration of shear deformation within the rock mass, particularly in the hangingwall under conditions of a vertical stress reduction.

- The extent of interaction of the rock bolts within the defined rock mass structure and loading environment can be estimated, and is dependent on the orientation of the discontinuities.

- The extent of the potentially unstable rock mass volume between the rock bolt reinforcement can be estimated under static and dynamic loading conditions and hence the demand on the fabric support.

- The load-deformation characteristics of the fabric support system influences the extent of interaction between rock bolt units and energy absorption capability of the rock mass itself. Consideration of the interaction between the fabric support and the rock bolt units is an important aspect of the support system design that ensures compatibility of the components of that support system.

2.1.2 Summary

Observations of the performance of tunnel support systems under rockburst conditions have allowed a mechanistic evaluation of support behaviour. Of significance for the improved design of support systems under rockburst conditions are the following:

- The depth of instability (fracture zone) of the rock mass around the excavation under dynamic loading conditions can be estimated from empirical data and conceptual models based on *in situ* strength-stress ratios.

- Consideration should be given to the loading of the fabric support due to the unstable rock mass between the rock bolt reinforcement and the influence of the characteristics of the fabric support. An important parameter in this respect is the fragmentation of the rock mass. Intense fragmentation typically directs the unstable rock mass towards the fabric, resulting in an ineffective support system in which the tendons are hardly activated. (The support resistance of typical fabric is significantly less than that of typical tendons).

- The fragmentation of the rock mass and the orientation and location of discontinuities is also an important parameter affecting the interaction of the rock bolt reinforcement with the unstable rock mass volume. In addition, the yielding capacity, and even strength, of typical bolts may in practice also be severely reduced due to various factors; corrosion in cracked rock for instance may cause local weakening, while bonding forces may be larger than anticipated, so that critical bond length and hence yielding length is reduced.

- The shear demand and capacity of the rock bolt reinforcement should be considered, particularly in the hangingwall of the tunnel. Of importance here is the presence and behavior of bedding planes especially when changes in field stresses are anticipated.

- Consideration should be given to the location of seismically active structures; most of the violent rockburst damage was observed in the immediate proximity of major dykes or faults. The relative position of stopes should also be considered, as the associated stress concentrations could affect tunnel stability.

2.2 Design considerations

In order to consider the influence of repeated dynamic loading on the performance of a support system for design purposes, estimation must be made of the demand on, and the capacity of the support system.

2.2.1 Repeated dynamic demand on the support system

The critical parameters with respect to support system performance are deformation capacity and support resistance. Both quasi-static and dynamic loading can be expected to play a role in deep-level mining environments. The loading history and the associated deformation history of a support system must be considered in order to determine current support capacity. Time dependent behaviour and stress changes associated with mining will induce deformations into the support system and thus reduce the remaining deformation capacity. The anticipated or historic demand on the support system may be evaluated on the basis of the seismicity, the mining-induced stress changes and possible time effects to which the excavation is exposed over its life. Repeated dynamic loading, the subject of this study, is directly linked to seismicity and the effects of seismic events. While it is impossible to quantify exactly the associated movements, certain relationships between magnitude, relative location and induced movements and associated forces exist. It is possible to qualify the potential for seismic excitation on the basis of seismic history and relative location. The level of static stress obviously plays an important role as well, as the dynamic stresses will be superimposed on the former.

2.2.2 Capacity of the support systems

Stacey and Ortlepp (1997) carried out impact tests on panels of containment support 1.6 m x 1.6 m suspended on a $1\,m^2$ rock bolt pattern with and without lacing. In total, 56 tests were carried out representing combinations of different types of wire mesh, wire rope lacing, and fibre reinforced shotcrete. The simulated rock mass comprised concrete blocks stacked within the defined rock bolt pattern in the geometry of a pyramid. The system was loaded dynamically by means of a drop weight from which the kinetic energy imparted to the system could be defined. The fabric support systems were evaluated on the basis of deformations associated with impacts of known kinetic energy. The maximum (accumulated) kinetic energy, which a system could sustain prior to substantial loss of fabric integrity, can be obtained from their results. Figure 2.4 shows the data set from their work.

Although Stacey and Ortlepp (1997) did not consider trendlines to be appropriate, they are used here to illustrate the concept that a support system may have a critical kinetic energy below which the support system can absorb the impact energy elastically and thus recover any deformation. Thus in Figure 2.4 the intersection of such a trendline with the y-axis would represent the critical kinetic energy level for zero deflection. Thus, for a given volume of unstable rock mass interacting with the support system, a critical impact velocity may be defined, below which no permanent damage to the support system will be sustained. Clearly noticeable is the influence of the lacing in this respect; only the presence of lacing seems to

lead to a measurable critical kinetic energy magnitude (i.e. velocity). The absence of lacing appears to result in negligible critical energy levels, or, in other words, even extremely small impact energy levels would lead to ultimate failure in the absence of lacing.

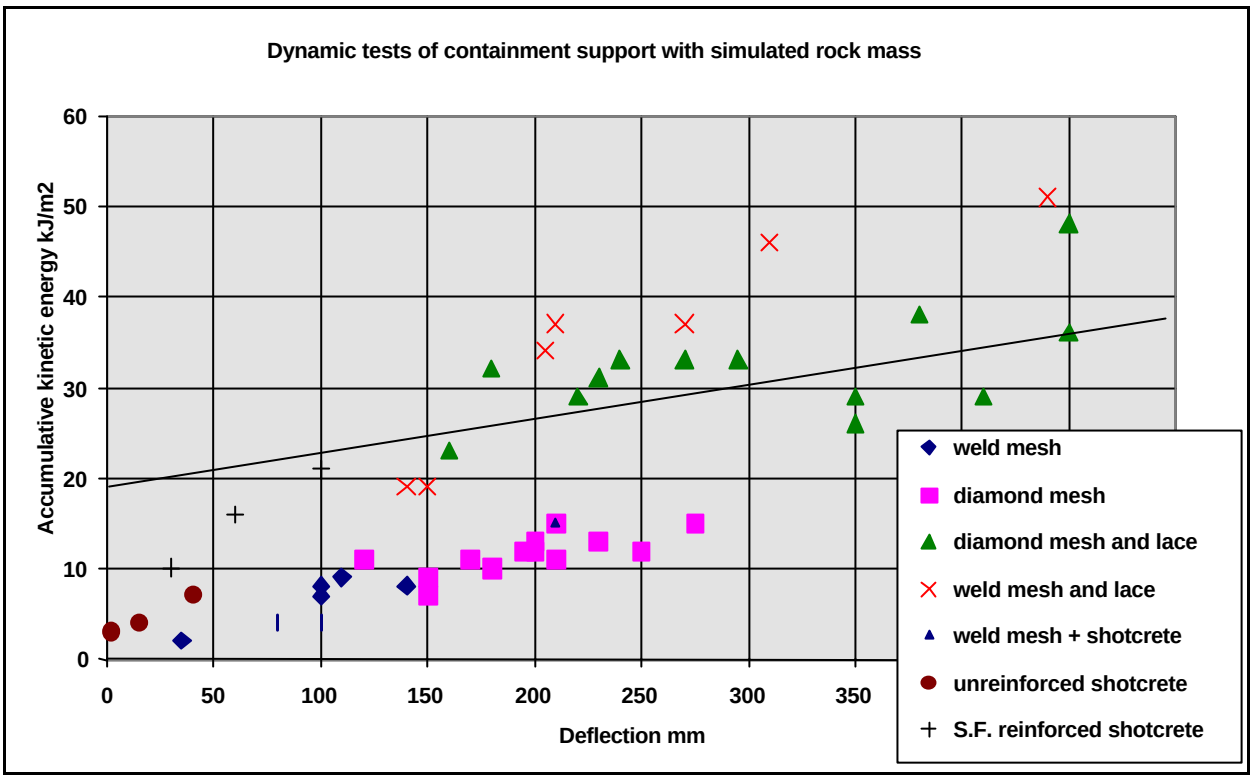

Figure 2.4. Relationship between accumulated impact kinetic energy and deformation for contained simulated rock mass system (Stacey and Ortlepp, 1997).

In this laboratory testing programme the kinetic energy, in addition to the constant gravitational loading of the fabric support, was imparted by a drop weight. *In-situ*, it would be the weight of unstable rock mass that would be accelerated to a maximum velocity (the peak particle velocity or PPV), from which the kinetic energy would be determined in a typical design process.

The relationship between deflection and kinetic energy in Figure 2.4 may be suitably represented by a linear fit of a trendline. However, it should be noted that the kinetic energy is represented by cumulative values, which could either be obtained by a small number of large impacts, or a large number of small impacts. The impact magnitude is not explicitly considered here, although this parameter can be expected to affect results substantially. In addition, it should be emphasized that the last data point within a series does not necessarily represent the failure of the system, but merely the end of a test.

Haile (1999) conducted a series of *in situ* tests on typical mesh and lacing configurations, which were directly loaded by static forces. Some of these configurations are similar to those tested by Stacey and Ortlepp (1997). If the results of these *in situ* tests and the impact tests are compared, substantial differences in energy absorption capacity can be observed. While the different boundary conditions in both situations may explain some of this difference, it is assumed that the bulk of the difference is associated with energy absorption within the rock mass structure. In the laboratory tests, this energy absorption can take place in the form of frictional resistance between blocks and the crushing of blocks.

3 Physical evaluation

3.1 Drop test rig

3.1.1 Introduction

The drop test rig, which was used for this project, was originally designed and used by SRK Consulting for impact testing on shotcrete panels. The test rig consists of a crane, which pivots around a central column and is guided in a circular track. A special foundation had to be constructed in order to support the central column, the guiding track and anchoring points for the pre-stressed lacing. A hook with a mechanical release mechanism is used to lift and release the1 ton impact weight. The lifting mechanism itself is powered by hydraulics and the hook is suspended from rails along the horizontal beam connecting the central column with the two other columns in the guiding track. This structure allows the hook to be positioned anywhere within the area enclosed by the circular track (see Figs.3.1 a and b)

3.1.2 Description of changes

In order to allow a realistic comparison between the case in which no fabric support was used and the various support systems, it was decided to redesign the test rig in such a way that the rock mass itself could also be represented. This required a substantial modification, enabling the interaction between a simulated rock mass and a tunnel support system to be analysed under repeated impact loading conditions. The interaction between the rock mass and the support system is of ultimate relevance. Testing the support system by itself might not provide a correct estimate of the practical support performance of an entire support system, as the contribution of the rock mass in resisting deformations and unravelling would be completely ignored in that case.

a

b

Figures 3.1 a and b. General views of the main test rig.

The rock mass in these tests was represented by a volume of relatively hard bricks which were suspended by 20 mm bolts from, and confined at the bottom layer by, a reinforcing frame. For this purpose special interlocking pavement bricks were selected which could be joined into a competent assembly. The resultant simulated rock mass structure was one in which the weakest discontinuity planes (those separating layers of brick) were normal to the applied impact load. When typical fracture patterns around a tunnel are considered, the laboratory set-up closely simulates vertical loading of the hangingwall or horizontal loading of the sidewall. A temporary support structure was used to assemble the bricks around four tendons inside the confining frame. Upon completion, the tendons were tensioned and confinement was applied by the confining frame, so that the supporting frame could be removed. This situation is sketched in Figure 3.2.

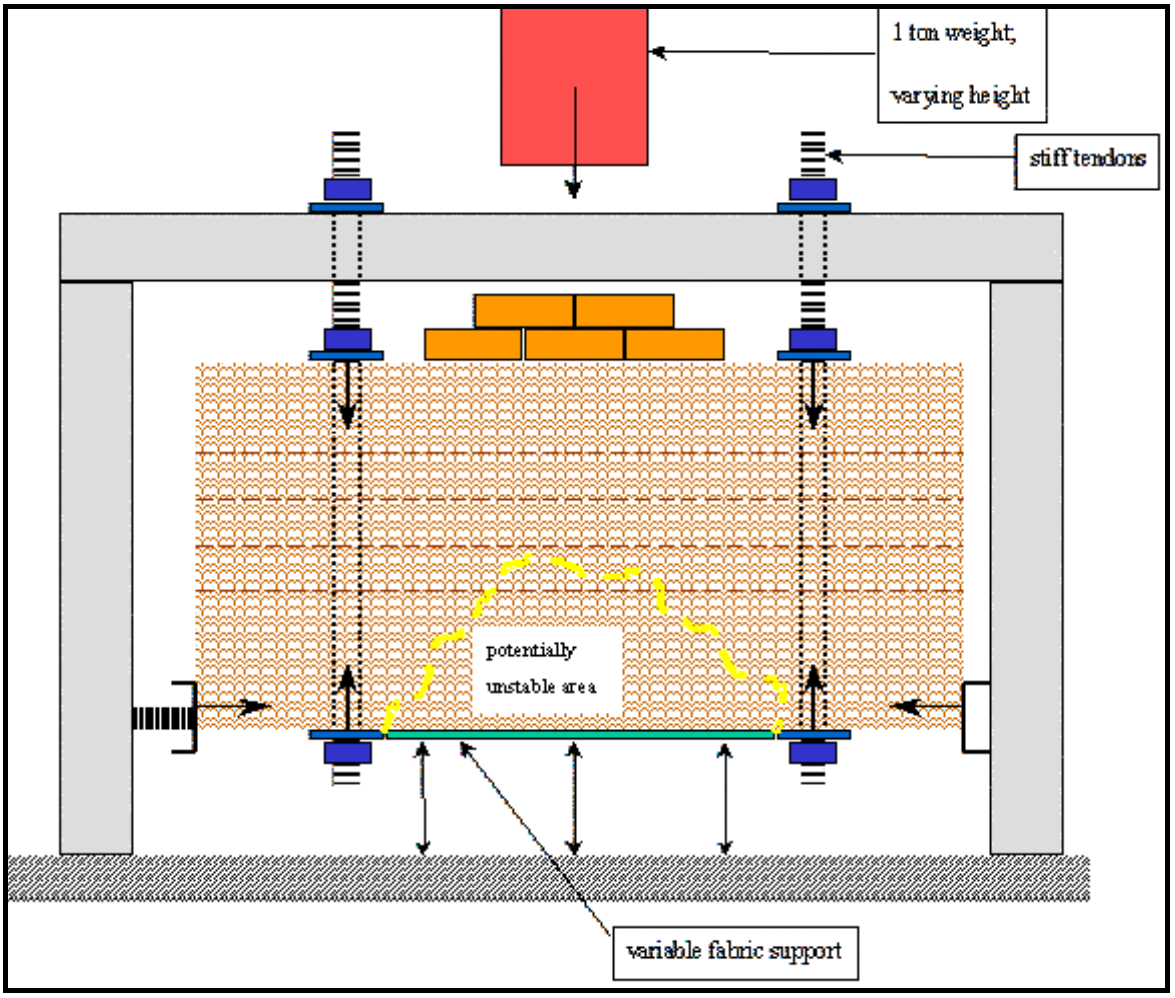

Figure 3.2. Sketch of the test frame with artificial rock mass and support system.

By dropping a mass of 1 ton from various heights, dynamic loading of the system was simulated. The impact energy was too small to cause failure or yielding of the tendons, but the brick size was sufficiently small to allow bulging of the "brick mass" in between the tendons. This deformation mechanism could lead to the fall-out of individual bricks and ultimately the total disintegration of the brick assembly.

The actual response of the system is strongly influenced by the presence of a support fabric, which fulfils a containing function. The magnitude of the impacts obviously plays an important role as well, while the accumulation of absorbed energy from a number of impacts is another crucial parameter. Each test was executed by dropping the mass from a fixed height, until the brick assembly was deemed to have failed. The drop height was constant during each test in order to maintain consistency. As the effect of an impact is not linearly related to its magnitude, variations in magnitude, during a test on an individual specimen, might result in non-linear

responses, which might be difficult to interpret. Therefore, different drop heights were used in different tests, so that the effect of the impact magnitude could be evaluated independently.

The artificial rock mass consisted of layers of interlocking concrete bricks, tightly packed in a volume of approximately 2 m X 1.5 m X 1.0 m (see Fig. 3.2). All tests were carried out until the unstable area (see Fig. 3.2) became dislodged.

In the current project, not only shotcrete was evaluated for its potential as fabric support, but also a membrane support (Evermine) and steel lacing. The unsupported situation was also tested and analysed in order to determine the reinforcing effect of a support system on the rock mass.

3.1.3 Tests performed

In total eleven drop tests were performed. Each of these tests required a complete reassembly of the artificial rock mass and the support system, which was a time consuming process. In order to obtain consistent results, the drop height during each individual test was maintained constant. Only two different drop heights were used, namely 10 cm and 50 cm. The smaller value was used for those fabrics which were assumed to be weak, while the greater drop height was used mainly for the shotcrete. The brick assembly consisted of nine layers, generating a height of approximately 1 m. Horizontal confinement was applied to the bottom layer through beams which were jacked against the testing frame. 20 mm bolts were used to push the beams from the testing frame against the bottom layer. The 20 mm tendons, which supported the brick assembly, were also pre-stressed so that vertical confinement of the assembly was induced as well. While the total length of the test specimens was approximately 2 m and their width about 1.5 m, the spacing between the tendons was approximately 1.5 m in one direction and 1.0 m in the other direction. The top layer of bricks was confined by pre-stressed strapping. The impact mass was dropped on a steel plate resting on a pyramid of concrete blocks. This concrete block structure effectively served as a load spreading device.

Three tests were performed without any fabric support, in order to obtain a datum value for the strength and deformation characteristics of the simulated rock mass itself. The only resistance against the impact in these tests was provided by the nominal confinement induced by the testing frame and the tendons. A drop height of 10 cm was used for two of these tests, while a drop height of 50 cm was used for the third.

The eight remaining tests were performed with varying support combinations. For fabric support, a structural membrane (Evermine) and fibre reinforced shotcrete were used. Evermine was sprayed onto the bottom layer of bricks while it was assembled in the testing frame. The

thickness of the Evermine layers was approximately 5 mm on average. Shotcrete panels were prepared separately in a special frame which could support a layer of bricks. Shotcrete was sprayed onto the layer of bricks in that frame and after a curing period of at least 48 hours, the shotcreted layer was placed in the testing frame and the other brick layers were placed on top of it. The shotcrete layers were on average 100 mm thick, although relatively large variations in thickness could be observed. Lacing was placed across the testing specimen (see Fig. 3.3) in such a way that it spanned diagonally from one tendon to the other. The lacing was pre-stressed and simultaneously pulled tight against the bottom of the testing rig by the use of special columns, anchoring points and tensioning devices. The following tests were conducted in chronological order:

1. Evermine and lacing; drop height 10 cm.
2. Evermine and lacing; drop height 50 cm.
3. Evermine; drop height 10 cm.
4. Lacing; drop height 10 cm.
5. No fabric support; drop height 10 cm.
6. No fabric support; drop height 10 cm.
7. No fabric support; drop height 50 cm.
8. Shotcrete; drop height 50 cm.
9. Shotcrete and lacing; drop height 50 cm.
10. Shotcrete and lacing; drop height 50 cm.
11. Shotcrete; drop height 50 cm.

In test 1, the bottom layer of bricks was flush with the confining beams and the testing frame. In this case the lacing was therefore in direct contact with the specimen from the first impact onwards. In the subsequent tests, the bottom layer of bricks was placed higher in the frame in order to maintain confinement and increasingly displaced downward during subsequent impacts. As a consequence, an initial gap between the lacing and the bottom layer was created in the remaining tests.

In test 6 and test 7 the monitoring frame with the telescopic bars was not placed against the brick assembly during any of the impacts. As it appeared that this frame affected the results in test 5, it was decided not to monitor during the impacts, but only afterwards.

3.1.4 Results

The deformations were measured with the assistance of a special monitoring frame, containing nine telescopic bars. These bars were positioned in a vertical direction, in touch with nine specific locations along the bottom of the assembly. After each impact, both the maximum and the permanent deformation of each individual bar were recorded. The difference between maximum and permanent deformation is representative of dynamic elastic behaviour, while the permanent deformations obviously represent inelastic behaviour.

In addition to these deformations, the peak particle velocities (PPVs) were monitored along the bottom of the testing assembly. The PPVs generated by repeated dynamic loading were thus measured on the skin of the simulated tunnel support rock mass system. A ground motion monitor (GMM) with eight geophones was used in this experiment. The position of the geophones with respect to the support is shown in Figure 3.3.

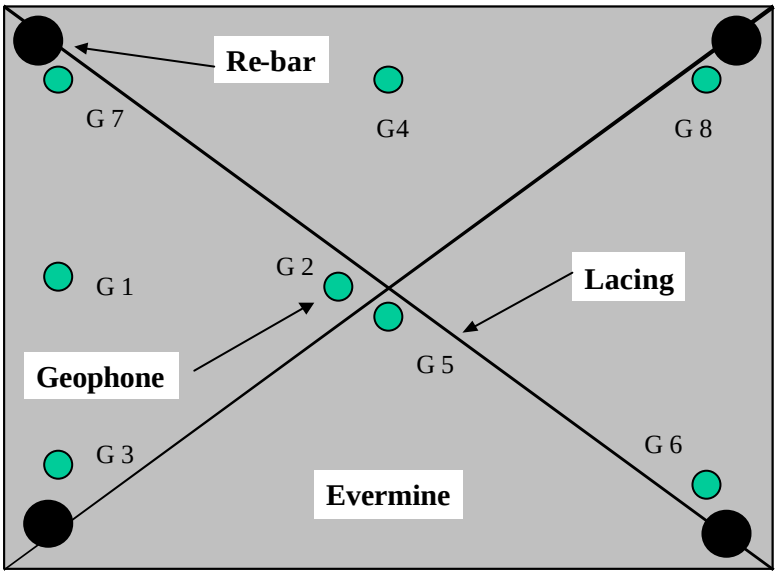

Figure 3.3. Plan view illustrating the position of various geophones at the bottom of an assembly supported with Evermine and lacing.

To improve the dynamic range of the recording system some of the geophones were over-damped with external resistors.

Three stages of rock mass behaviour are clearly identified in Figure 3.4. The first stage, drops 1 to 10, is associated with the initial compaction of the bricks used to build the sample. During this stage, the PPVs recorded in the middle of the sample (G2) are higher than the PPVs recorded in the periphery (G1 and G4). This stage is also characterized by minor or almost no damage. The second stage, drops 11 to 28, is associated with the post-compacted period

where damage of the sample begins to occur. The PPVs at all geophones during this stage are more consistent. There is no evidence of lacing yield during this stage. The third stage, drops 29 and above, is characterized by extensive cumulative damage, which spreads outward from the centre of the sample towards geophone G4 where PPVs are significantly higher. The effect of lacing support during this stage is demonstrated by the lower PPVs recorded at geophone G 2, which is located very close to the lacing intersection. The increased velocities at G4 can be associated which increased damage and a limited support influence. The general variations in the PPVs shown in Figure 3.4 ranged from 200 to 600 mm/s. This compares to impact velocities of 1400 mm/s for this particular experiment.

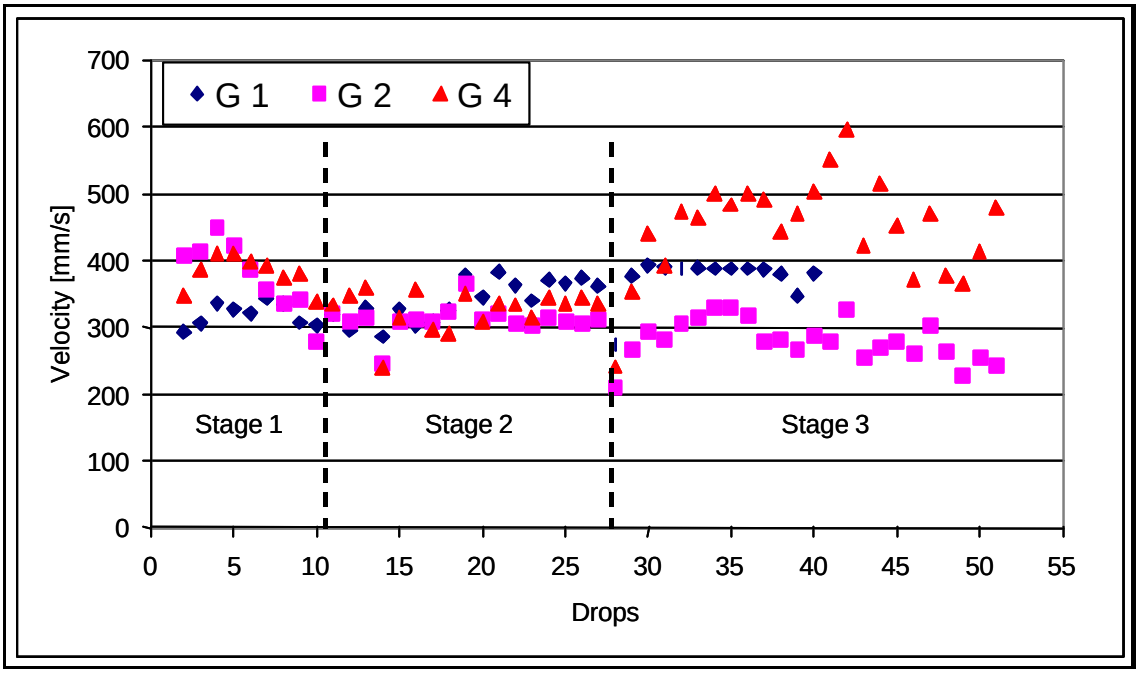

Figure 3.4. Peak particle velocities measured on the surface of the sample with Evermine and lacing.

3.1.5 Discussion of the results and Conclusions

The test results provide a relatively realistic reflection of the interaction between a tunnel support system and a rock mass subjected to (impact) loading. The fact that this interaction can now be quantified renders these tests valuable from a practical point of view. While the vast majority of results can be explained in a very logical manner, they could definitely not have been predicted in any detail. The test results thus allow a quantitative evaluation of the effectiveness of various fabrics.

In the drop test rig, the tendons can be assumed to be rigid for all practical purposes. During the impact, a certain percentage of the impact energy is used to mobilize boundaries between individual bricks and to accelerate a potentially unstable region of bricks. Parameters subject to variation may be the shear and normal stiffness and the frictional resistance across the brick interfaces. Increasing deformations and associated damage can be expected to affect these parameters in particular. In addition, support resistance may change with increasing deformation, while the difference between various support systems should be reflected in the actual support resistance provided.

The effect of support and fracturing on the PPVs was clearly illustrated in Figure 3.4, where less supported areas remote from the support were associated with higher PPVs in a fractured environment. Similar behaviour was measured underground during the simulated rock burst experiment (SIMRAC project GAP 530). The results from these measurements are shown in Figure 3.5.

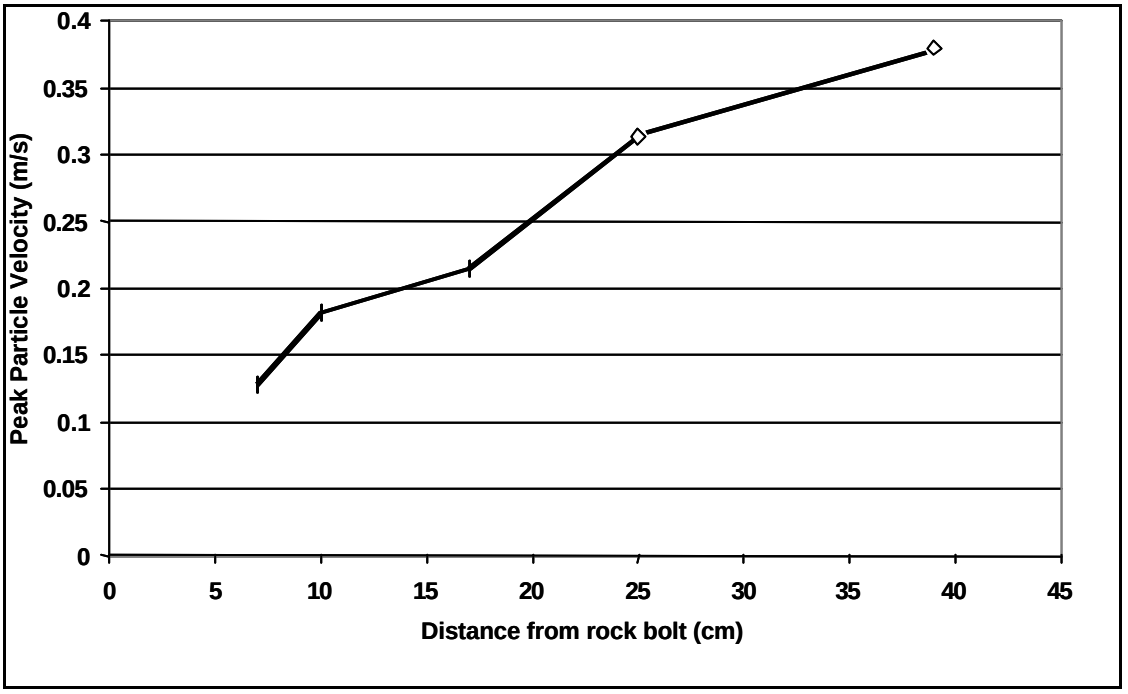

Figure 3.5. In situ relationship between PPVs and distance from a rock bolt reinforcement unit (Haile and Le Bron, 2001).

The general trend of increased PPVs with increased distance from the rock bolt reinforcement is clearly illustrated. This trend is in accordance with measurements at other tunnel sites (Haile *et al.*, 1998) under conditions of natural seismic events.

Figures 3.6 and 3.7 show the results of all impact tests performed, for 10 cm and 50 cm drop height respectively.

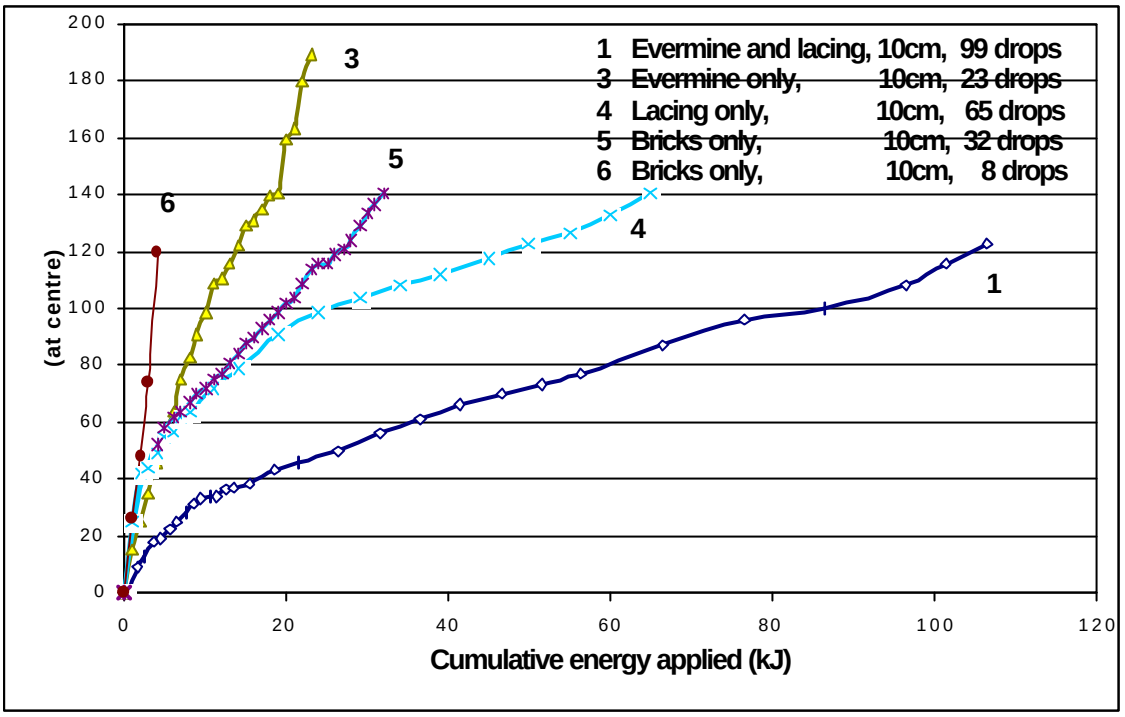

Figure 3.6. Results for 10 cm drops for various fabric supports (1 kJ per drop).

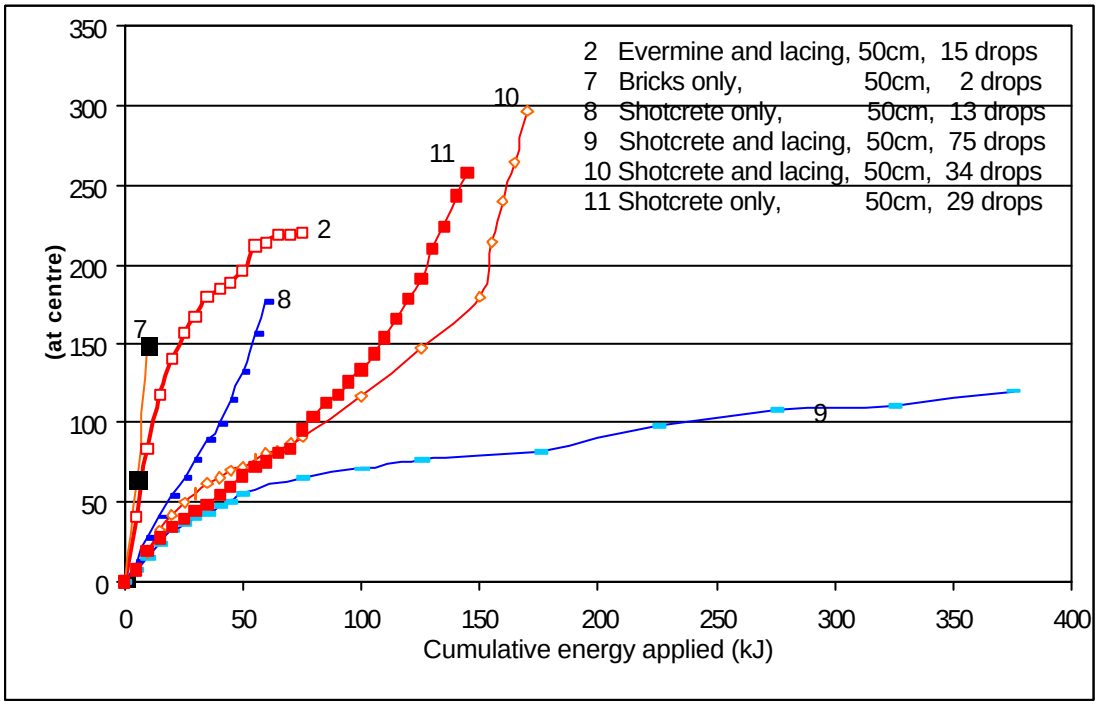

Figure 3.7. Results for 50 cm drops for various fabric supports (5 kJ per drop).

The termination of each test does not necessarily coincide with total specimen failure. In fact most of the tests resulted in the fall-out of a limited area only. Damage was often difficult to quantify, especially in those tests in which lacing was used. In these tests, the removal of lacing typically led to massive additional fall-out, which could not be anticipated correctly. Even the displacement monitoring frame, with its telescopic bars, appeared to have a considerable influence on stability in the absence of any fabric support. Removal of the frame also led to additional fall-out. The amount of damage or the degree of instability at the termination of each test is therefore not equivalent for all tests. However, it can be stated that all specimens were subjected to damage which would be far in excess of any acceptable standard.

The conclusions based on the impact tests can be summarized as follows (see also Figs. 3.6 and 3.7):

- Deformations accumulate with the number of impacts.
- The magnitude of accumulated deformation controls the stability of individual fragments (bricks in this case).
- The maximum deformation before failure is increased by the use of a structural membrane (Evermine in this case) or shotcrete.
- The magnitude of accumulated deformation is strongly reduced by the presence of lacing and/or shotcrete; the system stiffness increases noticeably, even in response to a relatively small lacing force.
- The use of fibre reinforced shotcrete of approximately 100 mm thickness resulted in a substantial improvement in energy absorption capacity (Note: a lack of manufacturing control of shotcrete thickness led to considerable performance differences between individual shotcrete panels).
- The best performance could be obtained with a combination of shotcrete and lacing; large fragments of shotcrete, which stabilize the small fragments (bricks), remain stabilized by the lacing, even when subjected to very large deformations.
- A large drop height has more influence on deformation than a number of small drop heights with equivalent total impact energy.

Lacing only becomes activated once sufficient deformation has been induced into the lacing. While the lacing was pre-stressed in all the tests, this is not likely to have a significant effect, as the lacing first has to assume a curved shape in order to provide effective support pressure.

Failure of the lacing did occur in test 10 (shotcrete and lacing) at deformations in excess of 200 mm. It is of interest to note that in test 2 (Evermine and lacing) the lacing did not fail at similar deformations, although the specimen itself was assumed to have failed due to excessive brick fall-out. Owing to the geometry of the testing frame, there was an initial gap between the lacing and the bottom surface of the specimen. Variations in this gap resulted in variations in lacing response; i.e. a larger gap required more deformation in order to activate the lacing. The difference in results from tests 1 and 4 can be explained by the difference in the initial gap of around 50 mm.

Variations in results from the different shotcrete tests can partly be attributed to variations in panel thickness. Although care was taken to construct panels of uniform and constant shotcrete thickness, relatively large variations in both the average panel thickness as well as local thickness could be noticed. Each shotcrete panel consisted of a single layer of bricks, which was sprayed with shotcrete on one side. The panels were manufactured in a special mould, but their relatively large size created some practical difficulties, which may have accounted for the inconsistencies.

The assembly of bricks in the testing frame was not supposed to be subject to variation. However, it should be appreciated that the results are probably very sensitive to the interface stiffness and frictional resistance. Therefore, small variations in interface conditions between individual bricks may also have affected the results to a certain extent.

The differences between test 5 and test 6, in which unsupported bricks were tested, is explained by the influence of the displacement monitoring frame. As no elastic rebound took place in test 5, the telescopic monitoring bars remained in continuous contact with the bottom layer of bricks after every impact. Removal of the monitoring frame at the end of test 5 resulted in a substantial additional fall-out. It was decided to detach the monitoring frame from the test specimen during the impacts in a similar test. In test 6 the displacement was measured after each impact and the telescopic bars did not affect the deformations. While the effect of the monitoring frame was intentionally minimized, it is possible that the combined resistance of the nine telescopic bars may be as much as 1 kN. Such a small force can apparently affect the results to a large extent in the absence of any support resistance. Test 7 was conducted in a similar fashion as test 6, namely with a detached monitoring frame. Due to the larger impacts only two drops could be accommodated by this particular specimen.

The effect of a structural coating is difficult to evaluate in a test like this. The support resistance of such a coating is relatively small and its effect is mainly to prevent individual blocks from dislodging. Test 3 shows that a support consisting of Evermine does not reduce overall

deformations, but it does enable larger deformations to occur before failure is deemed to have taken place. Compared with fibre reinforced shotcrete, it is clear that the support system consisting of Evermine and lacing (test 2) lacks initial stiffness, although its final performance is similar to that of shotcrete without lacing (tests 8 and 11). Another consideration in this respect is the effect of ejected blocks on the entire system. While a structural membrane may prevent individual blocks from being ejected, more energy will be contained within the system than if the blocks had been ejected. This may explain the difference between test 3 and test 5. In test 3 more impact energy is absorbed by the system as no blocks are dislodged, while the results of test 5 reflect a reduction in impact energy, which is effectively dissipated by ejected blocks.

It is difficult to estimate the critical minimum energy below which no damage is induced to the support system. Permanent deformations and associated damage appear to occur in all tests, from the first drop onwards. The minimum impact used in these tests is 1 kJ and it is therefore concluded that the critical minimum energy must be less than this. It is possible that the shotcrete panels might not have been damaged by 1 kJ impacts; however this was unfortunately not assessed.

The critical deformation for assemblies without fabric support is approximately 150 mm, while Evermine and shotcrete allow deformations of more than 200 mm. Both shotcrete and lacing increase the stiffness of the system. Although large variations, associated with differences in individual test specimens, were observed, these trends are obvious. Without support, stiffness ranges from 0.04 kJ/mm to 0.33 kJ/mm. Results with Evermine show a stiffness of 0.12 kJ/mm, shotcrete increases the stiffness to values between 0.43 kJ/mm and 0.80 kJ/mm. Lacing leads to stiffness values which range from 0.9 kJ/mm to 1 kJ/mm, while the combined effects of lacing and shotcrete result in a stiffness ranging from 0.8 kJ/mm to 5.4 kJ/mm. By comparison, a single tendon which is stressed to 20 tons, would only show a theoretical stiffness of 0.2 kJ/mm. In this respect it should be recalled that only a small portion of the impact may have to be absorbed by inelastic deformations in the fabric support, and actual stiffness values are thus proportionally smaller. The above evaluation therefore only serves to identify relative changes between different types of support.

3.2 Laboratory evaluations

3.2.1 Introduction / Methodology

In order to evaluate individual components of typical tunnel support systems, a laboratory testing programme involving repeated loading was designed. The purpose of this testing

programme was to determine the contribution of each component with respect to strength, stiffness and yielding capacity.

3.2.2 Tests performed

3.2.2.1 Tendons

Initial laboratory work was carried out in the Terra-Tek rapid loading machine (see Fig. 3.8), in order to establish the effect of repeated loading on individual support units. Two types of loading were used, namely quasi-static and cyclic dynamic loading on three different types of rock tendons. Re-bar, smooth bar and wire cable specimens were stretched until failure (see Fig 3.9.). These tendons were anchored by clamping jaws, spaced at 1 m, so that an effective tendon length of 1 m was obtained. Varying loading rates from 1 mm/sec to 20 mm/sec were used and the results are presented here. Note that the tendons were not grouted and that the loading velocities were relatively low when compared to expected maximum rockburst velocities. However, these velocities are within the range of commonly measured PPVs.

Deformation curves for the re-bar show that the yield range and the peak loads are very similar in all tests (see Fig 3.10). A stiffer elastic response can be observed with the 20 mm pulse loading, something which is not evident with the 10 mm pulse. The indicated yield range associated with the pulse loading may be larger than the actual yielding range. As the forced deformations related to the final pulse were recorded in total, the exact deformation at which failure occured during this last pulse may not be reflected. The actual yield range is obviously limited by the deformation at which failure takes place.

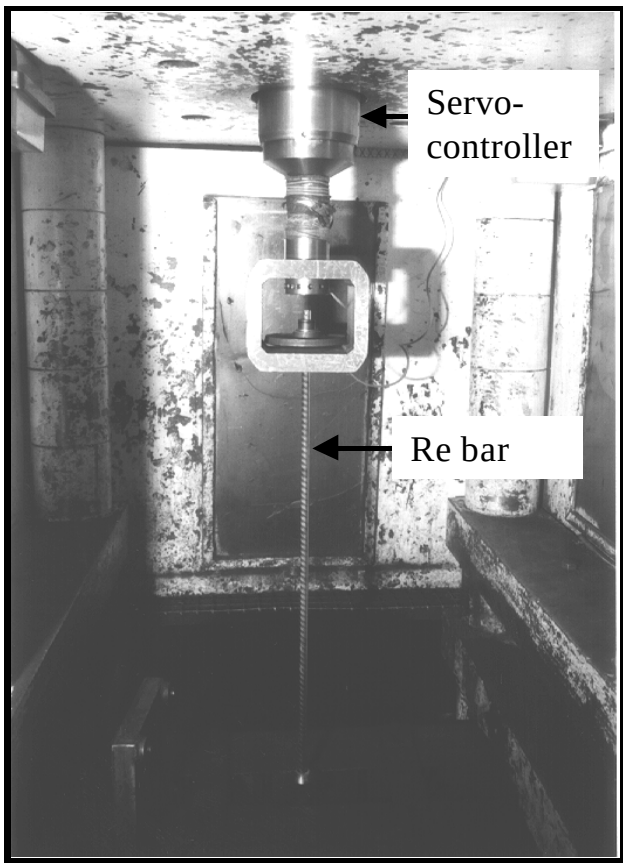

Figure 3.8. Servo controller with 2000 kN capacity.

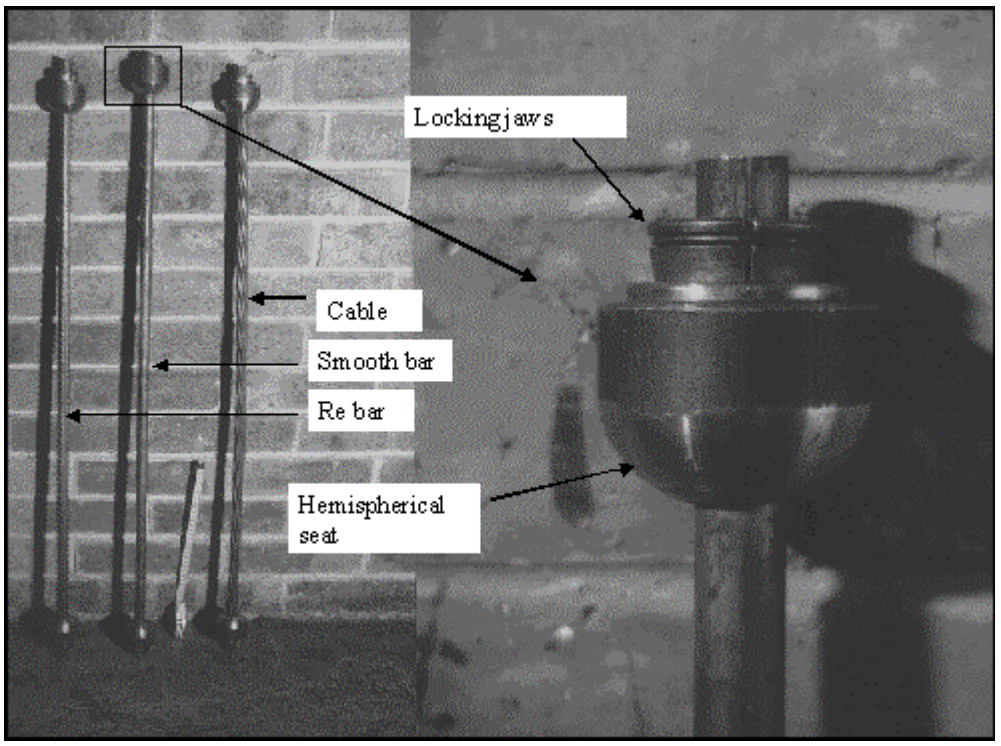

Figure 3.9. Various types of elements to be tested and mechanism of locking jaw.

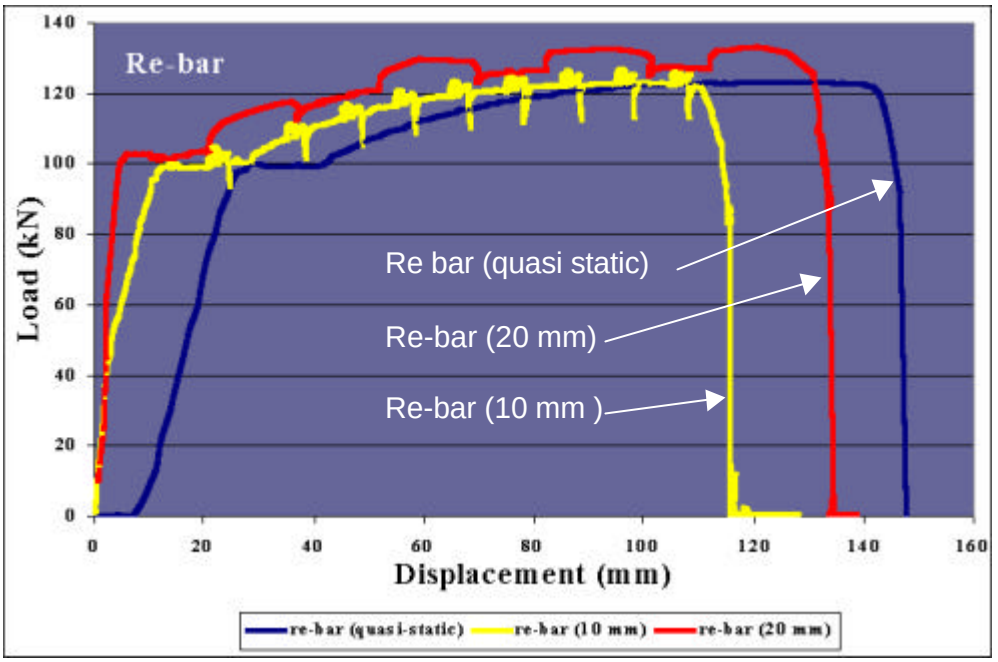

Figure 3.10. An example of re-bar testing results

Figure 3.11 shows an example of various deformation curves for smooth bar, the graph indicates an almost similar response for all loading conditions. No effect of pulse loading can be observed from these results. The final failure of both support units is controlled by necking, which results in a planar surface in the smooth bar and a more irregular surface in the re-bar (see Fig. 3.12). The maximum elongation of the re-bar was approximately 15 per cent while the maximum elongation of smooth bar was approximately 20 per cent. These values represent a considerable yielding range and hence energy absorption capability. It was observed that yielding occurred over the full tendon length of all specimens, as a considerable reduction in diameter was evident at the end of each test. It is clear that this yielding range is directly associated with the mechanical properties of the steel used in these tendons. The choice of an appropriate steel is therefore crucial to the performance of tendons, especially in rock burst conditions. It is highly recommended that this issue be thoroughly investigated in order to design more efficient rock tendons.

The re-bar has a 20 per cent higher strength than the smooth bar. However, because of a smaller yielding range, the energy absorption capacity of re-bar is slightly less than that of smooth bar (see Figs. 3.15 and 3.16).

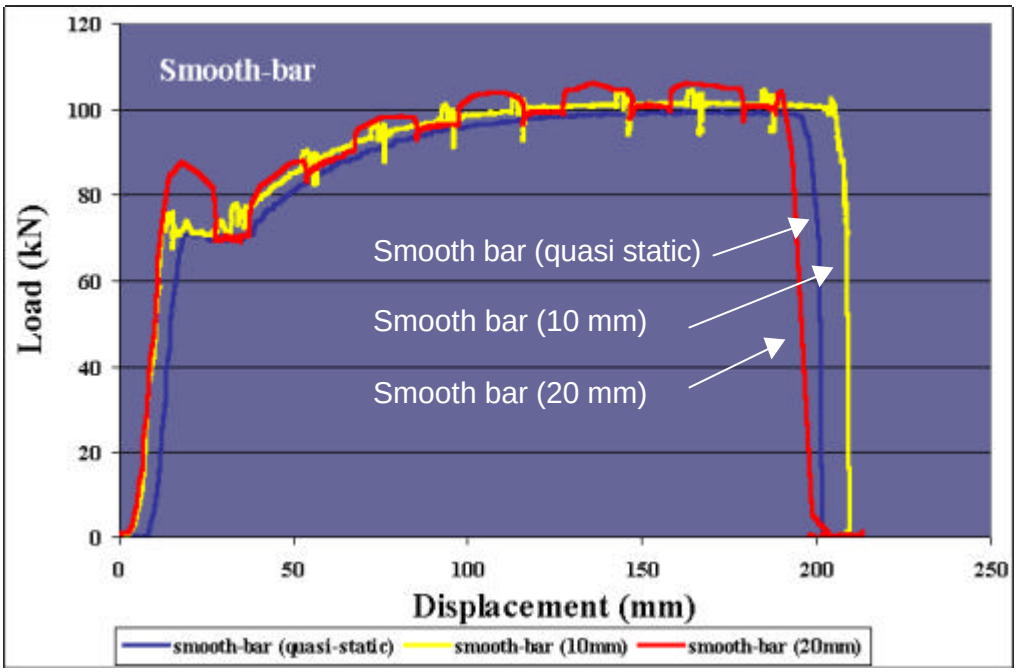

Figure 3.11. Deformation curve of the smooth bar.

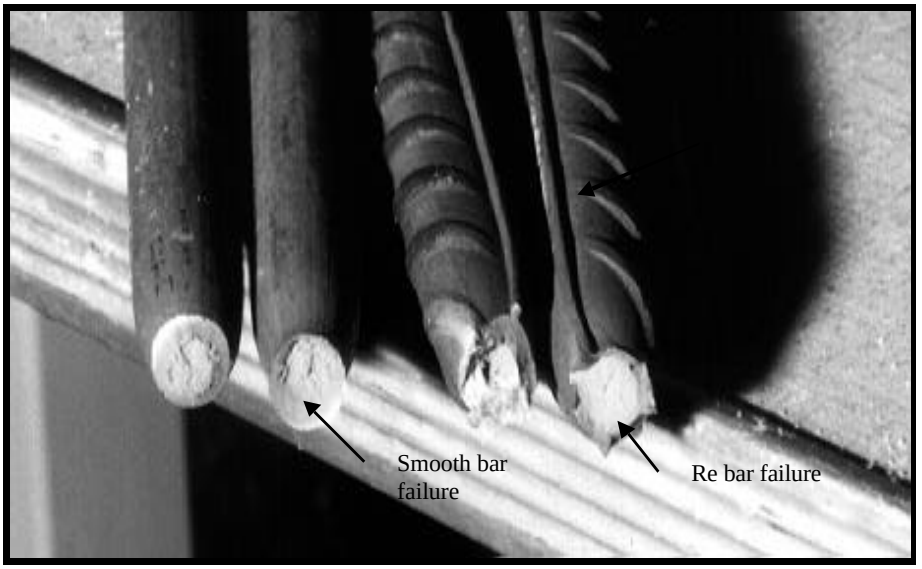

Figure 3.12. Failure mechanisms of smooth and re-bars.

Results from tension tests on wire cable do not demonstrate an effect of the type of loading applied either (see Fig. 3.13). The failure mechanism of the cable is associated with consecutive failure of individual strands of wire (see Fig. 3.14). This type of failure is induced by the clamping jaws, which effectively cut the strands at the circumference of the cable. The yielding range of the wire cable is noticeably less than that of the re-bar and smooth bar. Although this is most likely associated with the cutting effects of the jaws, it may nevertheless be quite representative of underground conditions as well.

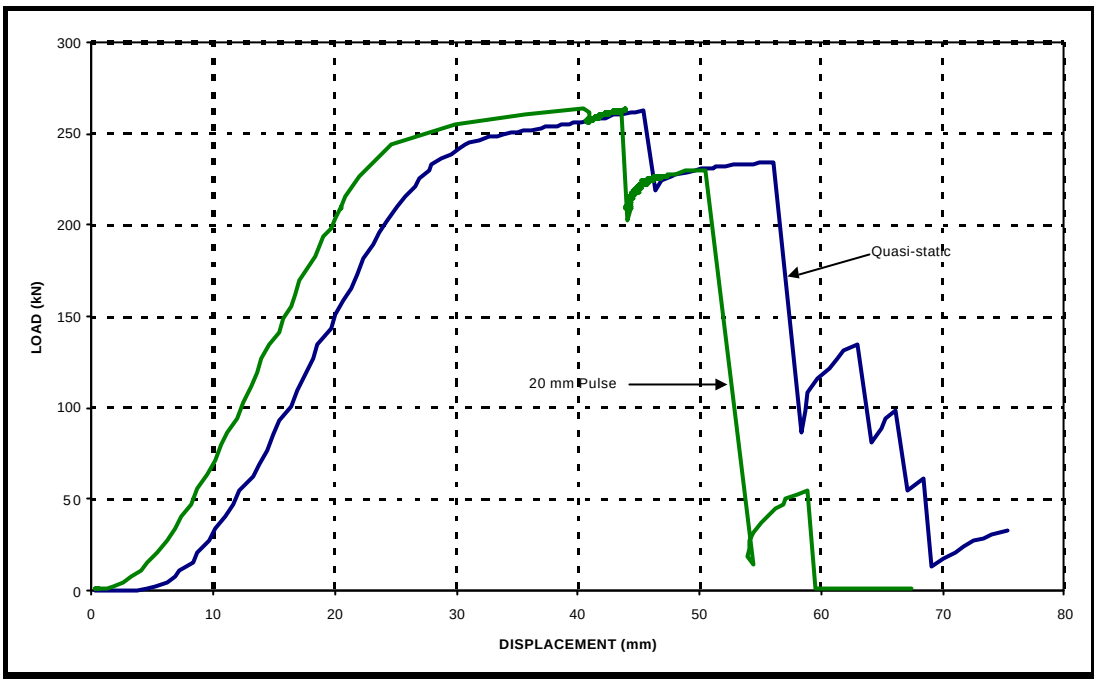

Figure 3.13. Deformation curve of the wire cable.

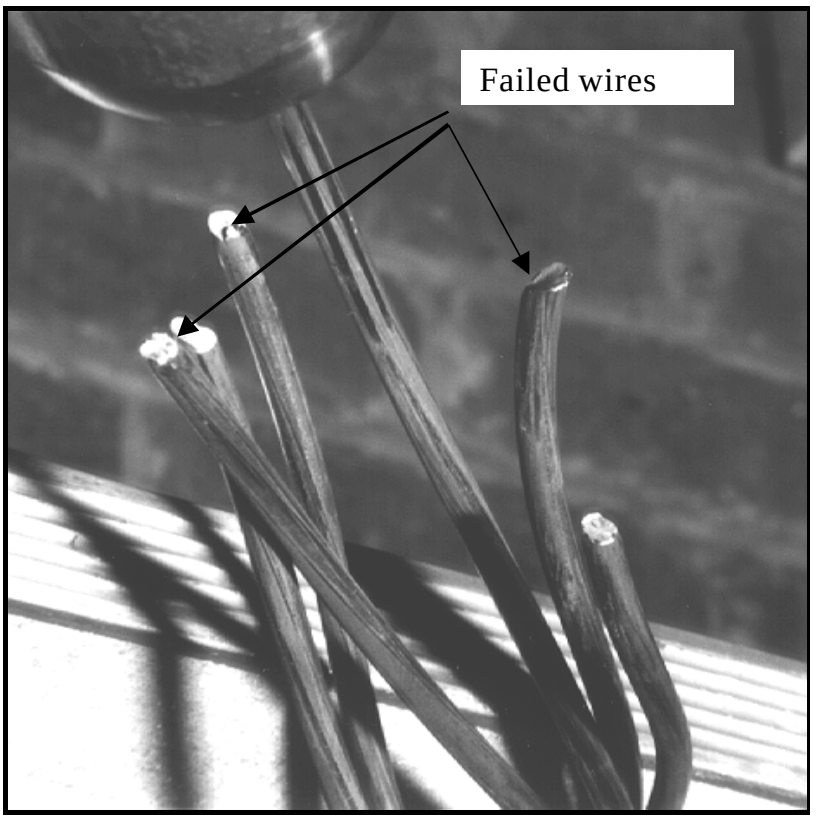

Figure 3.14. Failure mechanisms of wire cable.

The energy absorption capacity of each support unit is graphically expressed as well. Deformation curves of the re-bar show that the values range from 12.7 kJ to 16.1 kJ (see Fig. 3.15). Again, no correlation between loading rate and results could be observed.

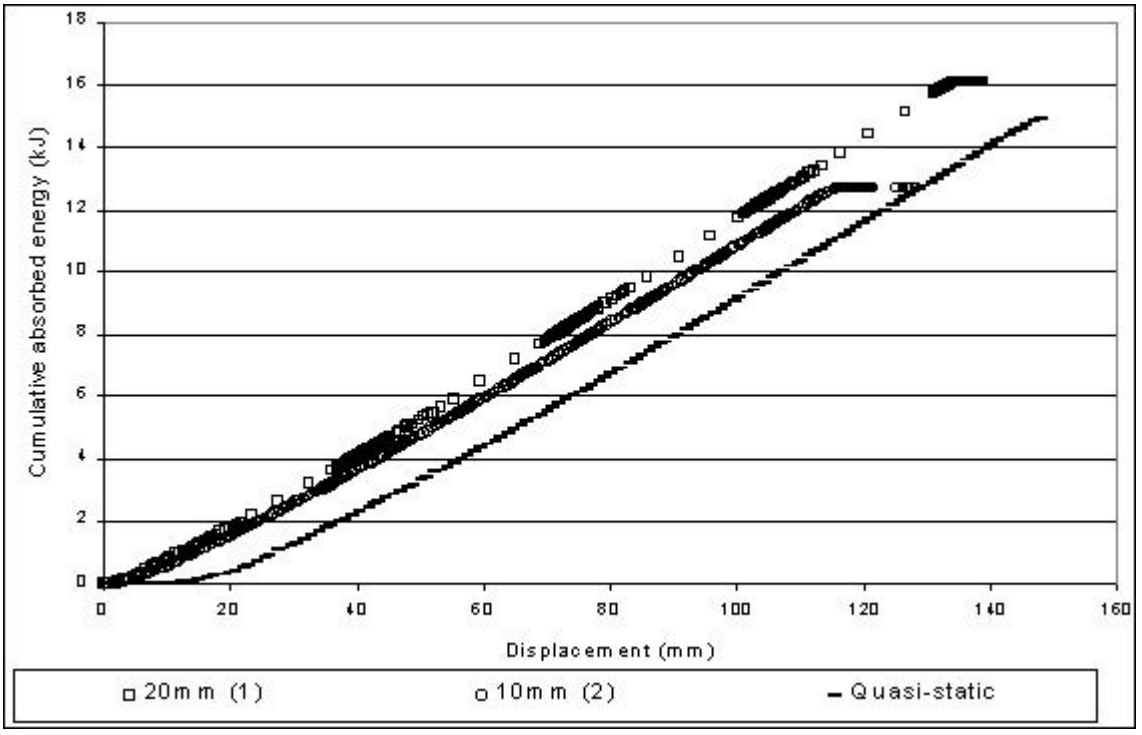

Figure 3.15. Energy absorption capabilities of re-bar under different types of loadings.

Deformation curves of the smooth bar show energy absorption capacities of about 17.1 kJ, 17.9 kJ and 18.8 kJ, for quasi-static, 10 mm pulse and 20 mm pulse dynamic loading conditions respectively (see Fig. 3.16).

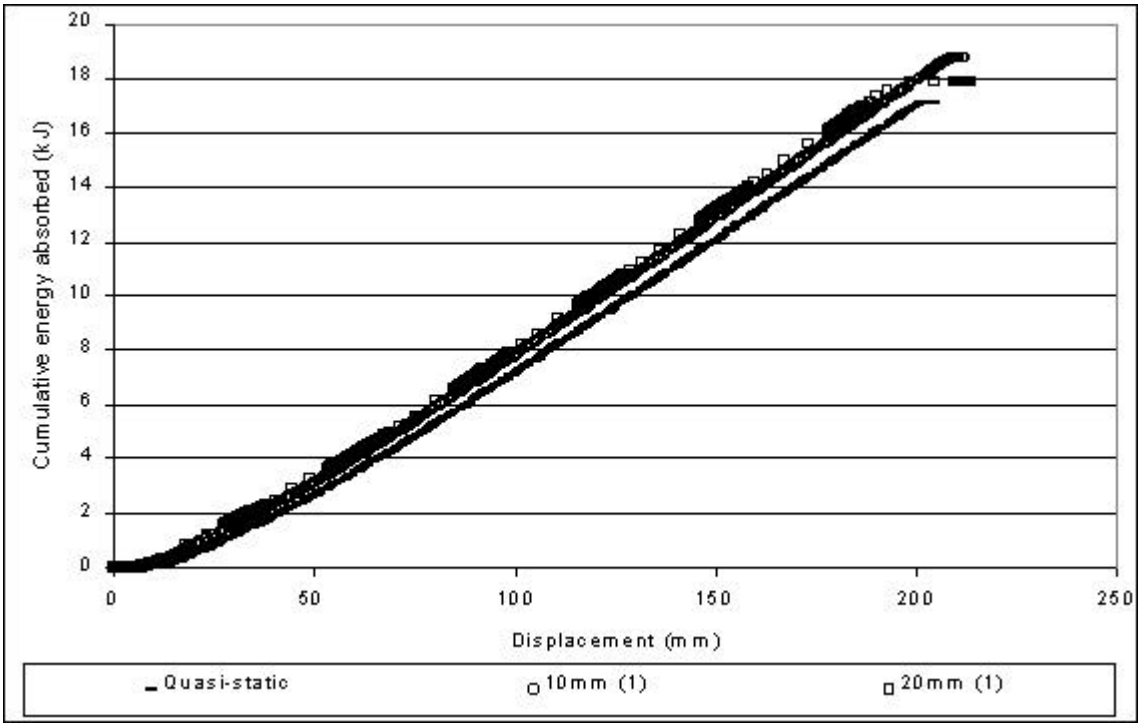

Figure 3.16. Energy absorption capabilities of smooth bar under different types of loadings.

More results of tests with re-bar and smooth bar are shown in Figures 3.17 to 3.20. These results indicate more clearly that the variation in results is not associated with the loading rate, but most likely with variations in the test specimens themselves. The fact that the spread in results is larger for the re-bar than for the smooth bar may be explained from a larger sensitivity to variations in the manufacturing process.

The results can be summarized as follows:

- The type of loading appears to have no noticeable effect on energy absorption capacity in steel tendons at the loading rates applied (up to 20 mm/s).
- Differences between individual specimens should be attributed to the manufacturing process.
- Stranded wire cables are approximately 100 per cent stronger than solid tendons of similar diameter, but their yielding range is about 50 per cent smaller.
- Re-bar is approximately 20 per cent stronger than smooth bar, but has a smaller energy absorption capacity due to a reduced yielding range.

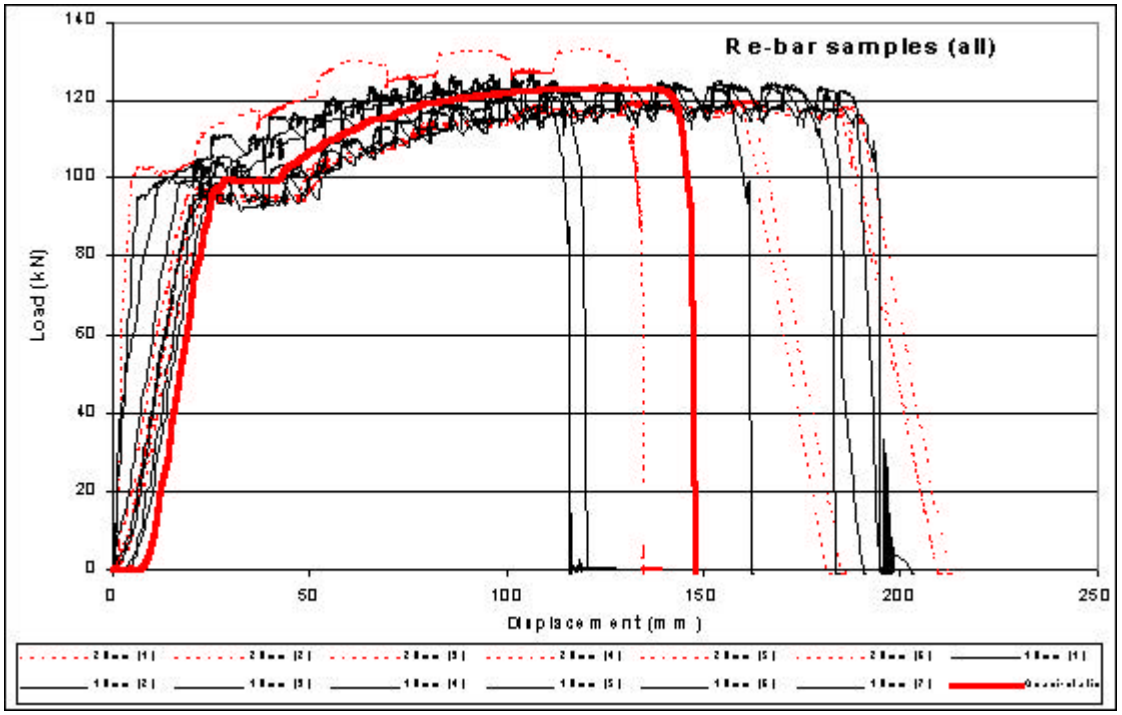

Figure 3.17. Deformation curves for all re-bars tested.

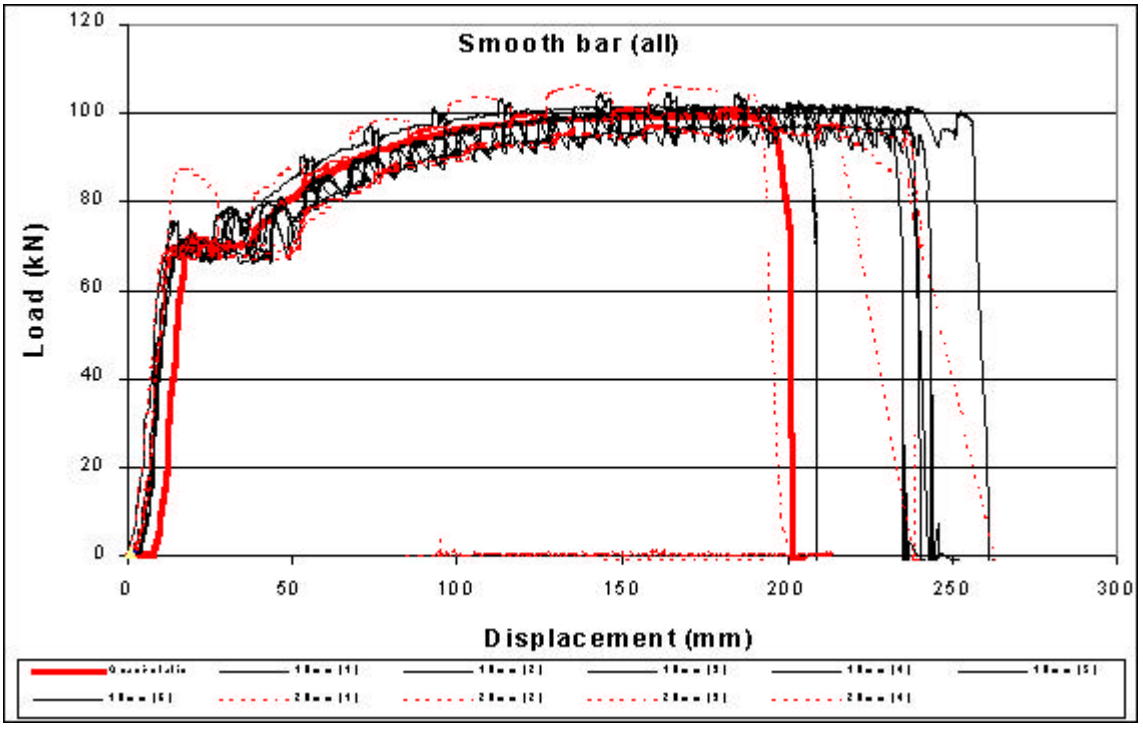

Figure 3.18. Deformation curves for all smooth bars tested.

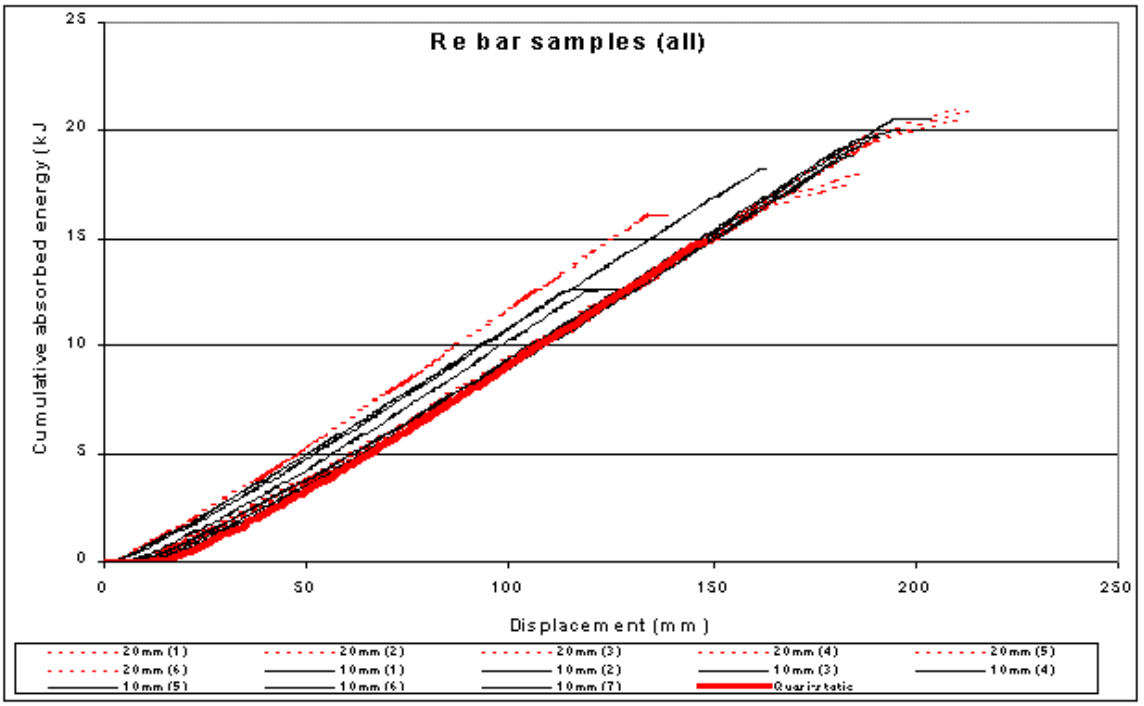

Figure 3.19. Cumulative energy absorbed (kJ) by all re-bars tested.

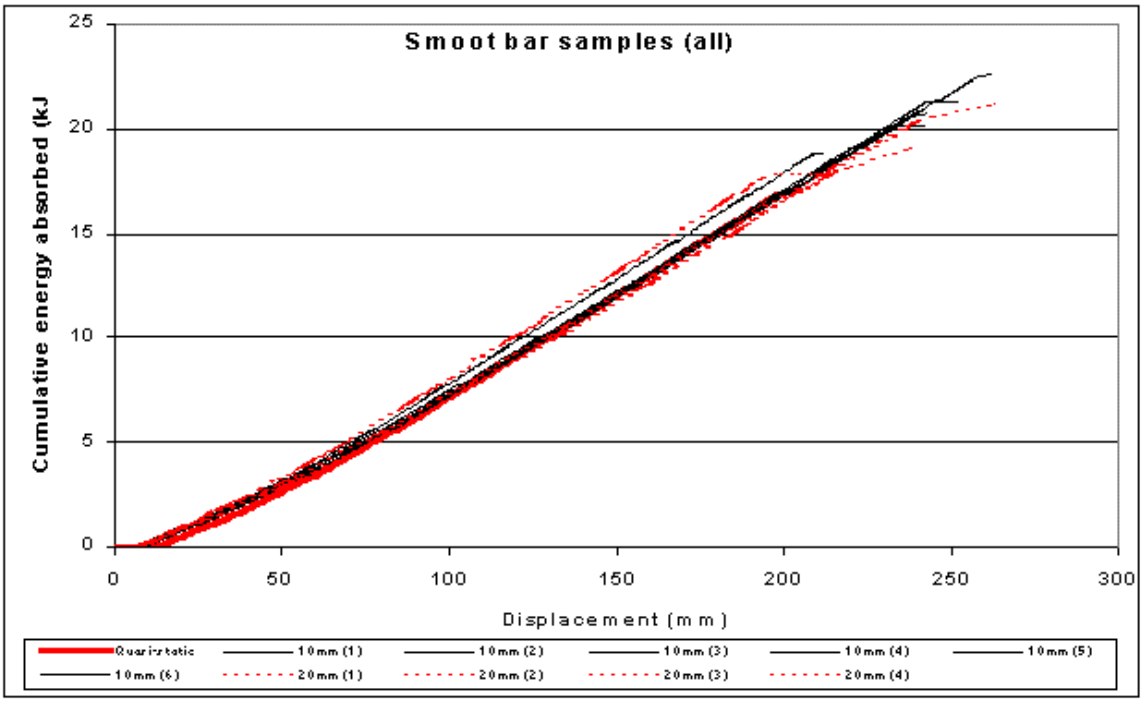

Figure 3.20. Cumulative energy absorbed (kJ) by all smooth bars tested.

3.2.2.2 Mesh

Testing of diamond and welded mesh was performed with a special testing frame in which a mesh panel could be clamped. The mesh consisted of mild steel with a diameter of 3.15 mm spaced at 100 mm, the dimensions of the testing frame being 600 mm x 600 mm. Varying loading rates, ranging from quasi-static to 2 m/s, were applied by the Terra-Tek to load the panel in the middle, in the direction perpendicular to the panel. The results are shown in Figures 3.21 to 3.24.

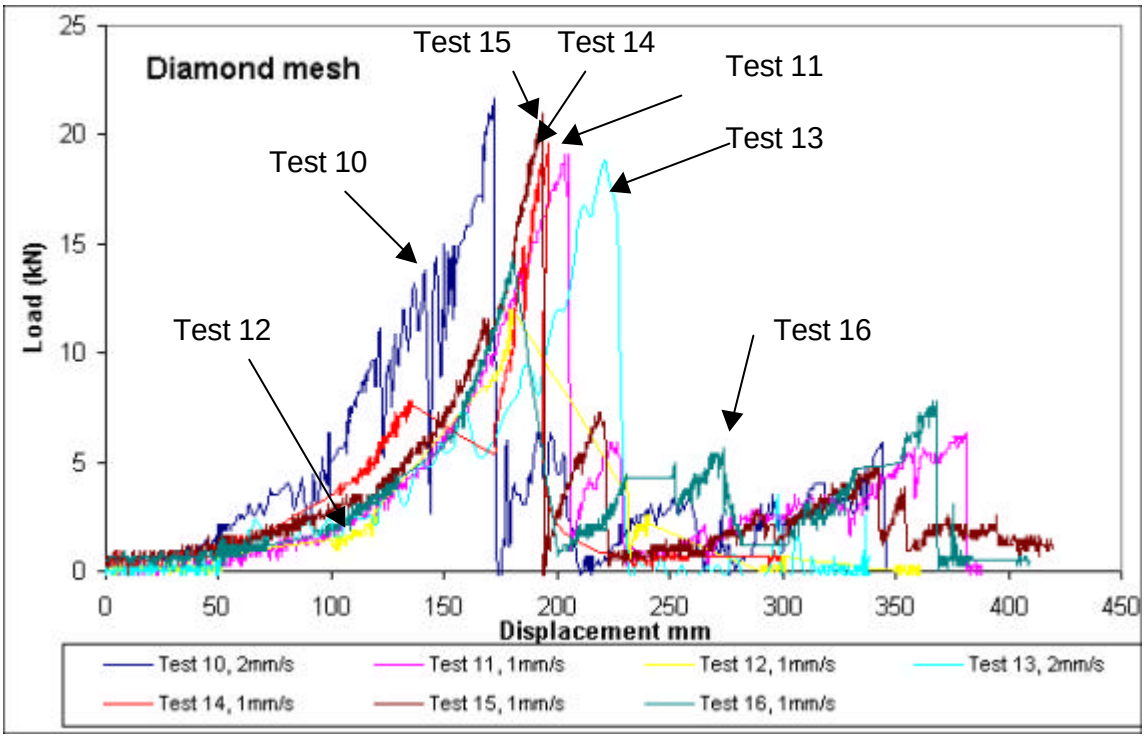

Figure 3.21. Deformation curves for all diamond meshes tested.

The diamond mesh is about three times stronger than the welded mesh, and its energy absorption capacity is about 75 per cent more. In the case of the welded mesh, stress concentrations at weld points limit the overall performance, whereas, in the case of the diamond mesh, deformations can follow a more natural course.

The variability in results with welded mesh is also associated with the presence of random stress concentrations and the limited potential for stress redistribution. The diamond mesh does not demonstrate this variability and is consistently stronger and more yieldable.

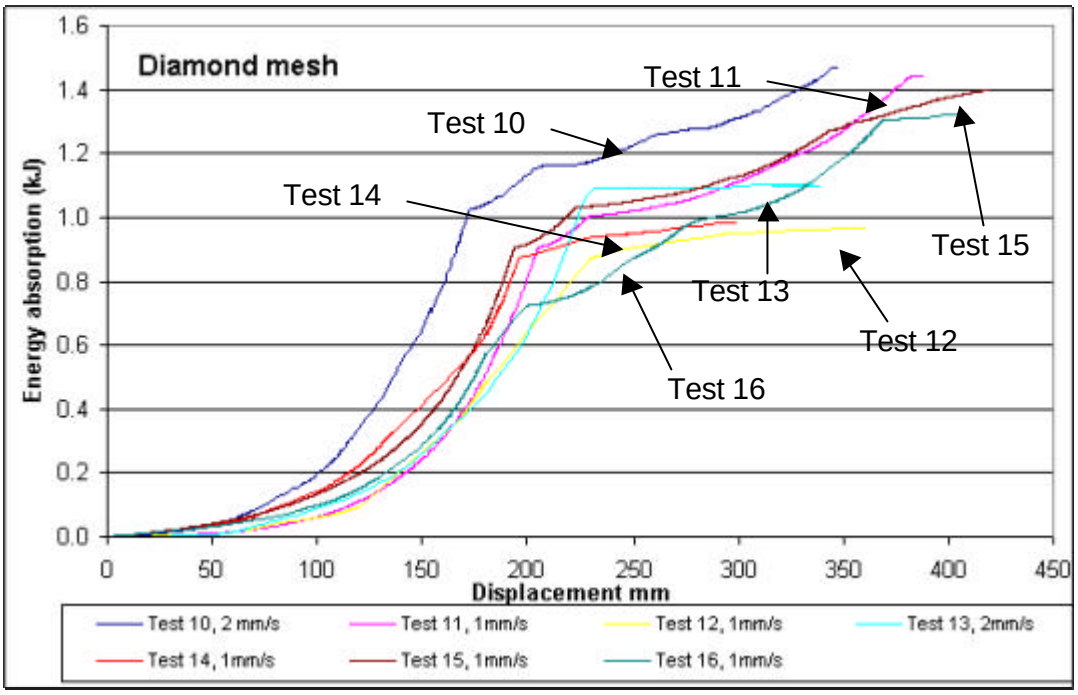

Figure 3.22. Cumulative energy absorbed in all diamond meshes tested.

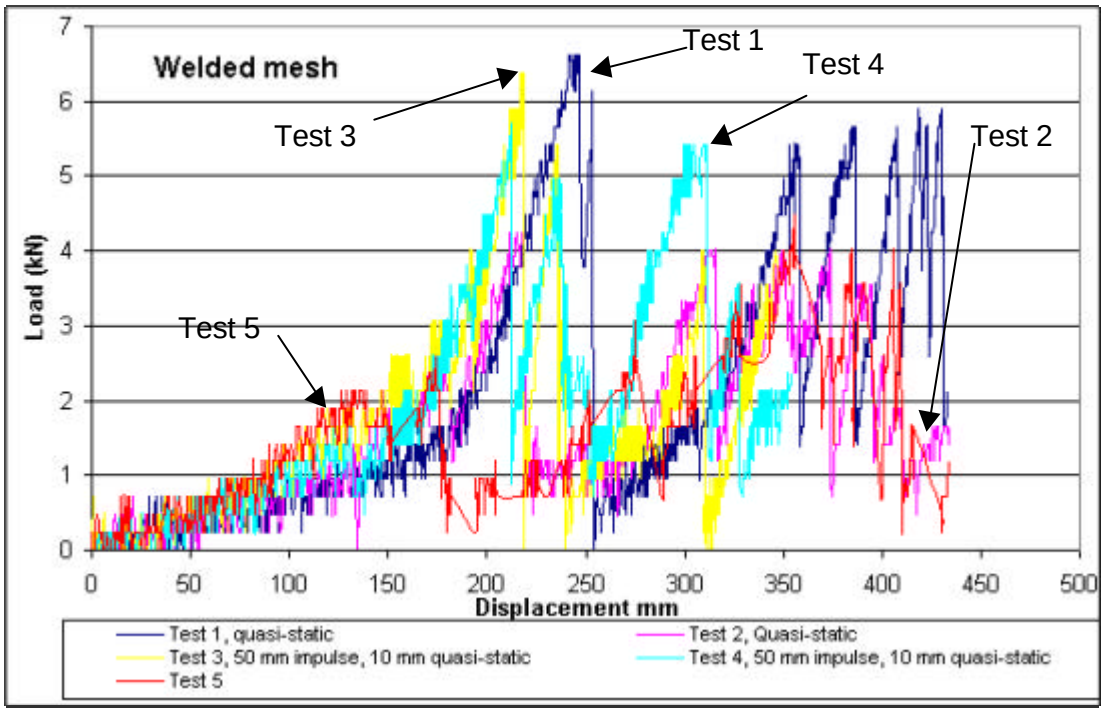

Figure 3.23. Deformation curves for all welded meshes tested.

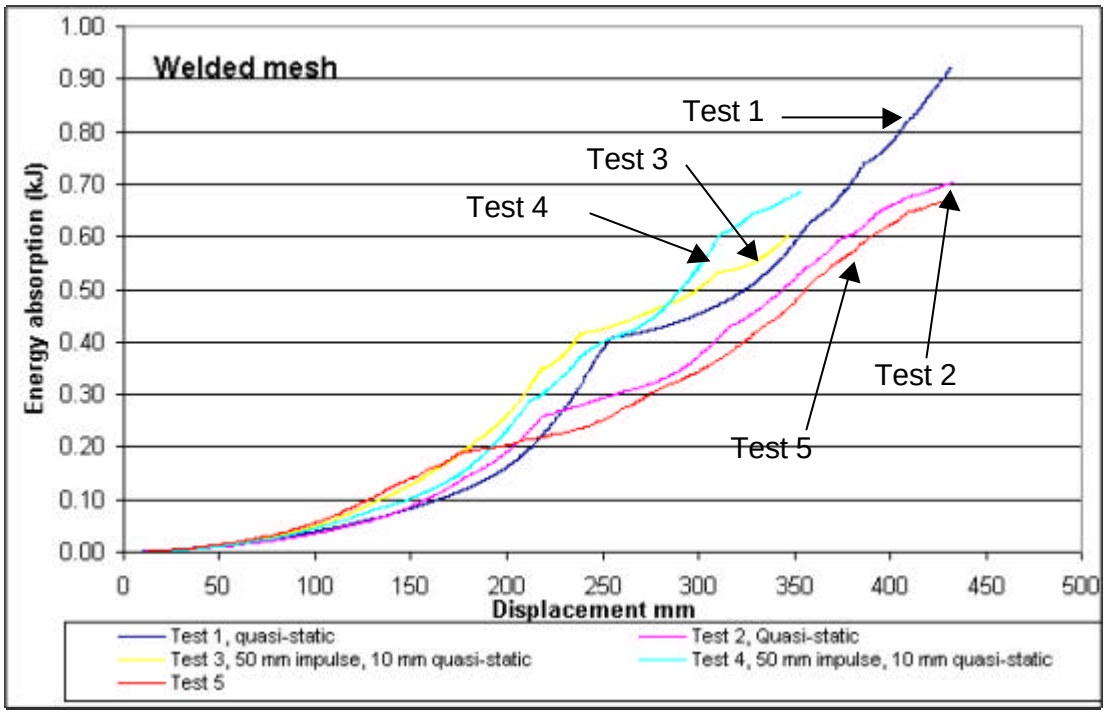

Figure 3.24. Cumulative energy absorbed in all welded meshes tested.

Loading rate variations from quasi-static to 2 m/s do not appear to affect the energy absorption capacity in a steel mesh.

Ultimate loads, in a panel of 0.4 m^2, can reach up to 20 kN, but are typically much lower in welded mesh.

It should be noted that in all tests on the welded mesh, the mesh was clamped near its four corners only. A similar clamping arrangement resulted in excessive deformations in the diamond mesh, where a maximum load was not reached after 500 mm of deformation. All subsequent tests on diamond mesh (shown in Fig. 3.21) were therefore conducted on mesh which was clamped along the full length of all its sides. While it was obvious that the diamond mesh is less stiff than the welded mesh, such behaviour is unfortunately not reflected in the results shown in Figures 3.21 and 3.23.

3.2.2.3 Lacing

Various types of lacing were tested in the same testing frame used for the mesh. Used lacing was obtained from Kloof Gold Mine and new lacing was obtained from Haggie Rand. Clamping of the lacing was done either by two jaws at each end of a length of lacing, or by using typical

cable friction clamps. Varying loading rates were used to load each cable in the middle and perpendicular to its axial direction.

The performance of the lacing is strongly controlled by the clamping device, e.g. the use of jaws results in stress concentrations at individual strands rather than a homogenous stress distribution along the lacing. This leads to a reduced performance as individual strands fail prematurely. On the other hand, the use of friction cable clamps result in a maximum clamping force which is far lower than the tensile strength of the lacing; sliding of the cable through these clamps could be observed at relatively low loads. (Note: Similar behaviour may be expected in underground applications).

The results are highly variable, as can be appreciated from the following Figures 3.25 to 3.27.

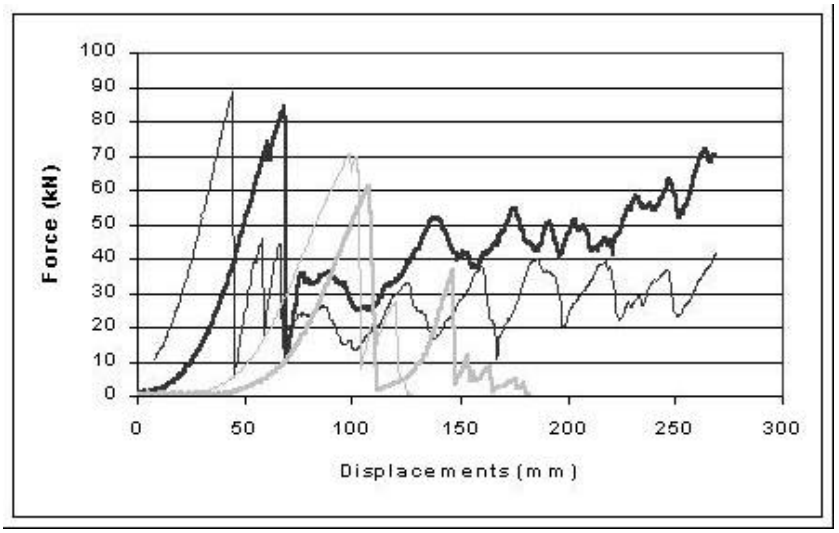

Figure 3.25. Lacing tested with clamping jaws.

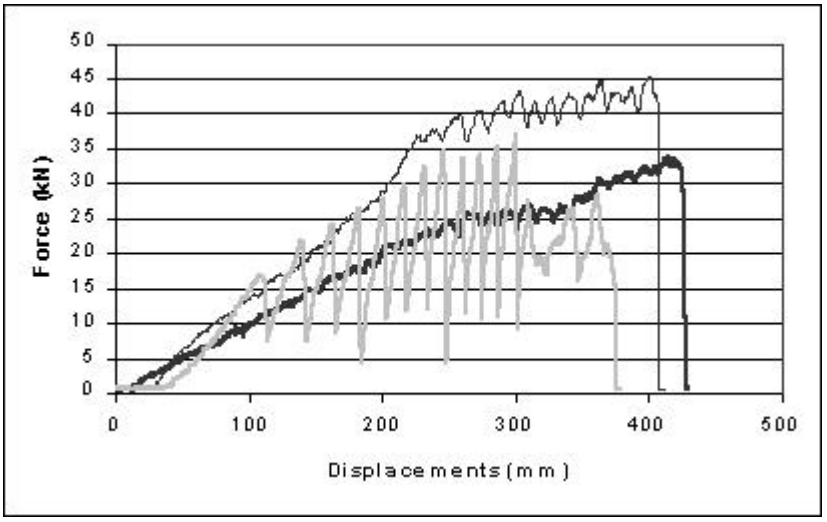

Figure 3.26. Lacing tested with a single friction clamping device.

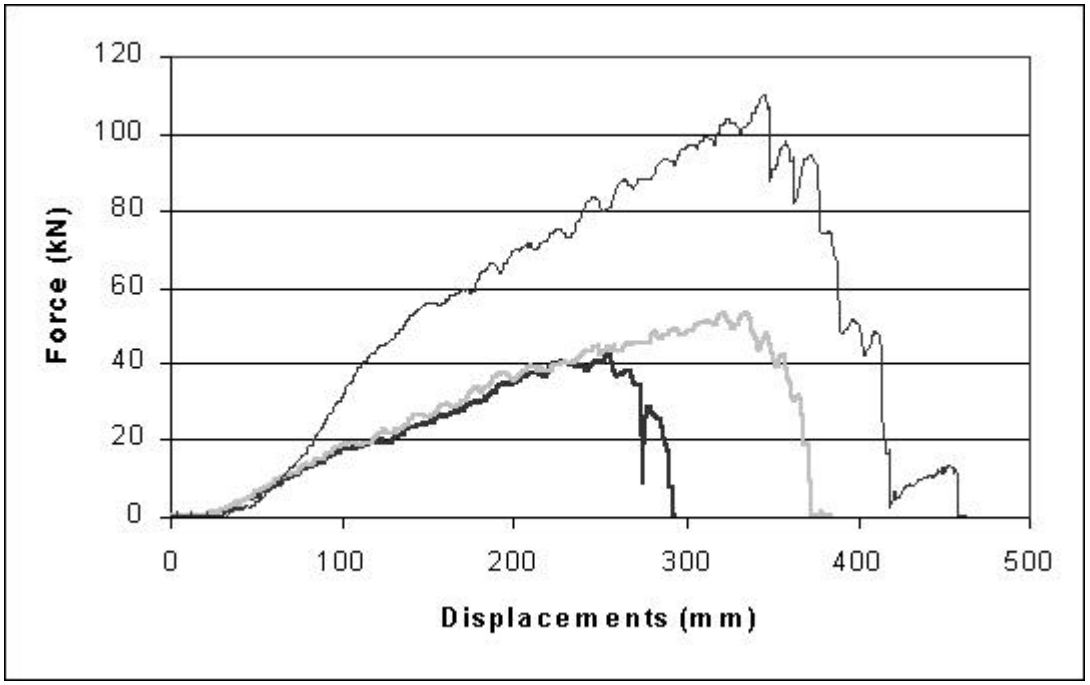

Figure 3.27. Lacing tested with three friction clamping devices.

The peak resistance forces obtained in these laboratory tests range from 35kN to 120kN. This was achieved under controlled conditions and across a relatively small span of 600mm. The displacements associated with friction clamping devices were extremely large as peak loads were only obtained at displacements in excess of 300mm. Such behaviour reflects a very soft support response. The use of clamping jaws leads to a stiffer response, but a more brittle post failure behaviour is observed in this case. Lacing typically acts as a passive support unit, and relatively large deformations are generally required before lacing units are loaded. If lacing elements could be used more efficiently their support capacity could be improved substantially. Two aspects need to be addressed in this respect. The first is the initial interaction between the lacing and the rock mass. A minimum amount of rock mass dilation should meet with immediate lacing resistance. The second aspect deals with the limiting capacity of the clamping devices used. Sliding of the lacing in the friction clamp has been observed to occur at stress levels which are far below the tensile strength of the lacing. Jaw clamps induce brittle tendon failure at relatively low stress levels, although they allow a stiffer initial response. It appears that the performance of lacing support could be substantially improved if more efficient clamping devices, inducing yield at higher stress levels, could be identified. It is strongly recommended that further research be conducted for this purpose. In addition it is recommended that the underground performance of lacing elements be investigated, in order to identify potential *in situ* problems with the lack of efficiency of such elements.

4 Preliminary design recommendations

Under rockburst conditions tendons should be able to accommodate large shear and axial deformations (by yield). In the case of a relatively massive rock mass, in which only large blocks can be dislodged, tendons can be designed according to the original concept of block retainment. The function of fabric support may be limited to that of a safety net in such case. The presence of bedding planes in the hangingwall needs to be considered as they may cause shearing of tendons.

In the case of a relatively fragmented rock mass, the effect of tendons is reduced, as deformations of the rock mass will be concentrated in the areas in between the tendons. Bulking and unravelling of the local rock mass may lead to overall instability. This situation requires an appropriate fabric support. Relatively stiff fabric such as shotcrete appears to give the best results, as deformations are limited to minimum values. Under more demanding conditions, additional yieldability may be obtained from fibre reinforcement and lacing. Other support systems such as mesh and lacing do not provide similar initial stiffness, and may, therefore, cause initial instability under relatively low loading conditions. Nevertheless, mesh and lacing can provide resistance against large deformations, which may prevent total instability.

The results from the testing programme demonstrate the capacity of various support units and systems. The drop tests showed the superior performance of reinforced shotcrete and lacing in providing support resistance. The effect of a flexible membrane such as Evermine was not directly reflected in these results, as its influence on overall resistance is relatively small. However, with the use of Evermine, larger deformations could be accommodated before local failure occurred. As the capacity of lacing was found to be strongly affected by the clamping devices used, it is strongly recommended that the efficiency of lacing be thoroughly investigated. The lack of initial stiffness of lacing systems should also be addressed; it might be possible to develop more efficient systems by appropriate pre-stressing and curving of the lacing. Welded mesh appears to be less suitable than diamond mesh under rock burst conditions. Compared to diamond mesh, both its strength and its yield range are small. Mesh is typically used as a passive support and is therefore not truly integrated with the support system. Its relative weakness, compared to tendons, lacing and shotcrete render it less suitable in highly fragmented rock under rock burst conditions. Mesh should be regarded as acting independently of the support system in a similar fashion to a safety net. Individual blocks may be contained by the mesh, but large amounts of fragmented rock may require improved support under rock burst conditions.

The demand on any support system is obviously determined by the loading conditions. As has been discussed previously, these loading conditions can vary largely and are strongly controlled by local seismic activity. In addition, the local rock mass conditions and stress environment largely determine the extent of the fragmentation of the rock mass around the excavation. The fragmentation of the rock mass in turn largely determines the requirements for areal support, while the potential for seismic excitation determines the required energy absorption capacity of the rock tendons. As a rough guideline the following table contains support recommendations for various combinations of seismic excitation and rock mass fragmentation:

Table 4.1. Support recommendations.

Intensity of fragmentation / Ground motion	Low	Medium	High
Low	Pinning of key blocks	Pinning of key blocks plus a safety net	Adequate anchorage plus complete areal coverage with active fabric support (shotcrete or Evermine)
Moderate	Pinning of key blocks with yielding tendons	Pinning of key blocks with yielding tendons plus active fabric support (shotcrete or membrane)	Adequate anchorage with yielding tendons plus complete areal coverage with active and competent fabric support (reinforced shotcrete and lacing)
High	Pinning of key blocks with yielding tendons of sufficient capacity plus a "safety net"	Pinning of key blocks with yielding tendons of sufficient capacity plus a competent and active fabric support (reinforced shotcrete, lacing and membrane)	Either a system with high capacity tendons and reinforced shotcrete plus lacing or an alternative in the form of a competent shell.

5 Detailed underground evaluation

5.1 Site selection / history

A site at Tau Tona Mine was instrumented and monitored during this project. Two seismically active faults are located near the site and repeated dynamic loading of the support system was therefore expected. Seismic data recorded by the mine's seismic network was collected around the monitoring site. A hypocentral map of the seismic events recorded by the mine network during the period of observation is shown in Figure 5.1.

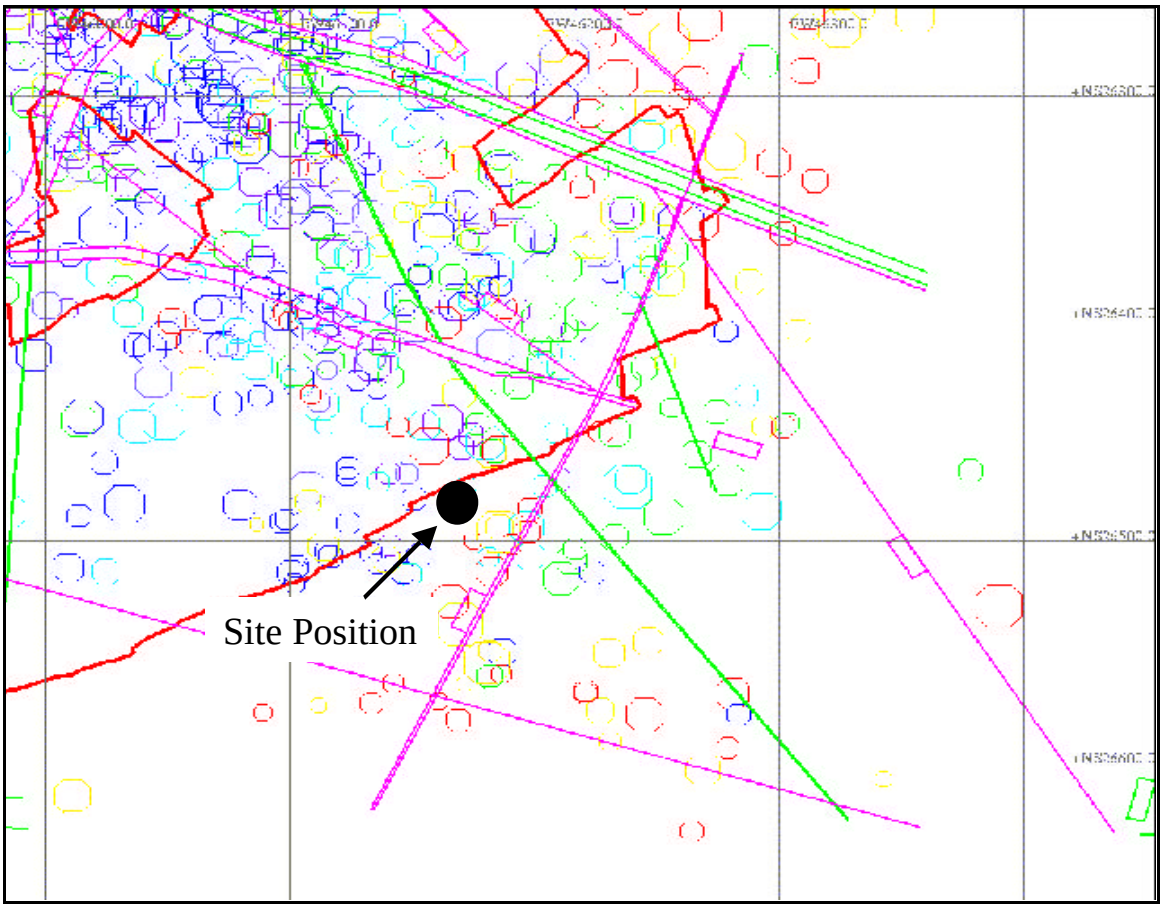

Figure 5.1. Mine layout, geological structures and seismicity around the site. Data from the Rock Mechanics Department, Tau Tona Gold Mine.

It can be seen from Figure 5.1, that the majority of the seismic events are associated with the active working faces and the geological weaknesses. The overall seismic activity in this area was found to be relatively high. The monitored area was also modelled to assess the stress environment from the virgin stress through the subsequent mining steps. To improve the stress conditions a de-stressing slot was mined out at 5 m above the tunnel. Figure 5.2 shows a plan view of the tunnel and the de-stressing slot and the position of the monitoring instrumentation is also indicated.

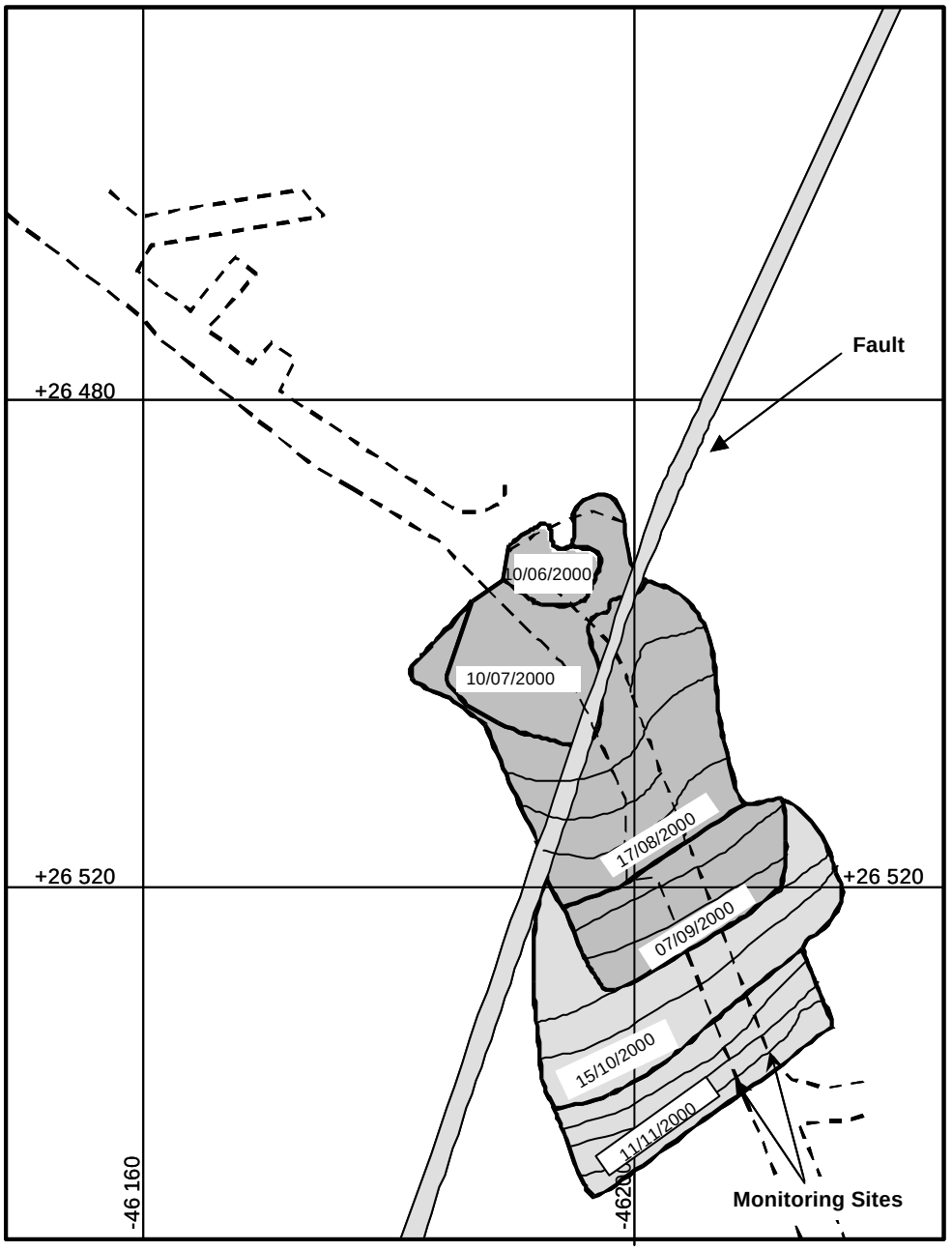

Figure 5.2. A plan view of the monitoring site and de-stressing slot.

5.2 Evaluation of support system performance

5.2.1 General

One of the objectives of this project was to evaluate the support performance along a monitored section on 100 Level in the 3c cross-cut south. Monitoring was done with the aid of two strain gauged hollow bars, various geophones, closure measurements and visual observations. Owing to the expected direction of the major principal stress, dilatation was expected to occur in the sidewalls of the excavation. To obtain quantitative data on the forces induced by these dilatational movements, two instrumented tendons were end-grouted with resin and subsequently pre-tensioned. The tendons were located at the monitoring site as indicated in Figure 5.2.

The tendons consisted of smooth hollow bar with a length of 2.5 m with three pairs of strain gauges evenly distributed along their length to ensure reliable data collection. Each tendon was installed in a hole drilled through the existing integrated support comprising Shepherd Crooks, wire mesh, rope lacing and shotcrete.

As illustrated in Figure 5.3, each instrumented tendon was incorporated into an integrated monitoring system that allowed for both dynamic and quasi-static measurements.

Figure 5.3. Instrumented rock tendons.

The stress history was analysed and related to overall conditions in the subject tunnel, which was supported in accordance with Tau Tona Mine support standards.

The monitored area was modelled to assess the changing stresses imposed on the tunnel. The tunnel was developed in the down-dip abutment of a longwall and subsequently overstoped by a 20 m wide de-stressing slot 5 m in the hangingwall as schematically illustrated in Figure 5.4.

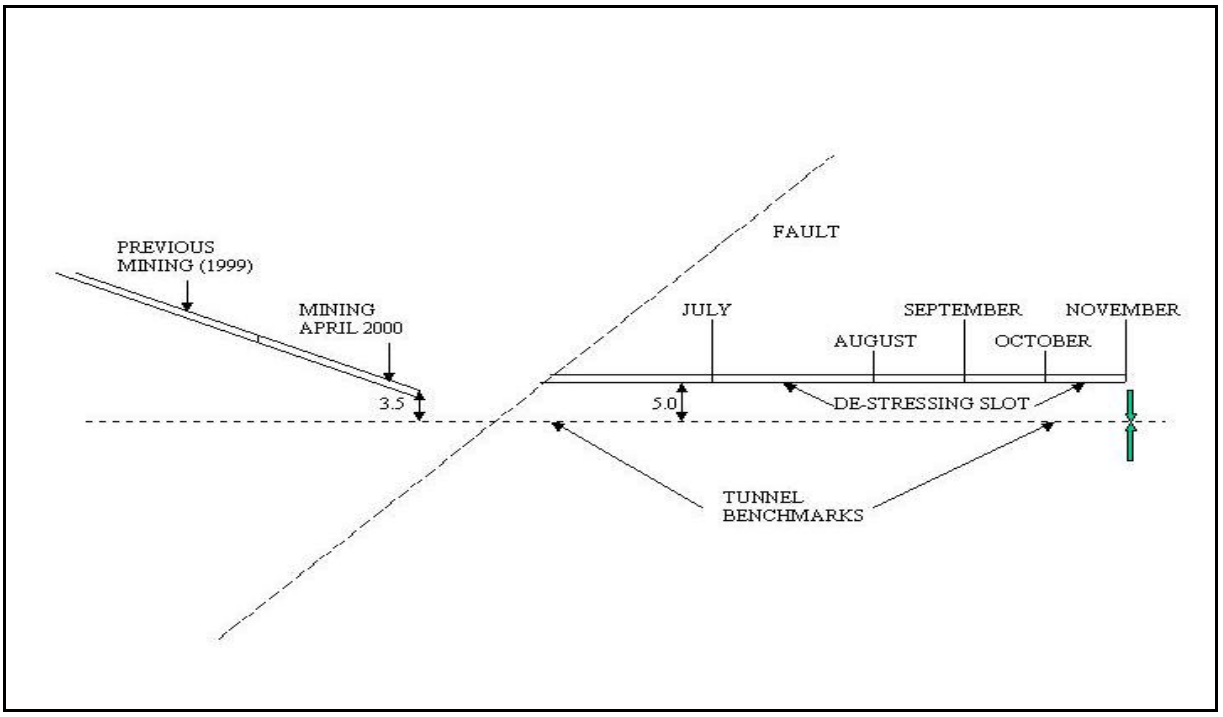

Figure 5.4. Layout of excavations and position of de-stressing slot.

In calculating principal stresses, a k ratio of 0.5 was assumed and the slot geometry was taken into account for a three-dimensional stress distribution. Although the numerical simulation was done with DIGS, which is a two-dimensional plane strain boundary element method, the out of plane dimension of the de-stressing slot was indirectly included by proportional reduction of the stress distribution onto the face of the slot.

The orebody dips at approximately 25 degrees and a fault is present - dipping at about 45 degrees, as illustrated in Figure 5.4. The double arrows indicate the position of the strain-gauged bar. The de-stressing off-reef slot, as shown in Figures 5.2 and 5.4, was developed away from the fault with advance rates ranging from about 7 m to 14 m per month.

Seven mining steps were used in the numerical simulation of the slot cutting above the monitored tunnel. It was found that the monitored tunnel experienced a theoretical change in field stress from approximately 85 MPa to about 121 MPa.

The location of the strain gauged bars is indicated in Figures 5.2 and 5.4 and is referred to as monitoring site in Figure 5.2. Position 2 is located approximately 20 m west of this monitoring site, while position 3 is located approximately 6 m east of it.

Simulated principal stresses representing the changing stresses are listed in Table 5.1 for three benchmarks. These benchmarks are located at the following positions:

- Position 1: furthest away from the tunnel face which is being developed to the east.
- Position 2: 20 m east of position 1.
- Position 3: 26 m east of position 2, and 6 m east of the strain gauged bars

Table 5.1. Stress history for monitoring positions along 100-3c cross-cut south.

Benchmark	Mining Step 1	Mining Step 2	Mining Step 3	Mining Step 4	Mining Step 5	Mining Step 6	Mining Step 7
Principal stress history, MPa							
1	94	112	121	40	40	40	40
2	88	97	99	116	103	40	40
3	85	91	92	94	97	103	118

5.2.2 Observations and monitoring

Closure measurements at position 1 showed insignificant deformations of the tunnel walls. Between October 2000 and January 2001:

- No sidewall closure was observed.
- Average hangingwall – footwall closure of only 2 mm was recorded.

Such small rock movement did not cause any notable damage to the supported tunnel as illustrated in Figure 5.5. Measuring points on the hangingwall and sidewall of the excavation can be seen in the photo as well.

The presence of the de-stressing slot above and good quality support installed prior to the cutting of the slot that started in June 2000, are responsible for the relatively good tunnel condition.

Figure 5.5. Overall tunnel condition around monitoring position 1. (October 2000).

The monitoring position 2 which is located 20 m east of position 1 in the direction of the tunnel end, showed slightly larger closure. Between October 2000 and January 2001:

- About 20 mm sidewall to sidewall closure was measured.
- About 5 mm hangingwall to footwall closure was measured.

The way sidewall to sidewall and hangingwall to footwall closure measurements were taken is illustrated in Figures 5.6 and 5.7, respectively.

Figure 5.6. Overall tunnel condition around the monitoring position 2.

Figure 5.7. Measuring hangingwall – footwall closure at monitoring position 2.

The monitoring position 3, which was situated about 46 m east of position 1 and 6 m east of the strain gauged bars, is the only one of three monitoring positions which was not located under the de-stressing slot during the monitoring period. Again, no significant closures were measured at this position:

- Approximately 15 mm sidewall to sidewall closure was measured.
- Approximately 5 mm hangingwall to footwall closure was measured.

The closure measurements were done with telescopic bars. Although the accuracy of such measurements should be in the order of millimetres, it is conceivable that due to the roughness of the tunnel walls, a reduced accuracy may have been obtained. Therefore, the inelastic deformations of the tunnel walls were assumed to be negligible for all practical purposes during the monitoring period.

According to the numerical simulations the stress changes during the monitoring period were as follows:

Section 1 No stress change
Section 2 6 MPa drop in principal stress
Section 3 15 MPa increase in principal stress (almost vertical -dipping at 86^0)

The overall good condition of the excavation in the immediate vicinity of position 3 is shown in Figure 5.8. No visible damage to the excavation or support (including a relatively brittle shotcrete) was observed.

Figure 5.8. Section of monitored excavation in proximity of position 3.

More detailed pictures of a supported hangingwall in this section are shown in Figures 5.9 and 5.10.

It should be noted that despite the generally poor rock conditions the hangingwall appears to be stable and well controlled by the integrated support system as will be described later.

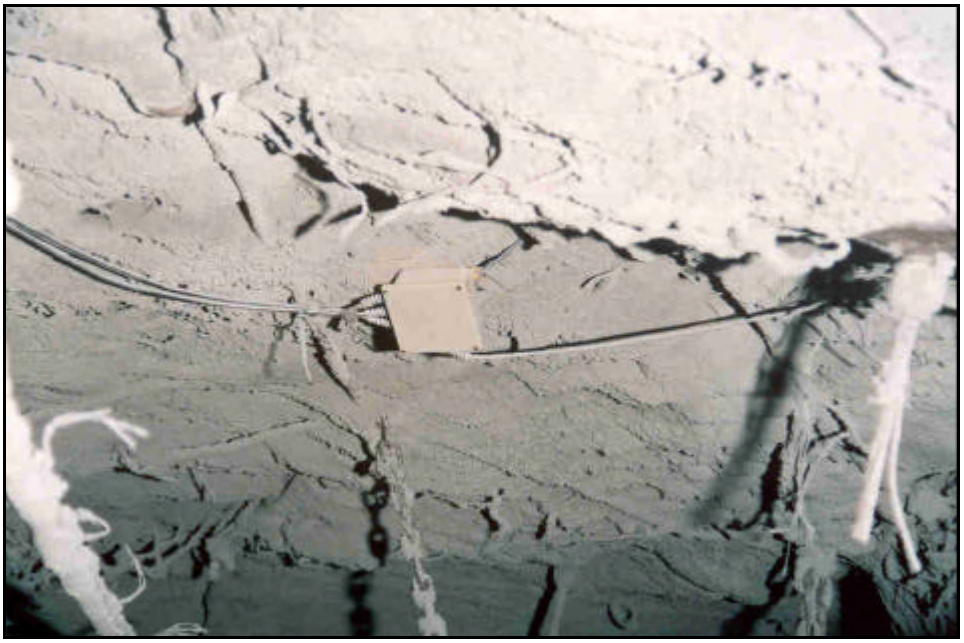

Figure 5.9. Close-up of the hangingwall condition adjacent to position 3.

Figure 5.10. Overall stability of hangingwall in the vicinity of position 3.

5.2.3 Support used in the monitored area of the 100-3c-x/c south

Primary support in the monitored excavation (with dimensions of approximately 3.0 m x 3.0 m) comprised seven smooth bar 16 mm diameter, full column grouted tendons for each row of support. Maximum spacing between rows was about 1.5 metres (1.5 m square pattern). Two of the support tendons were installed into the top corners of the excavation at approximately 45^0. In each row of support two tendons (one per sidewall) were installed below the grade line oriented downwards at about 30^0.

In addition, diamond wire mesh and 10 mm – 12 mm diameter rope lacing was incorporated into the support system as shown in Figure 5.11. It also illustrates a layer (from about 10 to 75 mm thick in places) of shotcrete. Shotcrete was applied in two phases. The second layer of shotcrete was applied after the installation of the tendons, mesh and rope lacing support.

Figure 5.11. Wire mesh, rope lacing and shotcrete integrated support.

To further ensure that the monitored cross-cut remained stable despite expected stress changes and seismicity, additional support in the form of bird-caged, full column grouted cable anchors was installed. The 25 ton strands, with diameter of about 16 mm were pre-stressed to a maximum load of about 10 tons. The tendons were full column grouted. The cable anchors were 4 m long with effective grouted length of about 3.8 m. They were installed at 3 m spacing in the side and hangingwalls. An example of such a tendon together with wire mesh and lacing is illustrated in Figure 5.12.

Figure 5.12. Pre-tensioned and post-grouted cable anchor.

It should be noted that the overall condition of the 100-3c cross-cut south, along the monitored length schematically illustrated in Figure 5.4, and for the calculated stress history as given in Table 5.1, appears to be well controlled by the integrated support system comprising full column grouted smooth bar Shepherd's Crooks, 4 m cable anchors, wire mesh, rope lacing and shotcrete. Despite the presence of relatively high stresses, both the general condition of the excavation as shown in Figure 5.13, as well as the condition of a relatively brittle shotcrete layer, which is shown in Figure 5.14, appear very stable.

It should be noted that two similar tunnel drives, which were excavated previously and further back from the current longwall face, were damaged in previous rockbursts and inaccessible.

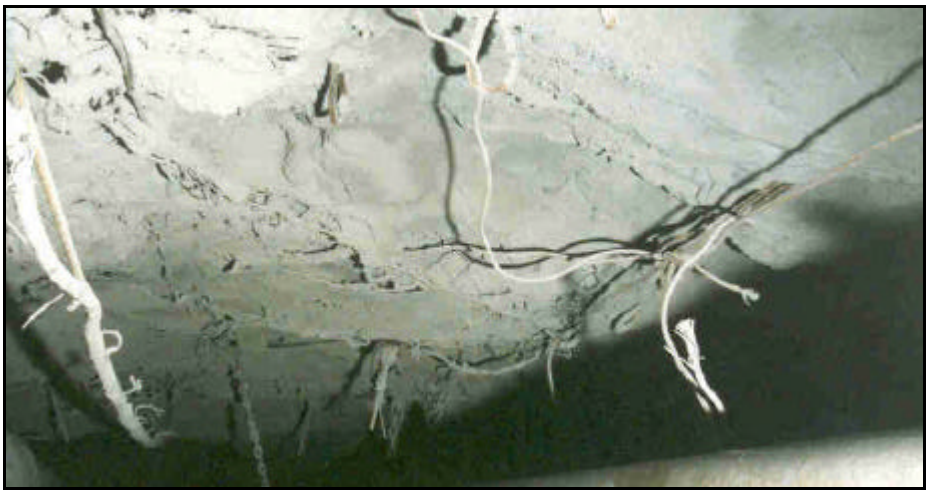

Figure 5.13. General condition of the hangingwall in the 100-3c cross-cut south.

Figure 5.14. A close-up of the hangingwall condition.

Figure 5.15 shows the only local support failure, which has been observed in this tunnel. The location is however quite far away from the monitoring area and the failure appears to be associated with stress concentrations due to the presence of a pillar above the tunnel (see Figure 5.4).

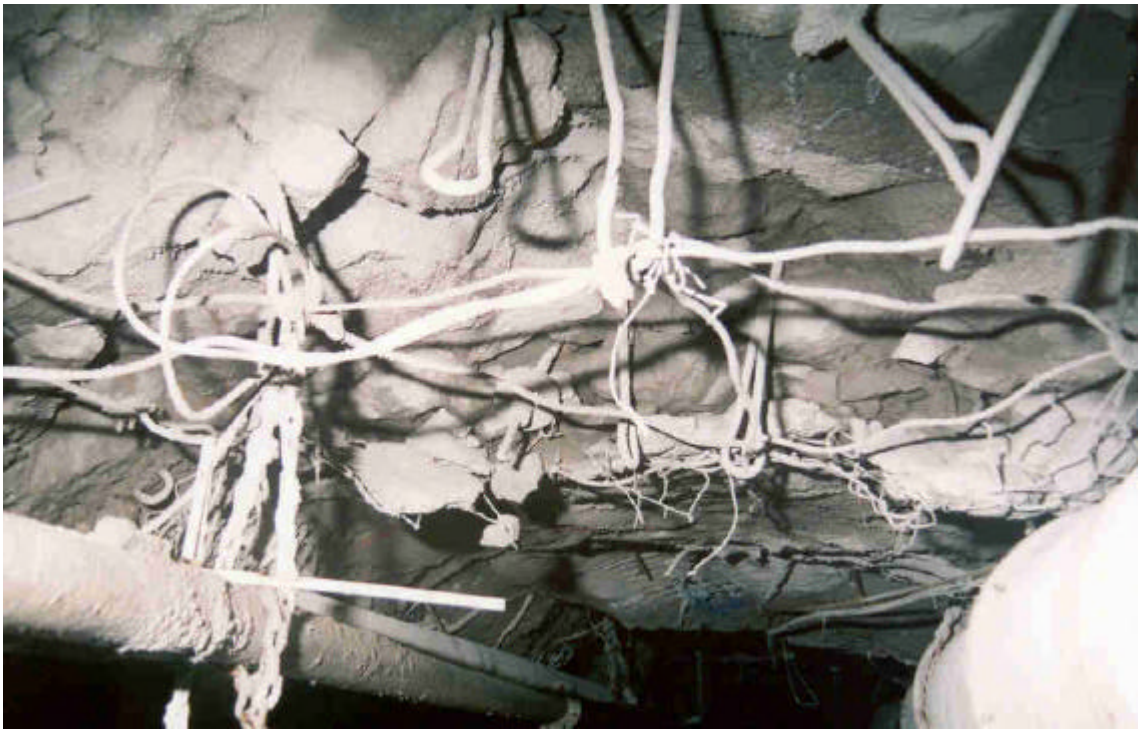

Figure 5.15. Rehabilitated area, exposing a brow.

5.3 Underground monitoring results

5.3.1. Quasi-static and dynamic monitoring

The monitoring programme collected quasi-static and dynamic data, which relates PPVs and deformation to support behaviour. The tunnel support system consisted of a primary set of Shepherd Crooks and an initial layer of shotcrete, complemented by a secondary system consisting of 3.8 m end-anchored, stranded cables, which were pre -stressed, mesh, lacing and a second layer of shotcrete covering the mesh.

The instrumentation consisted of two geophones and specially designed strain gauged tendons installed in boreholes in both sidewalls of the tunnel. One geophone was placed on the sidewall and the other one on the hangingwall of the tunnel. Each tendon had three pairs of strain gauges located along their length, one at the beginning, one at the middle and one at the end of each tendon. A cross-sectional view of the tunnel with the position of the instrumentation is shown in Figure 5.16.

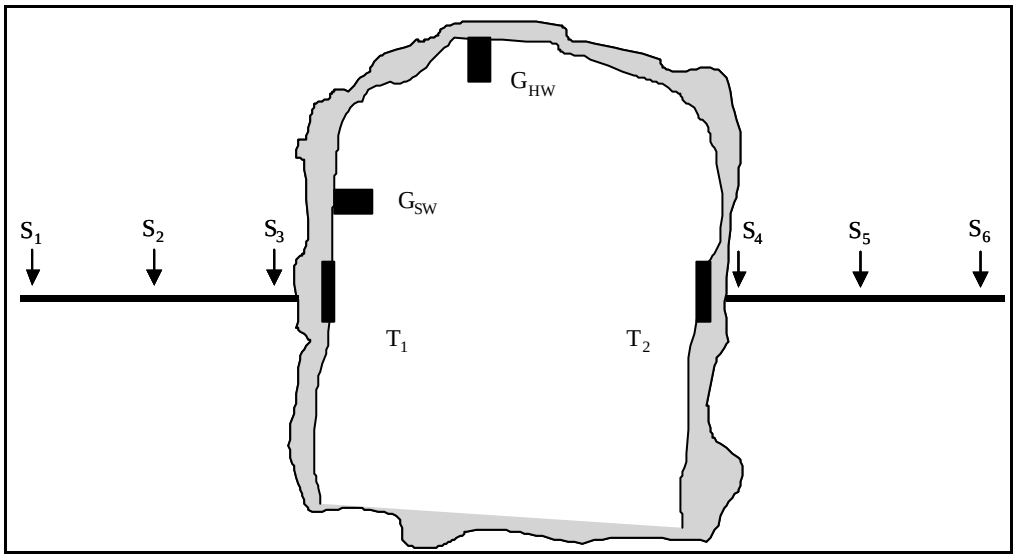

Figure 5.16. A cross-sectional view of the tunnel and the position of the monitoring instrumentation; G_{SW} and G_{HW} are geophones, S_1 to S_6 are strain gauges and T_1 and T_2 are tendons.

The site was monitored from 26 of July until 29 of December 2000. During the monitoring period 2684 seismic events were recorded. The PPVs of these events are shown in Figure 5.17.

The PPVs shown in Figure 5.17 ranged between 0.01 mm/s and 67 mm/s. Both sidewall and the hangingwall show similar behaviour in the PPVs. However, most of the higher PPV values were recorded on the sidewall.

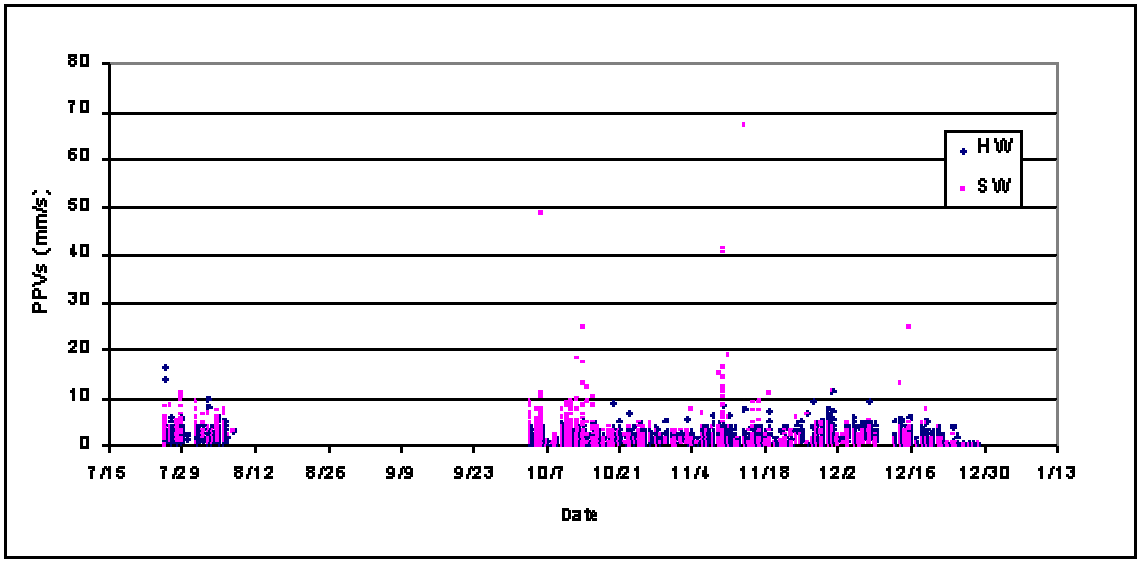

Figure 5.17. PPVs recorded on the hangingwall and the sidewall of the tunnel.

The strain measured in both tunnel walls as indicated by the strain gauges in the tendons is shown in Figures 5.18 and 5.19. The strain is plotted as a function of the advance of the de-stressing slot 5 m above the tunnel.

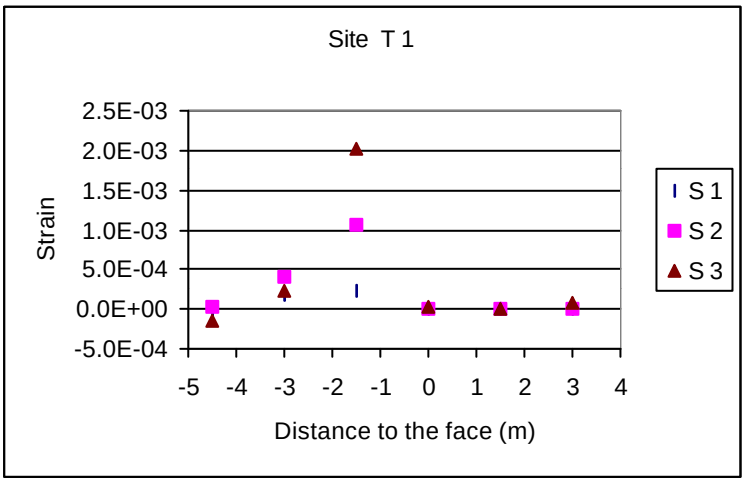

Figure 5.18. The strain at site T_1 as the face of the de-stressing slot progressed towards the instrumentation.

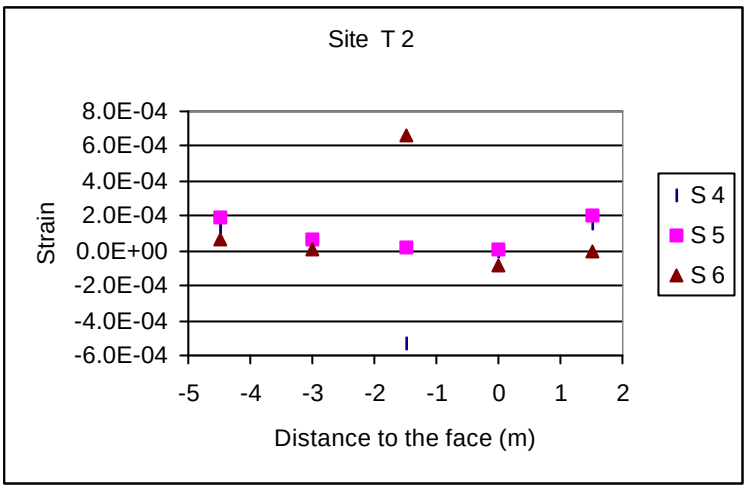

Figure 5.19. The strain at site T_2 as the face of the de-stressing slot progressed towards the instrumentation.

The different pattern and level of the strain clearly indicated in Figures 5.18 and 5.19 may be due to the asymmetric loading of the tunnel associated with the geometry of the de-stressing slot and the monitored tunnel. The T1 site has experienced higher strain then site T2.

It is interesting to note that as the tunnel was overstoped and the vertical stress reduced, the strain in the tendon reverted to zero.

There was no permanent deformation in the tendon due to repeated, though small, dynamic loadings.

The dynamic strain induced during the propagation of the seismic waves through the site was inferred from the readings from the strain gauges. This strain was compared to the PPVs recorded on the hangingwall to estimate a trend. The results are shown in Figures 5.20 and 5.21.

It is clearly indicated in Figures 5.20 and 5.21 that small PPVs close and below the noise level, 0.3 mm/s, have no correlation with strain changes. A linear relationship between strain and PPV was found for PPV values above 3 mm/s at both sidewalls. Extrapolating this relationship and assuming a uniform distribution of velocities and deformations, relevant velocities may be determined. Assuming a tendon yield strain of 10^{-3}, it follows that velocities, which induce higher strains, are associated with irrecoverable deformations.

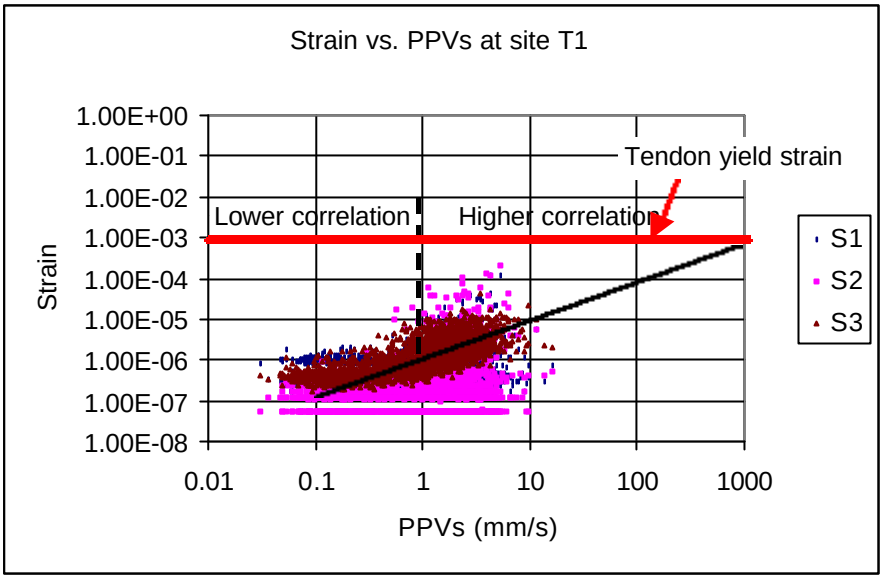

Figure 5.20. The dynamic strain measured in site T_1 as function of the PPVs measured on the hangingwall.

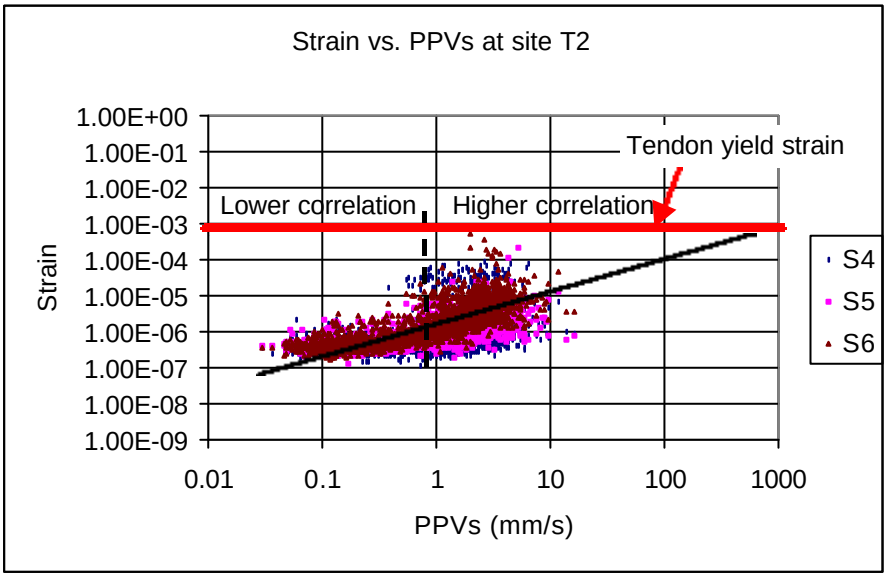

Figure 5.21. The dynamic strain measured in site T_2 as function of the PPVs.

A threshold PPV, beyond which yielding strains are induced in the tendon, can be inferred from Figures 5.20 and 5.21 for both monitoring sites. Threshold velocities of 0.8 m/s at site T1 and 0.6 m/s at site T2 appear to be reasonable estimates.

The relationship between the PPVs and the rock-mass strain is assumed to be associated with the volume of rockmass restrained by the tendon. In highly fractured and damaged rock this volume may be relatively large, while in solid rock no restraining function is required from the tendons. The threshold velocity is therefore indicative of the local rockmass damage and tendon action. The restrained rock mass can be derived from the principle of energy conservation:

$$\frac{1}{2}Mv_t^{\,2} = \frac{1}{2}F_y\boldsymbol{d}$$

where v_t is the threshold velocity

F_y is yield force

$\boldsymbol{d}$ is the deformation of the tendon

l is the length of the tendon and

M is the restrained rock mass

Permanent strains are induced beyond the threshold velocity and can be quantified as:

$$\frac{1}{2}M(v - v_t)^2 = \frac{1}{2}F_y\boldsymbol{d}$$

where v is the peak particle velocity

Relationships between PPV's and permanent strains are graphically illustrated in Figure 5.22 for various threshold velocities, using estimated tendon properties.

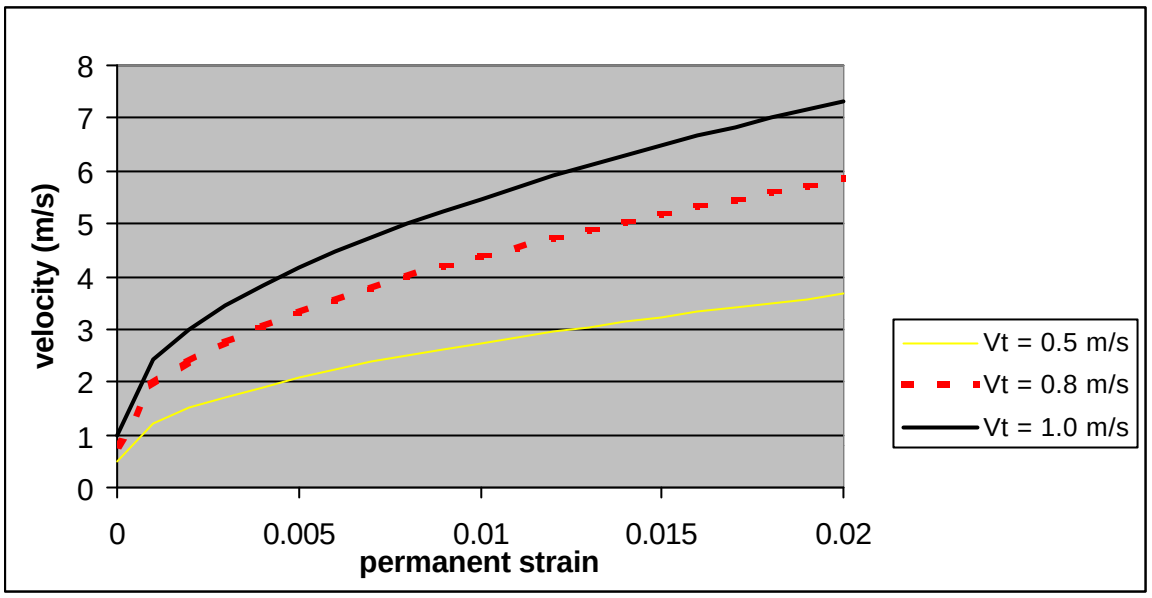

Figure 5.22 Relationship between velocities and non recoverable strain

Velocities in excess of 0.8 m/s were found to be associated with damage at the wall of an underground tunnel in a simulated rockburst experiment (Milev et al. 2001). This value is represented in Figure 5.22 as well. Although this observation is strictly related to the ejection of rock, it may nevertheless be of use in quantifying the relationship between velocities and induced deformations.

6 Impact test model

6.1 Parameter study on support requirements for impact loading

A model, describing the impact tests, is presented here. This model makes use of a minimum amount of parameters, namely the maximum impact force, impact duration and the resisting force. As the impact force and duration are directly related to the system stiffness (i.e. rock mass, tendons, fabric and lacing), these parameters will change from system to system. The resisting force is related to the support resistance and an internal rock mass component.

While these parameters may vary between subsequent impacts, due to induced damage and deformation, they are assumed to remain constant during a single impact. In this way, a particular system can be calibrated by matching monitored deformations and or velocities with model predictions. The model can thus be used for improved analyses of the impact tests. It should be emphasized here that the modelled deformations are permanent, non recoverable deformations associated with a single impact. The effect of multiple impacts is cumulative and reflects the effect of repeated dynamic loading due to seismicity in underground applications.

The impact of the drop weight on the artificial rock mass induces a dynamic force. By quantifying this force, as well as the resisting forces, it is possible to determine the associated velocities and displacements.

In order to derive suitable expressions, it is necessary to make certain simplifying assumptions about the impact forces and the resisting forces. The following assumptions are used in the impact model:

- Rise and decline of the impact force are linear and equivalent.
- Different impact magnitudes cause congruent (self-similar) impact force-time relationships, therefore the ratio $\frac{dF(t)}{dt}$ is constant (C). (6.1)
- The resisting force is made up of an internal shear component and a support force component.

- The impact can be related to the force amplitude $\hat{F}$ by:

$$mv = \frac{1}{2}\hat{F}T\,, \tag{6.2}$$

where by T is the duration of the pulse.

Figure 6.1 shows the assumed relationship between the impact force and time. In this figure, the resisting force is indicated by F^*. This resisting force consists of some internal frictional resistance and a support resistance. Both of these components may change with increasing deformation and increasing damage, but it is assumed that they are constant during one single impact. Positive values of $F(t) - F^*$ are conducive to relative movements between the potential "wedge" and the surrounding material. These movements can be computed from the impact by using (6.1) and (6.2) in combination with Figure 6.1. The following additional relationships can be found:

$$\hat{F} = \sqrt{mvC} = \frac{CT}{2};$$

$$T = 2\sqrt{\frac{mv}{C}} = \frac{2\hat{F}}{C} \tag{6.3}$$

$$C = \frac{4mv}{T^2} = \frac{2\hat{F}}{T}$$

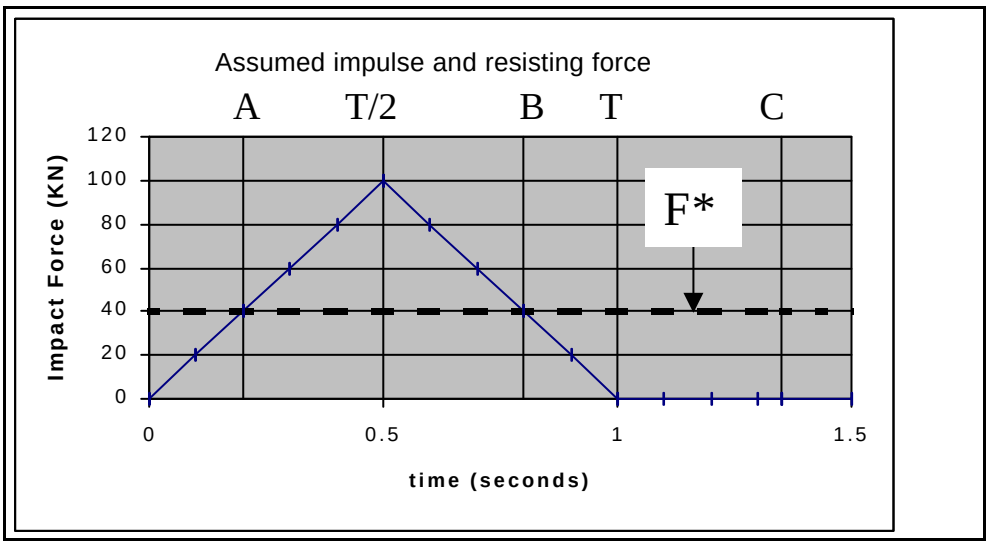

Figure 6.1. Relationship between the impact force, resisting force, and time.

The force is expressed as follows:

$$F(t) = Ct \text{ for } t \le \frac{T}{2}$$

$$F(t) = \hat{F} - C(t - \frac{T}{2}) \text{ for } \frac{T}{2} \le t \le T$$

$$F(t) = 0 \text{ for } t \ge T$$

If $\hat{F} \ge F^*$, the following conditions apply as well:

$$t_A = \frac{T}{2} - \frac{T}{2}(1 - \frac{F^*}{\hat{F}}) = \frac{TF^*}{2\hat{F}} = \frac{F^*}{C};$$

$$t_B = \frac{T}{2} + \frac{T}{2}(1 - \frac{F^*}{\hat{F}}) = \frac{T}{2}(2 - \frac{F^*}{\hat{F}}) = T - \frac{F^*}{C};$$

$$t_C = T(\frac{\hat{F}}{2F^*} + \frac{F^*}{4\hat{F}}) = \frac{CT^2}{4F^*} + \frac{F^*}{2C}$$

Associated velocities can now be computed by integration. A mass M, representing the potentially unstable region, has to be identified so that the acceleration induced by the impact force can be quantified. The relevant velocity for this particular problem is thus:

$$v(t) = \int \frac{F(t) - F^*}{M}$$

At A, the velocity is zero;

$$v_A = 0;$$

From A to $\frac{T}{2}$, the velocity can be expressed by:

$$v(t^*) = \frac{C(t^*)^2}{2M},$$

where by t^* is the time from t_A.

At $t = \frac{T}{2}$, $t^* = \frac{T}{2}\left(1 - \frac{F^*}{\hat{F}}\right)$ and the velocity is:

$$v(\frac{T}{2}) = \frac{CT^2}{8M}\left(1 - \frac{F^*}{\hat{F}}\right)^2 = \frac{1}{2M}\left(\frac{CT^2}{4} - F^*T + \frac{(F^*)^2}{C}\right)$$

From $\frac{T}{2}$ to B, the velocity can be expressed by:

$$v(t^*) = \frac{CT^2}{8M}\left(1 - \frac{F^*}{\hat{F}}\right)^2 + \frac{(\hat{F} - F^*)}{M}t^* - \frac{C(t^*)^2}{2M}$$

where by t^* is the time from $\frac{T}{2}$.

At $t = B$, $t^* = \frac{T}{2}\left(1 - \frac{F^*}{\hat{F}}\right)$ and the velocity is:

$$v(B) = \frac{CT^2}{4M}\left(1 - \frac{F^*}{\hat{F}}\right)^2 = \frac{1}{M}\left(\frac{CT^2}{4} - F^*T + \frac{(F^*)^2}{C}\right)$$

From B to T, the velocity can be expressed by:

$$v(t^*) = \frac{CT^2}{4M}\left(1 - \frac{F^*}{\hat{F}}\right)^2 - \frac{C(t^*)^2}{2M}$$

where by t^* is the time from B.

At $t = T$, $t^* = \frac{T}{2}\left(\frac{F^*}{\hat{F}}\right)$ and the velocity is thus:

$$v(T) = \frac{CT^2}{8M}\left[2\left(1 - \frac{F^*}{\hat{F}}\right)^2 - \left(\frac{F^*}{\hat{F}}\right)^2\right] = \frac{1}{M}\left(\frac{CT^2}{4} - F^*T + \frac{(F^*)^2}{2C}\right)$$

From T to C, the velocity can be expressed by:

$$v(t^*) = \frac{CT^2}{8M}\left[2\left(1-\frac{F^*}{\hat{F}}\right)^2 - \left(\frac{F^*}{\hat{F}}\right)^2\right] - \frac{F^* t^*}{M}$$

where by t^* is the time from T

At $t = C$, the velocity is zero and $t^* = T\left(\frac{\hat{F}}{2F^*} - 1 + \frac{F^*}{4\hat{F}}\right)$

Figure 6.2 shows the relationship between velocity and time for an example with the following parameters: $T = 1s$; $M = 5000kg$; $\hat{F} = 100N$; $F^* = 40N$

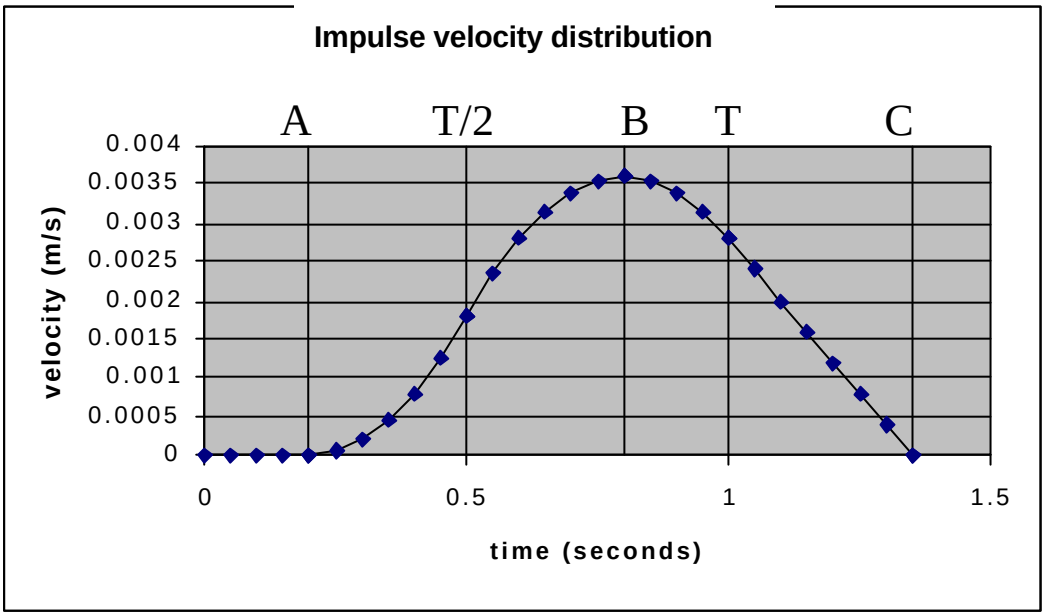

Figure 6.2. Relationship between impulse velocity and time for given parameters.

The permanent displacements associated with a single impulse can be derived from further integration:

At A, the displacement is zero, as the resisting force has not yet been exceeded;

$$s(A) = 0;$$

From A to $\frac{T}{2}$; the displacements are expressed as:

$$s(t^*) = \frac{C(t^*)^3}{6M},$$

where by t^* is the time from t_a.

At $t = \frac{T}{2}$, $t^* = \frac{T}{2}\left(1 - \frac{F^*}{\hat{F}}\right)$ and the displacement is:

$$s(\frac{T}{2}) = \frac{CT^3}{48M}\left(1 - \frac{F^*}{\hat{F}}\right)^3 = \frac{1}{48M}\left(CT^3 - 6F^*T^2 + \frac{6(F^*)^2T}{C} - \frac{2(F^*)^3}{C^2}\right)$$

From $\frac{T}{2}$ to B, the displacement can be expressed by:

$$s(t^*) = \frac{CT^3}{48M}\left(1 - \frac{F^*}{\hat{F}}\right)^3 + \frac{CT^2}{8M}\left(1 - \frac{F^*}{\hat{F}}\right)^2 t^* + \frac{(\hat{F} - F^*)}{2M}(t^*)^2 - \frac{C(t^*)^3}{6M}$$

where by t^* is the time from $\frac{T}{2}$.

At $t = B$, $t^* = \frac{T}{2}\left(1 - \frac{F^*}{\hat{F}}\right)$ and the displacement is:

$$s(B) = \frac{CT^3}{8M}\left(1 - \frac{F^*}{\hat{F}}\right)^3 = \frac{1}{24M}\left(CT^3 - 6F^*T^2 + \frac{6(F^*)^2T}{C} + \frac{2(F^*)^3}{C^2}\right)$$

From B to T, the displacements can be expressed by:

$$s(t^*) = \frac{CT^3}{8M}\left(1 - \frac{F^*}{\hat{F}}\right)^3 + \frac{CT^2}{4M}\left(1 - \frac{F^*}{\hat{F}}\right)^2 t^* - \frac{C(t^*)^3}{6M}$$

where by t^* is the time from B.

At $t = T$, $t^* = \frac{T}{2}\left(\frac{F^*}{\hat{F}}\right)$ and the displacement is thus:

$$s(T) = \frac{CT^3}{48M}\left[6\left(1-\frac{F^*}{\hat{F}}\right)^2 - \left(\frac{F^*}{\hat{F}}\right)^3\right] = \frac{1}{48M}\left(6CT^3 - 24F^*T^2 + \frac{24\left(F^*\right)^2 T}{C} - \frac{\left(F^*\right)^3}{C^2}\right)$$

From T to C, the displacements can be expressed by:

$$s(t^*) = \frac{CT^3}{48M}\left[6\left(1-\frac{F^*}{\hat{F}}\right)^2 - \left(\frac{F^*}{\hat{F}}\right)^3\right] + \frac{CT^2}{8M}\left[2\left(1-\frac{F^*}{\hat{F}}\right)^2 - \left(\frac{F^*}{\hat{F}}\right)^2\right]t^* - \frac{F^*\left(t^*\right)^2}{2M}$$

where by t^* is the time from T

At $t = C$, $t^* = T\left(\frac{\hat{F}}{2F^*} - 1 + \frac{F^*}{4\hat{F}}\right)$ and the total displacement is therefore:

$$S = \frac{1}{48M}\left(\frac{3C^2T^2}{2F^*} - 6CT^3 + 6F^*T^2 - \frac{2\left(F^*\right)^3}{C^2}\right) \qquad (6.4)$$

The last expression indicates the permanent deformation associated with a single impact. This parameter has been recorded for all tests and the model can thus be calibrated.

Equation (6.4) is shown in Figure 6.3 in graphical form for selected parameters.

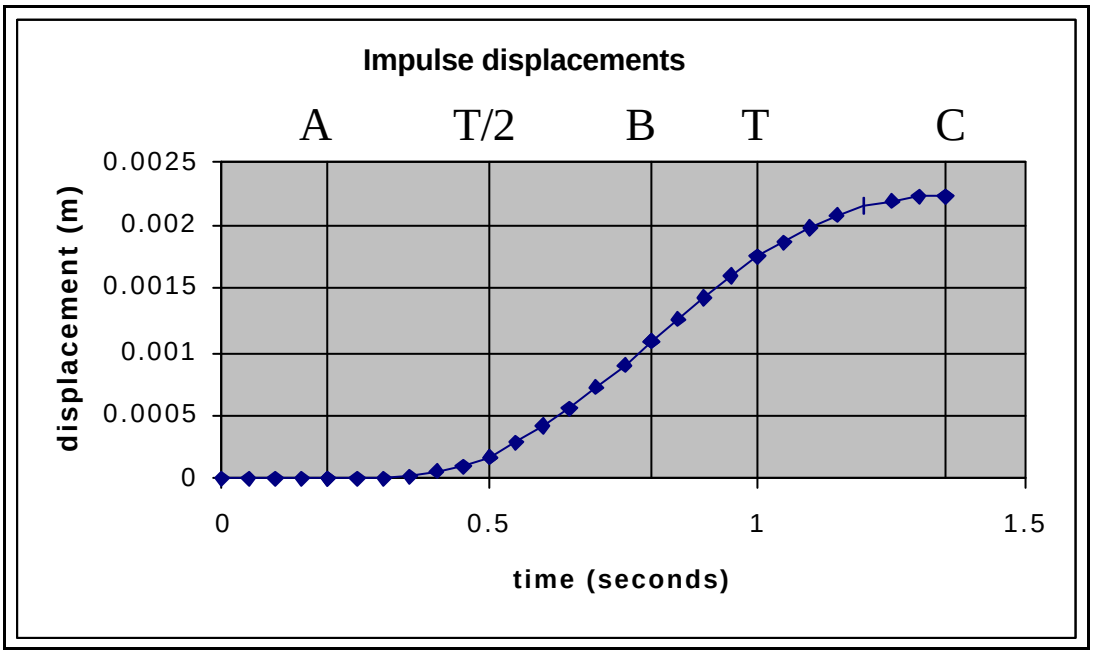

Figure 6.3. Relationship between impulse displacement and time for given parameters.

It should be emphasised that the model can be calibrated for a single impact only. Parameters such as internal resistance and support resistance may not remain constant, but could be affected by increasing deformations and associated damage.

In the drop test rig, the tendons can be assumed to be rigid for all practical purposes. During the impact, a certain percentage of the impact energy is used to mobilise boundaries between individual bricks and to accelerate the bottom layer of bricks. Part of the impact energy is expected to be lost in elastic deformation, local crushing and other, non-specified deformation processes. Equations (6.3) are therefore not strictly valid, but serve as an indication.

6.2 Discussion and Conclusions

Using the model described in Section 6.1, parameters can be calibrated for a particular impact. These model parameters must be expected to vary with increasing deformation and damage. If all parameters remained constant, a linear relationship would be obtained between deformation and applied energy. The fact that these relationships are typically non-linear (see Figure 3.6 and Figure 3.7) indicates variations in certain parameters. A reduction in internal resistance for instance would be associated with an exponential relationship between deformation and cumulative energy, while increasing support resistance would have the opposite effect.

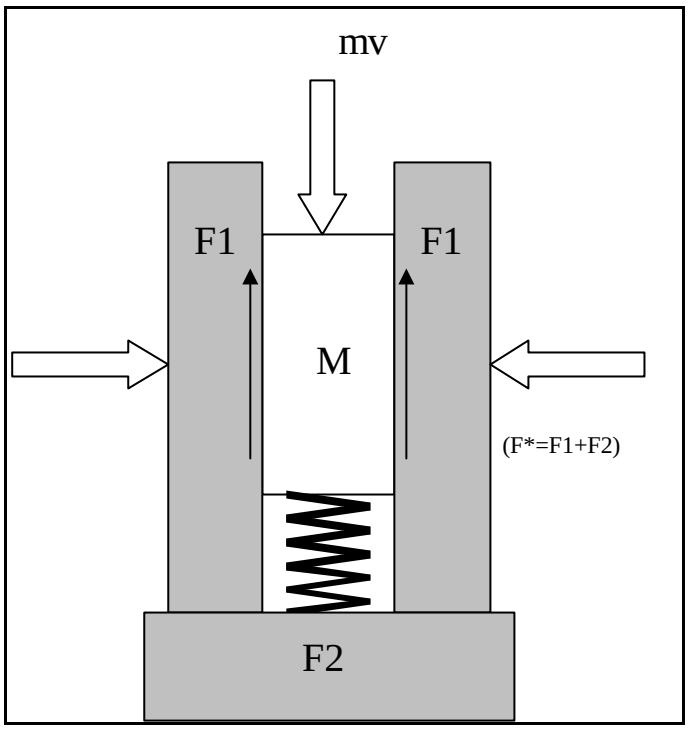

Figure 6.4. Model of impact testing.

The sketch shown in Figure 6.4 allows for visualization of the model and its controlling parameters. The relationship between impact energy and displacements is not necessarily linear such as in Figure 6.1. The shape of the impulse controls to a large extent the theoretical relationship between impact magnitude and the resulting displacements. In addition, the actual driving force is that force which exceeds the combined resisting forces in the system. Therefore, the difference between impact force and resisting force has to be considered and not just the impact force itself. This is an important issue, as the quantification of cumulative energy is directly affected. In order to avoid these complications, all tests were executed with constant impact magnitudes; by dropping the same weight from the same height in each individual test.

In the proposed model, the shape of the impact pulse was assumed to be self-similar for different impact magnitudes, while a triangular pulse shape was assumed as well. As can be appreciated from the derived expressions, the relationship between displacements (6.4) and impact magnitude becomes rather complicated and depends on parameters such as restraining force and rise time. In order to obtain simpler relationships, to allow a more direct comparison between displacements and impact energy, consider a pulse with zero rise time. The rectangular shape of this pulse is associated with a constant force and results in the following expression for the ultimate displacement:

$$S = \frac{T^2}{2M}\left(\frac{\left(\hat{F}\right)^2}{F^*} - \hat{F}\right) \qquad (6.5)$$

As the impulse can be related to the impact force by:

$$mv = \hat{F}T \tag{6.6}$$

and the velocity can be expressed by:

$$v = \sqrt{2gh}\,, \tag{6.7}$$

relationships between drop height and displacements can be established. Two extremes are considered here; the first one assumes a constant impulse time, while the second one assumes a constant impact force.

If the drop height is increased by a factor a, the velocity, as well as the impact force, increase by a factor $\sqrt{a}$ (from Equations 6.6 and 6.7), if the impulse time remains constant. Inserting in (6.5) and replacing $\frac{\hat{F}}{F^*}$ by X ($X \geq 1$), it follows that the ratio between the two displacement values is:

$$\frac{aX^2 - X\sqrt{a}}{X^2 - X} \tag{6.8}$$

Relatively large values of X would result in a relationship between drop height and displacement which approaches linearity. However, smaller values of the ratio lead to a relationship with varying values. Figure 6.5 shows how the relationship between drop height and displacement is affected by the ratio $\frac{\hat{F}}{F^*}$

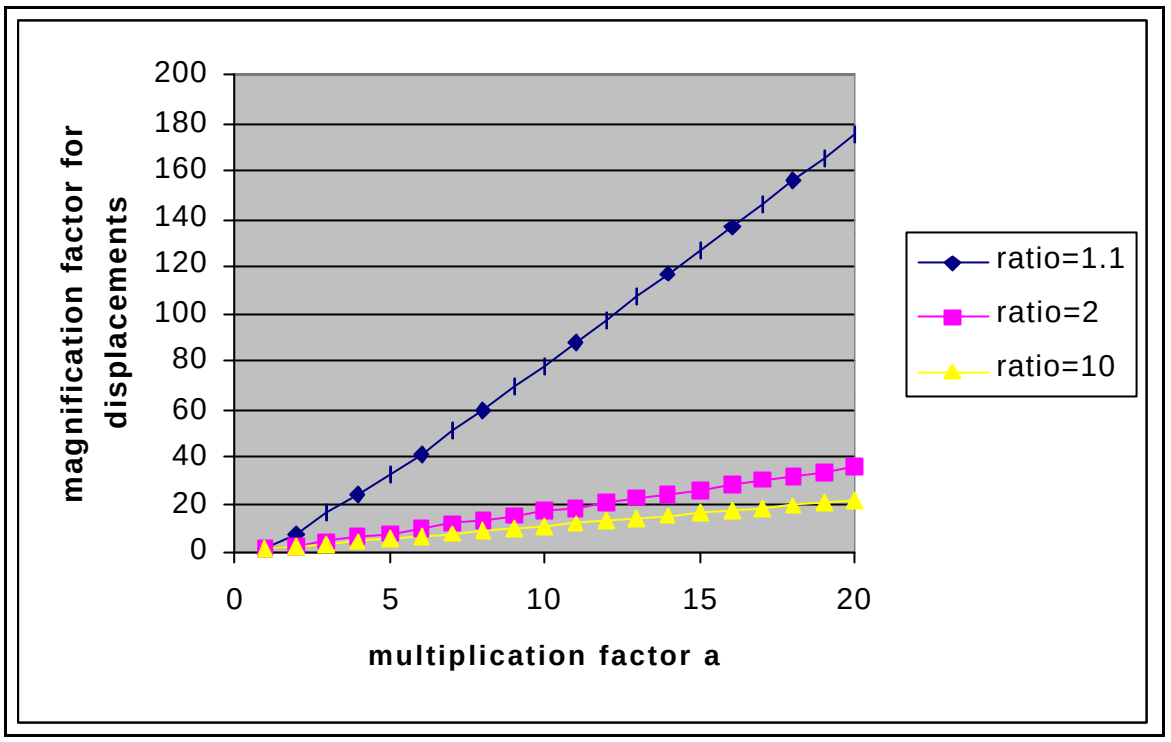

Figure 6.5. Displacement magnification factors for different ratios between impact force and resisting force with increasing drop heights.

From Figure 6.5 it is clear that the relationship between drop height and displacement is not linear. Depending on the ratio between impact force and resisting force, the exponent a in the expression:

$$S = \tilde{C}h^{a} \tag{6.9}$$

can reach values in excess of 1.0 and even in excess of 2.0 for relatively low values of $\frac{\hat{F}}{F^{*}}$.

If the impulse force were to remain constant, the ratio between the two displacement values would be equal to the multiplication factor a and a linear relationship would exist between drop height and induced displacement. If the impulse shape were not affected, both impulse time and impulse force would increase in response to increasing impact magnitudes. The effect would then be anything between the two extremes described above, so that the exponent in (6.9) would always be larger than 1.0. Although not explicitly demonstrated, a similar behaviour could be expected from the actual model used here. The results from the drop tests indicated that a large drop height has more influence on deformation than a number of small drop heights

with equivalent total impact energy. This observation is thus confirmed and substantiated by the current model.

The model could be further calibrated if the impulse time were monitored. In addition it should be emphasized that the resisting forces would be dependant on the deformations. Larger deformations typically lead to a reduction in internal resistance and may have various effects on the support forces. Increasing deformation would for instance result in an exponential increase in lacing resistance, while the resistance offered by a shotcrete panel will increase linearly until a maximum is reached at relatively small deformation levels. The deformation of tendons does not play a role in these particular tests, but could in principle also be incorporated into the model. The results from the drop tests can be readily explained from the current model if these considerations are taken into account as well.

Monitored velocities showed peak values of around 500 mm/s, while the velocities in the example reach a maximum value of 3.5 mm/s. The observed and modelled displacements show a smaller difference; observations varied between 1.2 mm and 60 mm per blow and the model predicts a value of 2.5 mm. Model parameters can be adjusted to match these observations by reducing the impulse time and increasing the impulse force. In order to obtain a hundredfold increase in velocity, it is necessary to increase the impact force by the same amount. Any additional reduction in impact time should be accompanied by an equivalent additional increase in impact force in order to maintain constant velocities. The displacements, however, are differently affected by impact force and time. A one thousand fold increase in impulse force, accompanied by a hundredfold decrease in impulse time and a tenfold decrease in affected rock mass would result in peak velocities of around 350 mm/s and maximum displacements of around 2.5 mm/s. An impact amplitude $\hat{F} = 100KN$ and an impact time $T = 0.01s$ result in matching values, while the impact energy is of an equivalent magnitude (10 cm drop height). As only test 1 has been monitored by geophones, the calibrated parameters may be different for the other tests. This can also be appreciated from the results shown in Figure 3.6 and 3.7.

The support resistance of the lacing can be estimated from its elastic properties. The lacing is assumed to be clamped at the tendons and no initial gap between lacing and assembly is considered. The total lacing force can be approximated from the displacements in the centre of the assembly as follows:

$$F_l = 2\left(\sqrt{1+\boldsymbol{d}^2} - 1\right)MN$$

a displacement of for instance 100mm would thus generate a force of approximately 100 kN. This force would balance the impact force. The yield force of the lacing configuration could however not be established clearly. From the results, it appears that some variation occurs and that yielding initiated at displacements ranging from 30 mm to 220 mm; initiation of yielding is assumed to occur when no further stiffening of the system takes place. Associated yield forces would therefore range between 30 kN and 220 kN. Fibre reinforced shotcrete can be expected to offer a similar peak resistance. Tests conducted by Kirsten (1992) show that similar shotcrete panels can withstand such loads as well. However, shotcrete would gradually lose this capacity with increasing deformation, after its peak resistance had been reached. The results indicate that deformations around 50 mm may be associated with such a peak resistance as the stiffness of the system decreases beyond this value. As variations in the results are relatively large, the influence of the different support systems cannot be determined with great accuracy. The occurrence of such large variations under controlled laboratory conditions suggests even larger variations in underground applications. This should obviously be an important consideration. The following conclusions on support effect are based on the results of the laboratory tests:

- Lacing provides a yield support resistance ranging between 30 kN and 220 kN.
- 100 mm Shotcrete provides a peak resistance of similar magnitude (around 100 kN).
- Evermine prevents local fall-out (stability), but does not affect overall deformations.
- Shotcrete provides an immediate stiffness, while lacing needs to be deformed first.
- Without fabric support, total failure occurs when deformations exceed 150 mm.
- The use of Evermine increases the damage threshold to 200 mm.
- The use of fibre-reinforced shotcrete increases the damage threshold to 250 mm.
- Velocities of around 500 mm/s and impact forces of around 100 kN appear to be associated with a drop height of 0.1 m.

7 Formulation of design criteria

The performance of various support fabric components was evaluated with the drop tests. From those observations it is clear that the combination of shotcrete and lacing provides the most competent fabric support. Shotcrete increases the initial stiffness of a system while it also offers a substantial peak resistance. Lacing is initially less stiff, but it is able to supply a similar resistance as the fibre-reinforced shotcrete. Evermine and lacing appear to provide a similar ultimate resistance as fibre-reinforced shotcrete, although the initial stiffness, associated with shotcrete, is lacking.

The tests were conducted in a relatively fragmented, blocky, medium, which seems to be fairly representative of fractured rock around deep level tunnels. The results of these tests demonstrate how such an assembly is destroyed because of support fabric failure. It can be argued that the support capacity of the fabric should at least match the support capacity of the rock tendons under these circumstances. If the fabric support fails before the tendons reach their yield strength, tendons are not effectively employed and are in fact under-utilised. This consideration should be reflected in any realistic design criterion. Rock tendons and fabric have to be compatible in the sense that the fabric strength exceeds the yield strength of the tendons.

In order to achieve practical improvements to an existing support system, the fabric support resistance should be increased. The main parameter to consider in any practical situation is the fragmentation or at least the potential for fragmentation of the tunnel walls. Identification of bulging between tendons would be an indication of high fragmentation and associated unravelling. The second parameter to consider is the magnitude of seismically induced velocities. Identification of seismic potential and location of seismically active structures may assist in quantifying potential velocities. A combination of high fragmentation and high velocities is considered to be particularly dangerous and warrants attention in the form of improved fabric support.

The main function of support in highly stressed tunnels in hard rock is to stabilize rock blocks. If these blocks are relatively large, this can be achieved by effectively pinning them. However when the rock is more fragmented, fabric support is required in order to provide a more uniform support distribution. The loads, which have to be considered, are gravitational forces and excitations due to seismic activity. The support is typically not required to control squeezing conditions, as tunnels would remain open in the absence of support pressure. Only the stability of the fragmented skin of the tunnels needs to be considered.

In exceptional circumstances, when extremely weak rock is encountered, squeezing conditions may occur and support pressure will be required to ensure overall tunnel stability. Required support pressures may be relatively large in that case and can be quantified with a design procedure similar to that used in soft ground conditions.

The demand on a support system in seismically excited hard rock depends mainly on the location and magnitude of the seismic event and the volume of unstable rock (depth of fragmentation). As seismic events cannot be predicted, potential excitations at certain locations have to be estimated. Such estimates may be based on seismically active structures in the surroundings of a particular tunnel. Induced support forces can be derived by using empirical relationships, which have been established for seismic activity. A methodology for establishing support requirements and designing fabric support was formulated in Miningtek's Step project Y2263, titled: "Tunnel Support Design Methodology". This methodology enables the matching of support components by requiring that the combined fabric/ rock mass strength should exceed the yield strength of the tendons. By using this methodology minimum required tendon spacing are initially determined for various tendons. In the next step the fabric properties can be determined. As the fabric requirements are strongly related to the tendon spacing, a reduction in tendon spacing would typically lead to a reduction in fabric requirements. On the other hand, a reduction in tendon spacing would obviously lead to in increase in tendon costs. Optimum combinations can be found for different design conditions.

From relationships such as shown in Figure 7.1, seismically induced forces on the support system can be determined. Figure 7.2 shows how the strength of wire mesh reinforced shotcrete (WMRSC) is related to tendon spacing. The yield strength and yielding range of tendons can easily be derived from appropriate laboratory tests and a matching type can be selected based on support requirements and fabric strength. As Figure 7.2 shows, the strength of the wire mesh reinforced shotcrete depends on its thickness and the panel span (=tendon spacing). Many combinations of tendons and fabric may satisfy the imposed support requirements, but obviously the most cost effective combination should be selected. Figure 7.3 shows an example of a cost analysis, which can be conducted after the support requirements have been determined. An increase in panel strength can be obtained by reducing the panel span and/or by increasing the panel thickness. An increase in panel thickness results in increased fabric costs, while a decrease in panel span is associated with denser tendon spacing and thus increased tendon costs. An optimum tendon spacing applicable for a particular combination of fabric and tendon, can be derived from this analysis. While any of these spacings would satisfy the support requirements, only one of those is associated with a minimum total cost. The graphs shown here are only applicable to certain selected conditions and support systems and serve to demonstrate the methodology. In order to establish similar

graphs for different applications, the methodology as described in the project report Y2263 should be used.

Table 4.1 can be used as a guideline for support requirements in seismically active regions, while the methodology as developed in step project Y2263 can be used for actual design purposes.

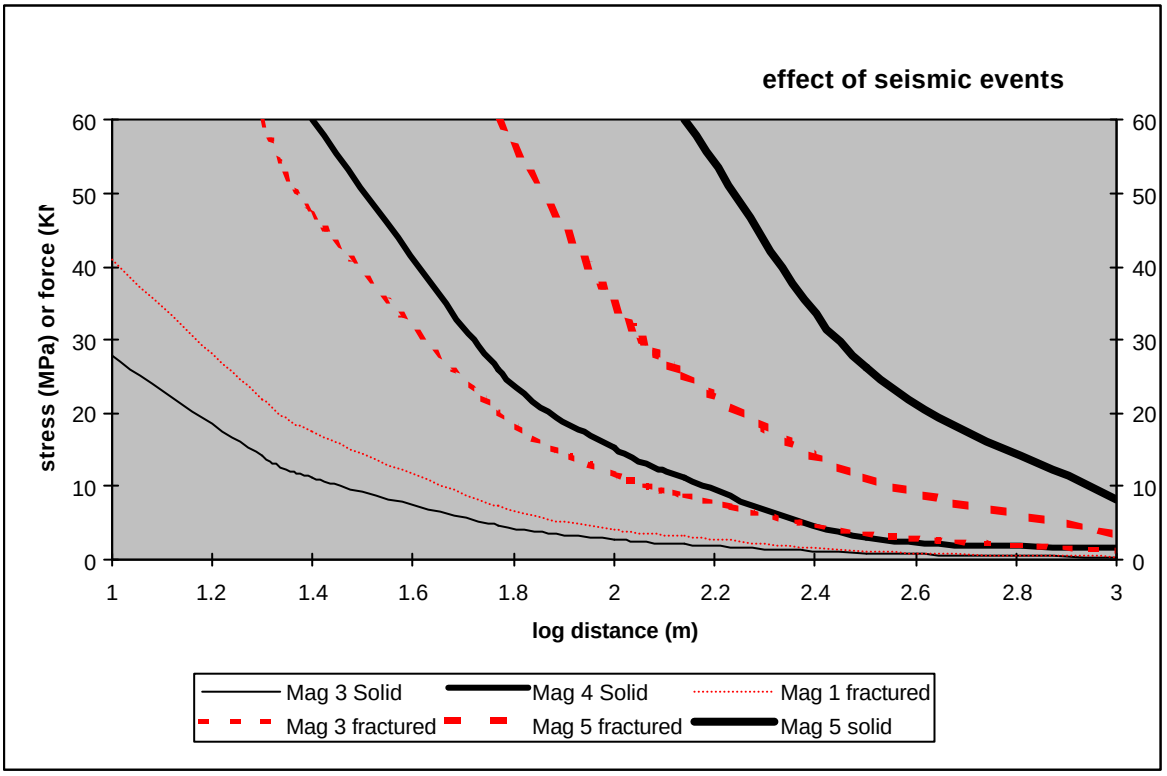

Figure 7.1. Relationship between distance from the seismic source and the induced stresses in solid rock and induced forces (volume of 1 cubic metre) for various magnitudes.

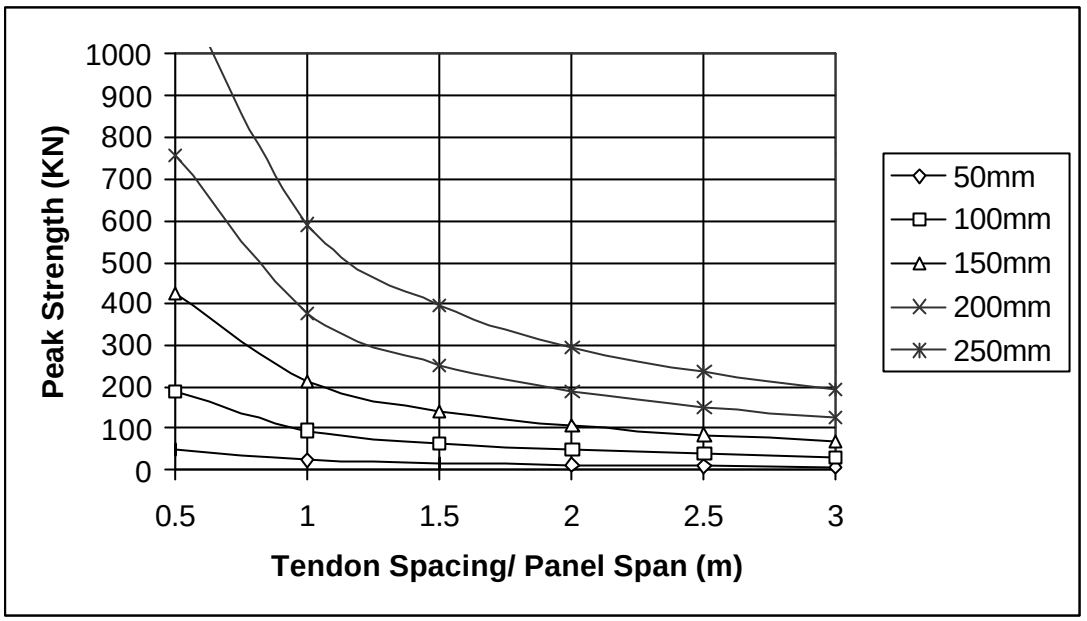

Figure 7.2. Theoretical relationship between strength and span for varying thicknesses of uniformly loaded WMRSC, based on a single calibration test.

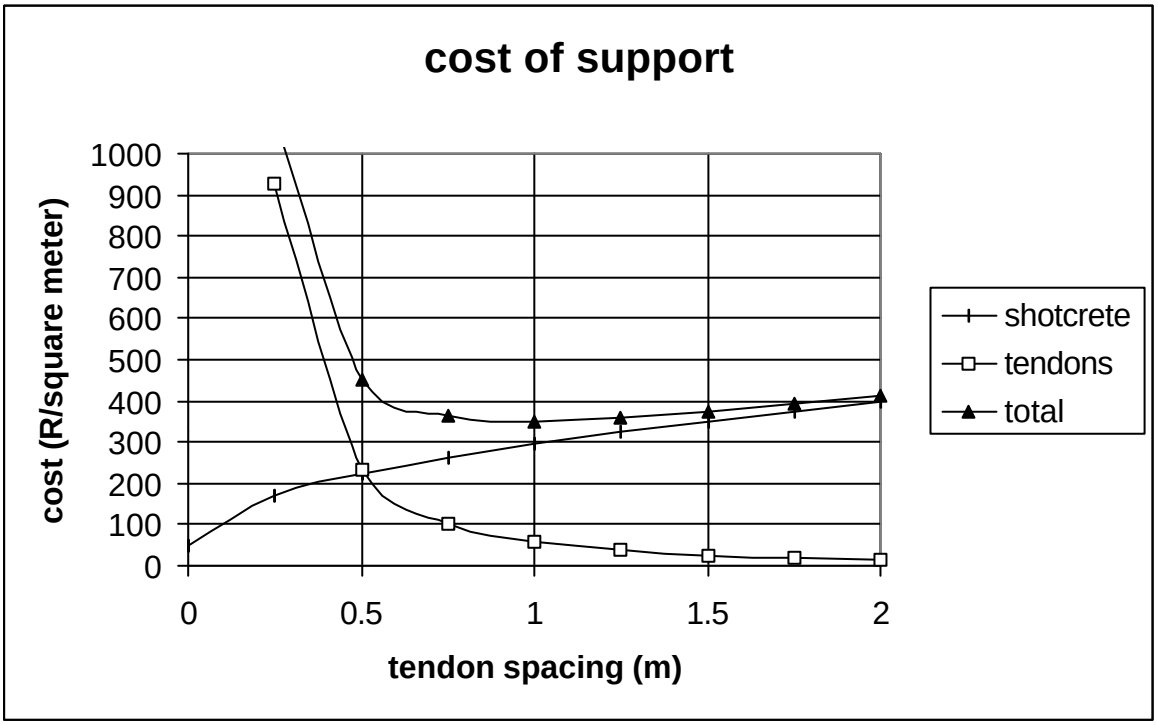

Figure 7.3. Cost analysis graph for cone bolts and WMRSC.

8 Recommendations for future work

Testing of additional support systems and components, including tendons and alternative support systems is recommended to complement these tests. In order to avoid large variations in test results, extreme care has to be given to specimen preparation, control and monitoring. Support components should be monitored individually so that their contribution can be evaluated directly. While the impact tests provided valuable and practical information on the deformation and failure mechanisms, it should, in principle, suffice to conduct static tests on individual components. The need for relatively large loading magnitudes may however present a practical obstacle in such tests.

In addition it is strongly recommended that statistically relevant data be obtained from underground sites. The current design criteria are based on indirect and sparse information and are likely to be inaccurate and irrelevant. Site specific design criteria, based on local seismicity, fragmentation and stress changes should result in more efficient use of support. Monitoring of local seismic activity can be done with fairly simple and cheap instruments, which are only triggered at relatively high accelerations.

Failure of support systems in highly fragmented ground is associated with the failure of the fabric, irrespective of the capacities of the tendons. The influence of fabric support may therefore be largely underestimated as it is often considered as a passive, containment support component. However, as has been highlighted before, fabric is most often the critical support component in highly fragmented rock and its support resistance should ideally exceed that of the tendons. This is typically not the case with current support systems and it is highly recommended that this inefficiency be addressed by research into cost effective solutions and improved safety.

The rock mass fragmentation has been identified as the major parameter determining fabric requirements. While this parameter is currently not quantifiable, only estimations can be made. It is therefore highly recommended that rock mass classification methods allow for a realistic quantification of the fragmentation, in such a way that it represents the potential for unravelling of a particular rock mass into an excavation such as a tunnel.

As the dynamically induced support forces are directly related to the system stiffness, there is a large potential to reduce these forces by reducing the system stiffness. Low fabric stiffness may be less desirable as it quickly leads to rock mass disintegration. However, reduced tendon stiffness does not necessarily cause disintegration and appears to be the preferred option for the reduction of dynamically induced support forces and associated requirements.

By addressing this aspect of support design mayor improvements may be expected, without increased costs. While the reduced stiffness obviously leads to larger deformations, these deformations may be recoverable as they are not associated with unravelling and disintegration of the rock mass, which is typically the cause of damage and injuries.

The *in situ* performance of support components should be monitored. Identification of premature failure may prevent subsequent failure of the support system. Tendons often corrode or shear or may not be properly installed. Any monitoring method or device, which could identify such deficiencies, is highly recommended.

Alternative support systems and/or components may offer more efficient solutions in highly fragmented rock which is subjected to seismic activity. The most important criteria for any support system are:

- Provide a support pressure which is as uniformly distributed as possible.
- Absorb the imposed dynamic energy.
- Keep the fragmented skin in position during seismic events.

The new Miningtek tunnel support design methodology attempts to address these issues and requires further evaluation from additional laboratory tests and *in situ* monitoring.

Possible alternative support systems, which may prove to satisfy the above criteria, may be found in structural shells, improved fabric and, possibly, weaker and/or softer tendons.

The *in situ* monitoring at Tau Tona mine could provide useful data in future as the site is in an area of relatively high seismicity. Funding would be required for data collection and interpretation. The costs of this exercise should be relatively low since the instruments are already in place. Miningtek is currently continuing the monitoring, but it is recommended that SIMRAC considers this in its 2001 budget.

References

DME (1996), Guideline for the compilation of a mandatory Code of Practice to combat rockfall and rockburst accidents in metalliferous mines and mines other than coal. Mine Health and Safety Inspectorate. Johannesburg.

Gürtunca, R.G. and Haile, A.T. (1999), Lessons learned from deep mining in South Africa, Proceedings of "Vorerkundung und Prognose der Basistunnels, editors Low and Wyss, Balkema, Rotterdam, pp. 349 - 357

Hagan, TO, Milev, AM, Spottiswoode, SM, Vakalisa, B & Reddy, N, (1998), "Improvement of worker safety through the investigation of the site response to rock bursts", Final Project Report GAP 530, Safety in Mines Research Advisory Committee, Johannesburg, South Africa.

Haile, A.T. (1999), A mechanistic evaluation and design of tunnel support systems for deep level South African gold mines, PhD thesis, University of Natal, South Africa.

Haile, AT, Grave, DM, Sevume, C & Le Bron, K, (1998), Strata control in tunnels and an evaluation of support units and systems currently used with a view to improving the effectiveness of support, stability and safety of tunnels, Appendix to Final Project Report GAP 530, Safety in Mines Research Advisory Committee, Johannesburg, South Africa.

Haile, A.T. and Le Bron, K.B. (2001), Simulated rock burst experiment – evaluation of rockbolt performance, J. of South African Inst. Of Mining and Metallurgy, submitted for publication

Kirsten, H.A.D.(1992), Comparative efficiency and ultimate strength of mesh- and fibre-reinforced shotcrete as determined from full-scale bending tests, J. S. Afr. Inst. Min. Metall., vol. 92, no. 11/12 Nov./Dec. 1992, pp. 303-323.

Kuijpers, J.S., (2000), "Tunnel Support Design Methodology", Final Step Project Report Y2263, Miningtek, Johannesburg, South Africa

Milev, A. M., Spottiswoode S. M., Rorke A. J. & Finnie G. J. (2001), Seismic monitoring of a simulated rockburst on a wall of an underground tunnel. J. S. Afr. Inst. Min. Metal, submitted.

Stacey, T.R., and Ortlepp, W.D. (1997), Testing of tunnel support: Dynamic load testing of rock support containment systems (e.g. wire mesh), Final Project Report, GAP 221, SIMRAC, Johannesburg, South Africa.

Tau Tona Gold Mine (2000), Rock Mechanics Department, Personal Communication.

Appendix A

Figure A.1. Preparation of bricks assembly.

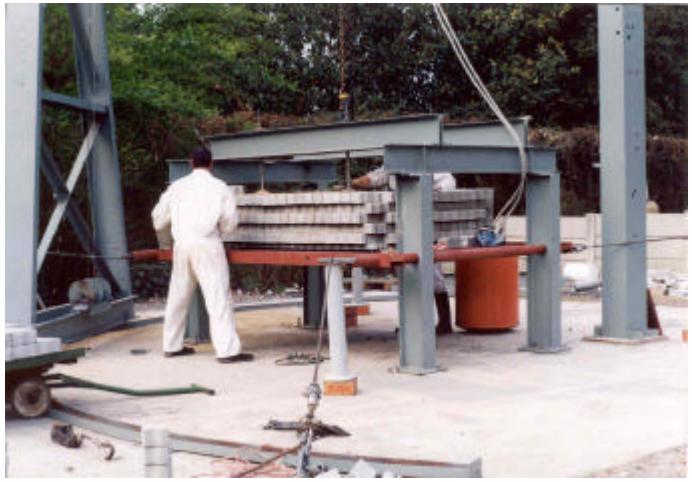

Figure A.2. Preparation of brick assembly.

Figure A.3. Brick assembly completed.

Figure A.4. Ready for testing.

Figure A.5. Ready for testing.

Figure A.6. Evermine and lacing 50 cm. drops.

Figure A.7. Evermine and lacing 50 cm. drops.

Figure A.8. Evermine and lacing 50 cm drops.

Figure A.9. Evermine and lacing 50 cm. drops.

Figure A.10. Evermine and lacing 50 cm. drops.

Figure A.11. Evermine and lacing 50 cm. drops.

Figure A.12. Evermine and lacing 50 cm. drops.

Figure A.13. Evermine and lacing 50 cm. drops.

Figure A.14. Evermine and lacing 50 cm. drops.

Figure A.15. Evermine and lacing 10 cm. drops.

Figure A.16. Evermine and lacing 10 cm. drops.

Figure A.17. Evermine and lacing 10 cm. drops.

Figure A.18. Evermine and lacing 10 cm. drops.

Figure A.19. Evermine and lacing 10 cm. drops.

Figure A.20. Evermine and lacing 10 cm. drops.

Figure A.21. Evermine 10 cm. drops.

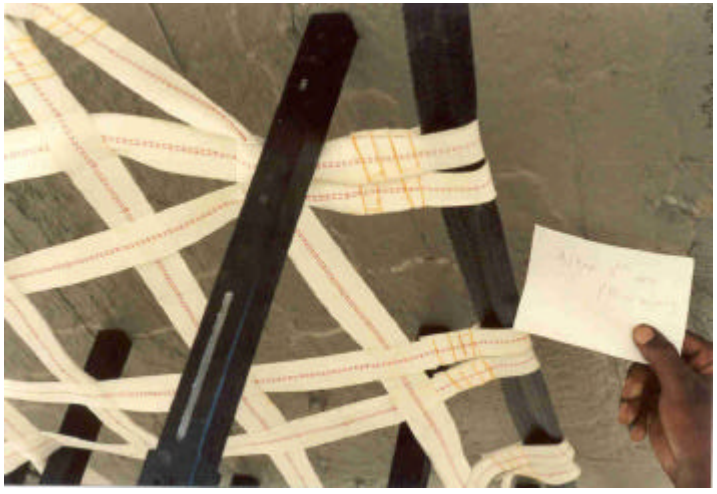

Figure A.22. Evermine 10 cm. drops.

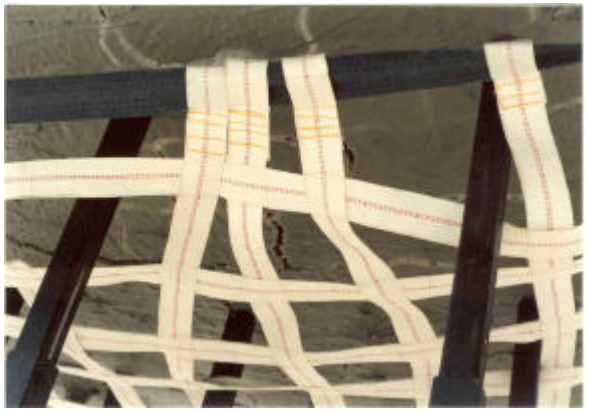

Figure A.23. Evermine 10 cm. drops.

Figure A.24. Evermine 10 cm. drops.

Figure A.25. Evermine 10 cm. drops.

Figure A.26. Evermine 10 cm. drops.

Figure A.27. Evermine 10 cm. drops.

Figure A.28. Evermine 10 cm. drops.

Figure A.29. Evermine 10 cm. drops.

Figure A.30. Evermine 10 cm. drops.

Figure A.31. Evermine 10 cm. drops.

Figure A.32. No fabric support 10 cm. drops.

Figure A.33. No fabric support 10 cm. drops.

Figure A.34. No fabric support 10 cm. drops.

Figure A.35. No fabric support 10 cm. drops.

Figure A.36. No fabric support 10 cm. drops.

Figure A.37. Lacing 10 cm. drops.

Figure A.38. Lacing 10 cm. drops.

Figure A.39. Lacing 10 cm. drops.

Figure A.40. Lacing 10 cm. drops.

Figure A.41. Detail of lacing.

Figure A.42. Shotcrete 50 cm. drops.

Figure A.43. Shotcrete 50 cm. drops.

Figure A.44. Shotcrete 50 cm. drops.

Figure A.45. Final failure of shotcreted assembly.

Figure A.46. Final failure of shotcreted assembly.

Figure A.47. Final failure of shotcreted assembly.

Figure A.48. Shotcrete and lacing 50 cm. drops.

Figure A.49. Shotcrete and lacing 50 cm. drops.

Figure A.50. Shotcrete and lacing 50 cm. drops.

Figure A.51. Shotcrete and lacing 50 cm. drops.

Figure A.52. Pull test diamond mesh (A).

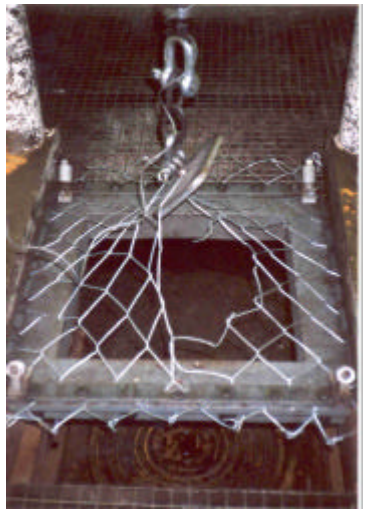

Figure A.53. Pull test diamond mesh (A).

Figure A.54. Pull test diamond mesh (B).

Figure A.55. Pull test diamond mesh (B).

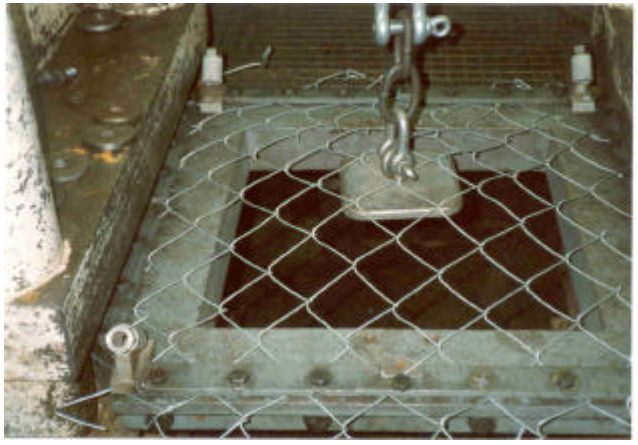

Figure A.56. Pull test diamond mesh (B).

Figure A.57. Pull test diamond mesh (B).